

Low-Head Pumped Hydro Storage with Contra-Rotating Pump-Turbines A Study on its Performance and Potential Contribution to Grid Stability

Hoffstaedt, Justus

DOI

[10.4233/uuid:f9274c7e-23e1-4f0b-b2f5-93ad7d44794c](https://doi.org/10.4233/uuid:f9274c7e-23e1-4f0b-b2f5-93ad7d44794c)

Publication date

2025

Document Version

Final published version

Citation (APA)

Hoffstaedt, J. (2025). *Low-Head Pumped Hydro Storage with Contra-Rotating Pump-Turbines: A Study on its Performance and Potential Contribution to Grid Stability*. [Dissertation (TU Delft), Delft University of Technology]. <https://doi.org/10.4233/uuid:f9274c7e-23e1-4f0b-b2f5-93ad7d44794c>

Important note

To cite this publication, please use the final published version (if applicable).
Please check the document version above.

Copyright

Other than for strictly personal use, it is not permitted to download, forward or distribute the text or part of it, without the consent of the author(s) and/or copyright holder(s), unless the work is under an open content license such as Creative Commons.

Takedown policy

Please contact us and provide details if you believe this document breaches copyrights.
We will remove access to the work immediately and investigate your claim.

LOW-HEAD PUMPED HYDRO STORAGE WITH CONTRA-ROTATING PUMP-TURBINES

**A STUDY ON ITS PERFORMANCE AND POTENTIAL
CONTRIBUTION TO GRID STABILITY**

Justus HOFFSTÄDT

LOW-HEAD PUMPED HYDRO STORAGE WITH CONTRA-ROTATING PUMP-TURBINES

**A STUDY ON ITS PERFORMANCE AND POTENTIAL
CONTRIBUTION TO GRID STABILITY**

Justus HOFFSTÄDT

LOW-HEAD PUMPED HYDRO STORAGE WITH CONTRA-ROTATING PUMP-TURBINES

**A STUDY ON ITS PERFORMANCE AND POTENTIAL
CONTRIBUTION TO GRID STABILITY**

Dissertation

for the purpose of obtaining the degree of doctor
at Delft University of Technology
by the authority of the Rector Magnificus, prof. dr. ir. T.H.J.J. van der Hagen,
chair of the Board for Doctorates
to be defended publicly on Tuesday, the 6th of May 2025 at 12:30 o'clock

by

Justus HOFFSTÄDT

Master of Science in Sustainable Energy Systems, University of Edinburgh, United
Kingdom
born in Düsseldorf, Germany

This dissertation has been approved by the promotor.

Composition of the doctoral committee:

Rector Magnificus,	chairperson
Dr. ir. R.L.J. Helmons,	Delft University of Technology, <i>promotor</i>
Dr. ir. A. Jarquin Laguna,	Delft University of Technology, <i>copromotor</i>

Independent members:

Prof. dr. ir. S.N. Jonkman,	Delft University of Technology
Dr. M. Marence,	IHE Delft, NL
Prof. dr. T. Sant,	University of Malta, MLT
Prof. dr. ir. T.J.C. van Terwisga,	Delft University of Technology / Marin, NL
Dr. ir. G.H. Keetels,	Delft University of Technology (reserve member)

Non-Independent members:

Prof. dr. N. Goseberg,	TU Braunschweig, GER
------------------------	----------------------

Prof. dr. ir. C. van Rhee † of Delft University of Technology has contributed greatly to the preparation of this dissertation.

This research was part of The ALPHEUS project (www.alpheus-h2020.eu) which has received funding from the European Union's Horizon 2020 research and innovation programme under grant agreement No 883553.



Keywords: Low-head pumped hydro storage, energy storage, grid stability, renewables integration, energy transition, reversible pump-turbine, experimental testing, physical modelling, fluid transients.

Printed by: Ridderprint.

Cover by: AI generated cover.

Copyright © 2025 by J. Hoffstädt

ISBN 978-94-6384-764-3

An electronic copy of this dissertation is available at
<https://repository.tudelft.nl/>.

*To my wife, Charlie, and my mother, Ulrike -
the two guiding lights of my life.*

CONTENTS

Summary	ix
Samenvatting	xi
List of Abbreviations	xiii
1. Introduction	1
1.1. Background and Motivation	1
1.1.1. The Role of Energy Storage and Ancillary Services in the Energy Transition	1
1.1.2. Overview, Historical Development and Limitations of Pumped Hydro Storage	3
1.1.3. The Challenges of Low-Head Pumped Hydro Storage	7
1.1.4. Low-Head Pumped Hydro Storage utilising Contra-Rotating Reversible Pump-Turbines	9
1.2. Research Scope and Objectives	10
1.3. Dissertation Outline	12
2. Low-Head Pumped Hydro Storage: State of the Art	15
2.1. Pump-Turbine Design	15
2.2. Electric Machines and Control	19
2.2.1. Electric Machines	19
2.2.2. Torque and Speed Control	21
2.2.3. Power Control	24
2.3. Grid Integration	28
3. Low-Head PHS system numerical model	31
3.1. Overview and Modelling Approach	32
3.2. Characterisation of the Reversible Pump-Turbine	33
3.3. Hydraulic Model	37
3.3.1. 1-D Compressible Flow Modelling in Pumped Hydro Storage Conduits	37
3.3.2. Reservoir and Valve Model	40
3.4. Drivetrain Model	41
3.5. Electric Machines and Control	42
3.5.1. Control Overview and Topologies	42
3.5.2. Axial-Flux PMSMs and Control Architecture	44

4. Experimental Evaluation and Model Comparison	47
4.1. Experimental Setup and Methods	47
4.1.1. Hydraulic Facilities with Open Surface Tanks	47
4.1.2. Contra-Rotating Reversible Pump-Turbine	49
4.1.3. Drivetrain Assembly	50
4.1.4. Instrumentation and Data Acquisition	52
4.1.5. Testing Protocol and Operating Range	54
4.2. Friction Torque Characterisation	55
4.3. Steady-State Results	56
4.4. Comparison of Steady-State Results to the RPT Model	59
4.5. Comparison of Dynamic Results with the Integrated System Model	62
4.6. Turbine Shutdown Sequence Simulation	65
5. Potential to Provide Energy Balancing and Frequency Support	69
5.1. The Prospective Storage Site	70
5.2. Performance and Sensitivity Analysis during Energy Balancing	71
5.3. Potential to provide Frequency Regulation Services	75
6. Conclusions and Recommendations	81
6.1. Conclusions	81
6.2. Perspectives and Recommendations for Future Work	86
A. Appendix	89
A.1. Control Maps used in the Numerical Model	89
B. Appendix	91
B.1. Steady-State Experimental Results for the RPT Efficiency and Power	91
Acknowledgements	109
Curriculum Vitae	111
List of Publications	113

SUMMARY

As the energy transition gains momentum globally, energy storage systems are becoming increasingly critical to balance intermittent energy sources such as solar and wind. Traditional pumped hydro storage has historically played a dominant role in energy storage due to its cost effectiveness, efficiency, and long lifecycle. However, its reliance on high-head applications limits its deployment to regions with specific topographical features. With an increasing demand for the provision of energy balancing and ancillary services, novel approaches are being developed to adapt pumped storage technologies for applications in regions where high-head installations are not feasible, including areas with limited elevation change or coastal regions. This study sets out to explore the potential of one such novel approach, low-head pumped hydro storage.

This work employs both experimental and numerical methodologies to evaluate the technical capabilities of low-head pumped hydro storage to provide energy balancing and frequency regulation services. Initially, a review is carried out, assessing different technologies including pump-turbine designs, electric machines, control and grid integration approaches for their applicability to low-head applications. Aside from this review, the majority of the work is centred around a new system concept developed by the ALPHEUS research project. The project proposes the use of contra-rotating reversible pump-turbines with adjustable speeds. These units are designed to handle the unique demands of low-head applications by using two independently controlled runners to achieve high efficiencies across a broad operating range. The integration of axial-flux permanent magnet synchronous machines allows for high torques at low speeds, making them well-suited for the large volumes of water required in low-head systems. By combining these novel pump-turbines and electric machines with state-of-the-art control systems, the major goals of the project are improved roundtrip efficiencies as well as fast power ramp rates and mode switching times.

To evaluate the technical potential of this technology and low-head pumped hydro storage as a whole, a medium-fidelity numerical system model has been developed. It integrates and couples a pump-turbine model with the dynamics of the hydraulic, mechanical, electrical and control subsystems. This model introduces a novel approach by incorporating the interaction between the two independent runners and their coupling with the other system components. A defining feature of this model is its flexibility and computational efficiency, enabling accurate simulations of various operational scenarios and dynamic responses without the high resource demands of high-fidelity computational fluid dynamics simulations. The individual model components are specifically tailored to the unique challenges of low-head applications, such as the increased inertia of the water column, which increases the risk of significant pressure transients. By incorporating the two coupled independent runners, as well as tailoring the approach to the demands of low-head systems, this model fills a critical gap in literature, providing a

robust tool for advancing the development of low-head pumped hydro storage.

To ensure the accuracy of the numerical model results, experiments are conducted with a 50 kW laboratory setup, featuring a 1:22 scale version of the reversible pump-turbine. The experimental campaign serves to evaluate the performance of the newly designed pump-turbine, explore the effects of utilising two independent runners and, crucially, benchmark the model. The setup is noteworthy for its gravity-fed design, aiding to create realistic in- and outflow conditions, reducing the risk of swirl and pressure pulsations occurring. These are typically induced by pumps used to create the required head for testing. Both steady-state and dynamic tests are performed in turbine and pump modes and compared to their corresponding numerical results. The benchmarking tests show that a medium-fidelity numerical model can effectively integrate the performance of two independent runners with the hydraulic and mechanical subsystems, capturing with sufficient accuracy the steady-state and dynamic behaviour as well as the interaction of the different subsystems of low-head pumped hydro storage.

Finally, the model is applied to a hypothetical grid-scale plant in the North Sea, providing, for the first time, detailed insights into the potential performance and operational capabilities of an integrated low-head pumped hydro storage plant. The results showed that the system could achieve a roundtrip efficiency of 73% during energy balancing as well as rapid power ramp rates suitable for providing frequency containment reserves. Sensitivity analyses further highlighted the potential for optimising the reservoir footprint and power input/output by scaling the electric machines.

Future work should focus on optimising energy management strategies, further refining control systems as well as detailed economic and environmental assessments. All of which can be aided by the developed numerical modelling approach. If a large-scale demonstration confirms its viability, low-head pumped hydro storage could play a transformative role in stabilising renewable energy dominated grids. This innovative approach may thus become a crucial component in advancing the global energy transition.

SAMENVATTING

Naarmate de energietransitie wereldwijd aan kracht wint, worden energieopslagsystemen steeds belangrijker om intermitterende energiebronnen zoals zon en wind in balans te brengen. Traditionele pompaccumulatiecentrales hebben historisch gezien een dominante rol gespeeld in energieopslag vanwege hun kosteneffectiviteit, efficiëntie en lange levensduur. Echter, de afhankelijkheid van hoogwateropstellingen beperkt de inzet ervan tot regio's met specifieke topografische kenmerken. Met een groeiende vraag naar energiebalancerend en ondersteunende diensten worden nieuwe benaderingen ontwikkeld om pompaccumulatietechnologieën aan te passen voor gebruik in gebieden waar hoogwaterinstallaties niet haalbaar zijn, zoals regio's met beperkte hoogteverschillen of kustgebieden. Deze studie onderzoekt de mogelijkheden van een van deze nieuwe benaderingen: laagwater-pompaccumulatie.

Dit onderzoek maakt gebruik van zowel experimentele als numerieke methoden om de technische mogelijkheden van laagwater-pompaccumulatie te evalueren voor energiebalancerend en frequentieregeling. Allereerst wordt een overzicht gegeven van verschillende technologieën, waaronder pomp-turbineontwerpen, elektrische machines, besturingssystemen en netintegratiebenaderingen, en hun toepasbaarheid voor laagwateropstellingen. Naast deze literatuurstudie richt het grootste deel van het onderzoek zich op een nieuw systeemconcept ontwikkeld door het ALPHEUS-onderzoeksproject. Dit project stelt het gebruik van contra-roterende omkeerbare pomp-turbines met verstelbare snelheden voor. Deze eenheden zijn ontworpen om te voldoen aan de unieke eisen van laagwateropstellingen door twee onafhankelijk aangestuurde rotors te gebruiken, waarmee hoge efficiënties over een breed werkbereik worden bereikt. De integratie van axiaalflux-synchroonmachines met permanente magneten maakt het mogelijk om bij lage snelheden hoge koppels te leveren, waardoor ze goed geschikt zijn voor de grote waterstromen die nodig zijn in laagwatersystemen. Door deze innovatieve pomp-turbines en elektrische machines te combineren met geavanceerde besturingssystemen streeft het project naar verbeterde rendementen over de hele cyclus, evenals snelle vermogensveranderingen en korte schakeltijden tussen modi.

Om het technische potentieel van deze technologie en laagwater-pompaccumulatie in het algemeen te evalueren, is een numeriek systeemmodel met middelhoge resolutie ontwikkeld. Dit model integreert en koppelt een pomp-turbinemodel met de dynamiek van hydraulische, mechanische, elektrische en besturingsonderdelen. Het model introduceert een innovatieve aanpak door de interactie tussen de twee onafhankelijke rotors en hun koppeling met andere systeemcomponenten op te nemen. Een onderscheidend kenmerk van dit model is de flexibiliteit en rekenefficiëntie, waarmee nauwkeurige simulaties van verschillende operationele scenario's en dynamische reacties mogelijk zijn zonder de hoge rekenkrachtvereisten van geavanceerde stromingssimulaties. De afzonderlijke modelcomponenten zijn specifiek afgestemd op de uitdagingen van laagwater-

opstellingen, zoals de grotere traagheid van de waterkolom, die het risico op aanzienlijke drukschommelingen vergroot. Door de twee gekoppelde onafhankelijke rotors op te nemen en het model specifiek af te stemmen op de eisen van laagwatersystemen, vult dit model een kritieke leemte in de literatuur en biedt het een robuust hulpmiddel om de ontwikkeling van laagwater-pompaccumulatie te bevorderen.

Om de nauwkeurigheid van de numerieke modelresultaten te waarborgen, worden experimenten uitgevoerd met een 50 kW-laboratoriumopstelling, voorzien van een schaalmodel van de omkeerbare pomp-turbine (schaal 1:22). De experimentele campagne dient om de prestaties van de nieuw ontworpen pomp-turbine te evalueren, de effecten van het gebruik van twee onafhankelijke rotors te onderzoeken en, cruciaal, het model te valideren. De opstelling valt op door het gebruik van zwaartekrachtgevoede stroming, wat helpt om realistische in- en uitstroomcondities te creëren en het risico op wervelingen en drukpulsaties te verminderen, die typisch worden veroorzaakt door pompen die de benodigde hoogte genereren voor tests. Zowel stationaire als dynamische tests worden uitgevoerd in turbine- en pompmodi en vergeleken met de corresponderende numerieke resultaten. De validatietests tonen aan dat een middelhoge-resolutie numeriek model effectief de prestaties van twee onafhankelijke rotors kan integreren met de hydraulische en mechanische subsystemen, waarbij het met voldoende nauwkeurigheid het stationaire en dynamische gedrag evenals de interactie tussen de verschillende subsystemen van laagwater-pompaccumulatie vastlegt.

Ten slotte wordt het model toegepast op een hypothetische installatie op netwerkschaal in de Noordzee, waarmee voor het eerst gedetailleerd inzicht wordt verkregen in de potentiële prestaties en operationele mogelijkheden van een geïntegreerde laagwater-pompaccumulatiecentrale. De resultaten tonen aan dat het systeem een rondrendement van 73% kan bereiken tijdens energiebalanceren en snelle vermogensveranderingen kan leveren die geschikt zijn voor frequentiebeheersingsreserves. Gevoeligheidsanalyses benadrukken verder de mogelijkheden om het reservoiroppervlak en de energie-input/output te optimaliseren door schaalvergroting van de elektrische machines.

Toekomstig onderzoek zou zich moeten richten op het optimaliseren van energiebeheersstrategieën, het verder verfijnen van besturingssystemen en het uitvoeren van gedetailleerde economische en milieubeoordelingen. Al deze aspecten kunnen worden ondersteund door de ontwikkelde numerieke modelleringsaanpak. Indien een groot-schalige demonstratie de haalbaarheid bevestigt, kan laagwater-pompaccumulatie een transformatieve rol spelen bij het stabiliseren van elektriciteitsnetten die worden gedomineerd door hernieuwbare energie. Deze innovatieve benadering kan daarmee een cruciale component worden in het versnellen van de wereldwijde energietransitie.

LIST OF ABBREVIATIONS

AC	Alternating Current
AF-PMSM	Axial-Flux Permanent Magnet Synchronous Machine
aFRR	Automatic Frequency Restoration Reserves
AS	Ancillary Services
CAES	Compressed Air Energy Storage
CFD	Computational Fluid Dynamics
CR-RPT	Counter-Rotating Reversible Pump-Turbine
DC	Direct Current
DQ	Direct-Quadrature
DSO	Distribution System Operator
DTC	Direct Torque Control
ESS	Energy Storage System
FCR	Frequency Containment Reserves
FOC	Field-Oriented Control
IRES	Intermittent Renewable Energy Sources
LCOE	Levelised Cost of Energy
LCOS	Levelised Cost of Storage
LH-PHS	Low-Head Pumped Hydro Storage
MMD	Modular Machine Drive
MPP	Maximum Power Point
MPPT	Maximum Power Point Tracking
MPC	Model Predictive Control
ODE	Ordinary Differential Equation
PI	Proportional-Integral
PHS	Pumped Hydro Storage
PLL	Phase-Locked Loop
PM	Permanent Magnet
PMSM	Permanent Magnet Synchronous Machine
PTO	Power Take-Off
PWM	Pulse-Width Modulation
ROCOF	Rate of Change of Frequency
RPT	Reversible Pump-Turbine
SSDR	Single-Stator Double-Rotor
SSSR	Single-Stator Single-Rotor
TRL	Technology Readiness Level
TSO	Transmission System Operator

1

INTRODUCTION

1.1. BACKGROUND AND MOTIVATION

1.1.1. THE ROLE OF ENERGY STORAGE AND ANCILLARY SERVICES IN THE ENERGY TRANSITION

THE integration of renewable energies into our power grids has gained significant momentum in recent years, driven by the urgent need to mitigate climate change and reduce greenhouse gas emissions. As a result of this global effort, renewables are now the second largest contributor to the world-wide electricity mix, claiming a total share of 30% in 2023 [1]. Although hydropower takes the largest share within that mix of renewables, solar photovoltaics and wind generation experience steep average annual growth rates of 36.5% and 23%, respectively, since 1990 [2]. Both of these technologies, however, significantly differ in their electricity generation characteristics when compared to traditional fossil-fuel and nuclear power plants. Rapidly increasing shares of such renewable power systems pose significant challenges to grid stability and reliability [3].

The first major challenge is their intermittency and variability. Conventional fossil-fuel power plants are able to control the power they generate by adjusting the amount of fuel that is burned. On the contrary, the power generated by intermittent renewable energy sources (IRES) depends on the apparent availability of the used natural resource, such as solar irradiance or wind speed. Consequently, the amount of power they supply varies over time. Cloud coverage, shading as well as the time of day and year all affect how much power solar plants are able to generate. Similarly, wind speed changes caused by localised gusts, weather systems and seasonal trends determine the possible power wind turbines can generate. These variations, manifesting over timescales from seconds all the way up to seasonal

Parts of this chapter have been published in J.P.Hoffstaedt et al. Low-head pumped hydro storage: A review of applicable technologies for design, grid integration, control and modelling. Renewable and Sustainable Energy Reviews. 2022. & J.P.Hoffstaedt et al. Low-head pumped hydro storage: An evaluation of Energy Balancing and Frequency Support. IET Renewable Power Generation. 2024.

differences, create a mismatch with the also fluctuating power demand.

The second challenge is the reduction of grid inertia. Conventional power plants operate their electrical generators at a fixed speed that is synchronous to the grid frequency. A large majority of these generators also have a large rotating mass and therefore store kinetic energy. In the case of generation or load fluctuations leading to sudden grid frequency deviations, the rotors combined inertia alleviates the deviation by providing additional power from the stored kinetic energy [4]. Traditional power grids relied on such synchronous generation to stabilise the grid. On the contrary, not all IRES have a large rotating mass and most are integrated into the grid via inverters, subsequently decoupling the rotating mass from the grid frequency. Increased fluctuations in grid frequency can have detrimental effects on the performance of sensitive electrical equipment and even lead to power outages [5].

To address the variability, and therefore the mismatch between the power supply of IRES and demand, large-scale short- and long-term energy storage solutions are required to store surplus energy during periods of high production and release it back to the grid during periods of high demand. In this context, short-term storage refers to energy storage durations ranging from sub-second timescales up to a full day, while long-term storage encompasses periods from several days, weeks, months or years. To tackle the second challenge, energy storage systems should be able to provide so-called ancillary services (AS). These are support services aimed at maintaining grid stability and reliability including frequency regulation, voltage support or power reserves [6].

While a direct correlation between renewable energy penetration levels and storage demand can be assumed, mitigating factors such as improved generation forecasting or the increased capability of renewable energy technologies able to provide ancillary services, will allow for later deployment of energy storage. Further factors to consider include the flexibility of remaining generators in the grids and the emerging need for additional operating reserves, improved demand management, as well as further grid expansion and interconnection.

Considering these factors, it becomes evident that energy storage demand will depend significantly on the specific characteristics of each power grid, leading to regional variations. Considering Germany as an example, additional short-term storage can be expected at renewable shares between 40% and 60% of the electricity supply and long-term storage between 60% and 80%. Above 80% and towards a fully renewable generation, bulk energy storage, short- and long-term, is not only required in order to avoid extensive renewable energy curtailment, ensure grid stability and power quality, but will be a cost-effective solution in the GW range [7]. In less flexible grids, for example utilising large-scale nuclear power to cover the base load, the need for extensive storage will be reached at much lower renewable penetration levels.

A wide variety of energy storage technologies, including capacitors, flywheels, electro-chemical batteries, compressed air energy storage (CAES), pumped hydro storage (PHS), molten-salt or hydrogen storage, are available to balance the grid across several timescales. Crucial factors for large-scale balancing include energy

and power capacity as well as fast response times while maintaining high roundtrip efficiencies. This roundtrip efficiency is the ratio between the energy retrieved from a storage system and the energy put in, accounting for all conversion losses. Aside from fulfilling these criteria, the major driver towards commercial deployment is the levelised cost of storage (LCOS); leading in this are PHS and CAES [8]. An alternative approach is based on the so-called energy stored on energy invested (ESOEI), which gives an estimate of the relation between the stored energy during the lifetime of a system and the energy required to construct the system. Also for this metric, PHS and CAES are, by far, in the lead [9].

1.1.2. OVERVIEW, HISTORICAL DEVELOPMENT AND LIMITATIONS OF PUMPED HYDRO STORAGE

PUMPED hydro storage is an amended concept to conventional hydropower as it cannot only generate, but also store energy. This is achieved by converting electrical to potential energy and vice versa in the form of pumping and releasing water between a lower and a higher reservoir. The energy conversion occurs by using pumps and turbines either combined in a reversible or separate configuration. A typical layout of a closed-loop pumped storage plant is given in Figure 1.1.

The hydraulic power of such a system is proportional to the product of the height difference (gross head) between the reservoirs and the total flow rate across the pumps or turbines. The amount of potential energy that can be stored is similarly proportional to the head and the reservoir volume. Hence, a higher head requires a reduced flow rate for a given desired power and smaller reservoirs for a given storage capacity. It does not, therefore, just correlate with scaled-down reservoirs but also smaller remaining civil structures and machinery, historically leading to reduced cost and a significant economic advantage of utilising high-head differences [11].

Of today's bulk energy storage integrated into the world-wide grids, over 90% is comprised of PHS of which the vast majority are high-head applications. According to the International Hydropower Association, in 2019, the global installed capacity reached 158 GW with the biggest contributors being China making up 30.3 GW of the share, Japan 27.6 GW, and the United States 22.9 GW [12]. Figure 1.2 shows the distribution of global storage capacity that is operational, under construction, planned, and announced as of 2021.

In comparison, the next largest contributors to bulk energy storage are electro-chemical battery storage – rapidly growing with a total capacity of 14.2 GW – and thermal storage with 2.9 GW in 2020 [14]. To explain the historic market dominance of PHS and understand recent trends, several factors have to be taken into account. Pumped hydro storage utilising reversible pump-turbines has been available as a mature and cost-effective solution for the better part of a century with an estimated energy based capital cost of 5–100 \$/kWh [15]. Today, compressed air energy storage is considered mature and reliable, offering similarly low capital cost between 2–50 \$/kWh. Electro-chemical batteries offer high energy density with higher costs and experience drastic growth while the impact of hydrogen-based storage in the energy transition is largely expected to be substantial [15].

However, PHS's dominance is not only due to its historic lead but can also be

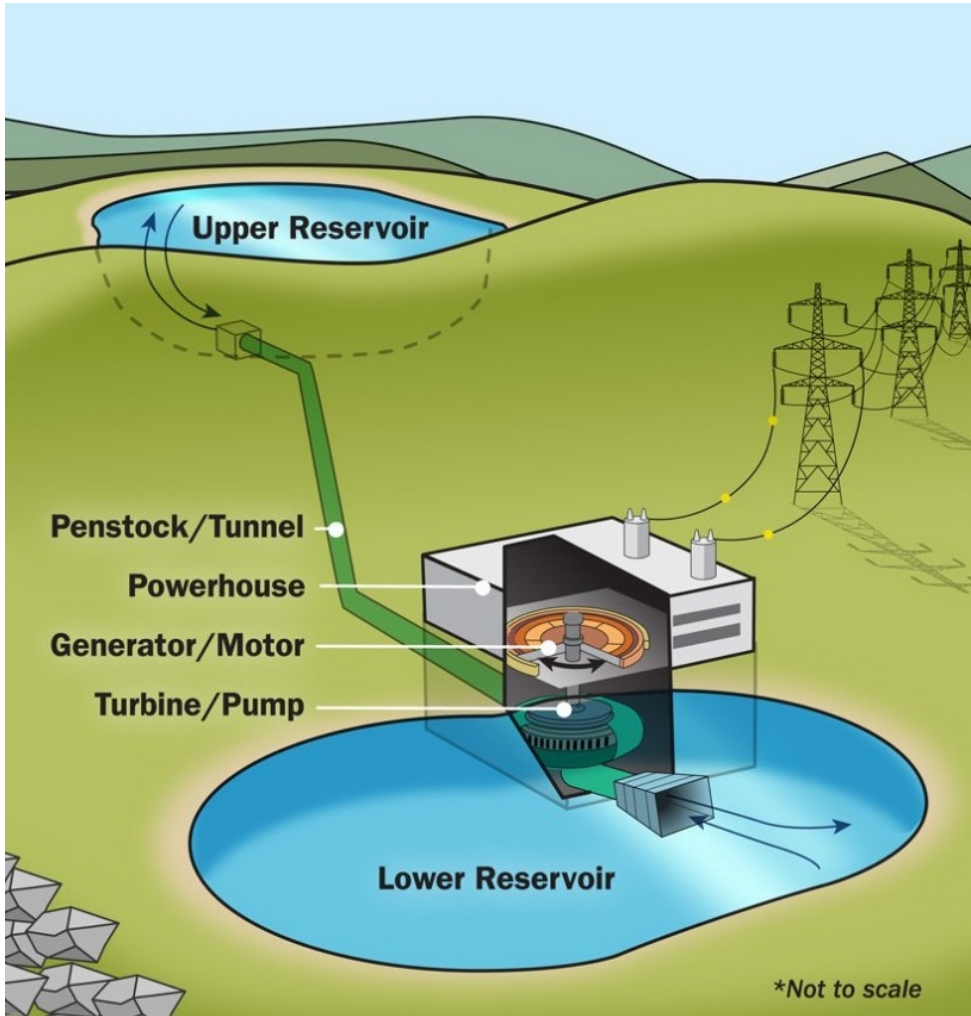


Figure 1.1.: Illustration of a closed-loop pumped hydro storage plant. [10]

attributed to its technical, economic, and sustainability advantages. These include high efficiencies, large achievable capacities, and long lifetimes. Compared to rapidly expanding battery storage that can be used wherever it is most needed, one clear advantage is this durability. It is currently assumed that a battery system will last around 15–20 years, but on the other hand, the oldest hydropower plant in Norway has been operating for over 120 years [16, 17]. Prolonged lifetimes are one factor improving the sustainability of PHS compared to other storage solutions. Others include maturity, low capital and operating cost, as well as low energy and carbon dioxide density. Based on these and other factors regarding economic, performance, technological, and environmental considerations, Ren et al. ranked PHS as the most

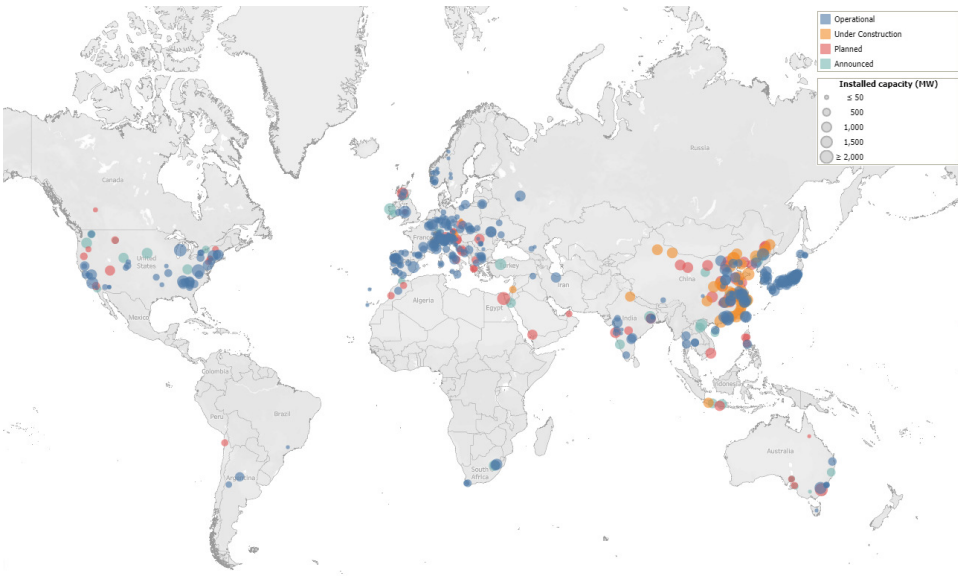


Figure 1.2.: Global PHS Capacity. [13]

sustainable storage technology [18].

Further advantages of PHS include suitability for long-term storage, since hardly any storage losses occur other than seepage and evaporation, and quick availability due to short switch-on and switch-off times. With these factors ensuring a significant share within a heterogeneous pool of storage technologies, one major disadvantage of PHS has historically been its topographic constraints. A switch from river-based to closed-loop off-river systems could overcome some of the constraints and increase the potential for deployment [19, 20]. Nonetheless, regions with flat topographies still do not offer viable sites.

EARLY DEPLOYMENT AND PROGRESSION IN THE 20th CENTURY

Not long after hydropower began to generate electricity, the first small-scale PHS plants were constructed in the mountainous regions of central Europe in the beginning of the 20th century. Initially using separate pumps and turbines, combined reversible pump-turbines have become the norm since the middle of the 20th century [21]. Experiencing a major boom in Europe, parts of Asia, and North America, a large portion of today's installed PHS capacity was constructed in the 1960s, 1970s, and 1980s; in most countries, this occurred alongside rapidly increasing nuclear power. The gained flexibility that PHS plants provided allowed them to match a varying demand with the baseload generation of nuclear power plants. An example where this was particularly relevant is Japan due to its lack of interconnections to other countries as well as their strong strategy towards nuclear energy.

In the United States, another reason for the growing capacity of PHS during that

period was the energy crisis in the 1970s, leading to an increased cost of fossil fuels allowing PHS to grow as a substitute for peak balancing [22]. After that period, development slowed down in most regions with the major exception of China. Its rapidly growing economy and correlated energy demand largely satisfied by non-flexible coal plants required major energy storage.

Up until this point, pump-turbines were coupled to fixed speed motor-generators. The next significant development occurred in the 1990s when variable speed operation was introduced in Japan. The ability to adjust the rotational speed of the runners allowed for higher efficiencies under changing conditions, reduced the switching time between pump and turbine mode, and facilitated higher ramp rates and quicker response times [23].

Later trends for PHS show the usage of ternary units. With ternary units, a separate pump and turbine are connected on a single shaft to an electric machine that can work either as a motor or a generator [24]. This configuration presents a very flexible and fast response range, shows higher efficiencies than reversible machines, and can utilise hydraulic short circuits for optimal power in- or outtake [25, 26]. The major drawback with ternary units is that they require higher investment and maintenance costs compared to a reversible unit [26].

CURRENT TRENDS

After an initial reduction of PHS deployment around the turn of the millennium, the rapidly growing share of intermittent renewable energy sources (IRES) in the last couple of decades sparked new interest in sustainable flexible generation as well as large-scale energy storage solutions. This caused increasing attention towards the rehabilitation of old hydropower plants and an expansion of PHS [27]. While PHS experienced a much longer development process than competitive technologies and could hence be considered mature, two major trends can be identified pushing further innovation in the field.

The first one is derived from the change in grid characteristics caused by the reduction in spinning reserves. The growing number of converter coupled renewables raise the necessity for an external provision of AS. To provide these using PHS, research efforts focus on developing improved control and machinery but also novel concepts, such as hybrid storage solutions. Examples of such concepts could be the coupling of conventional PHS with flywheels for frequency control or supercapacitors providing virtual inertia [28]. Hybrid storage solutions incorporating PHS, such as hybrid pumped and battery storage, are also particularly suited for off-grid applications [29].

The second major trend is expanding the operating range and application. One of the most limiting factors in the potential use of large-scale PHS has been the fact that not many locations could offer economically viable deployment. These were traditionally mountainous regions accessing water with enough space to construct extensive civil structures. There is a large potential in Europe to deploy further mini (100 kW – 1 MW) and small (1 MW – 10 MW) hydropower plants to counteract the effects of higher renewable penetration levels [30]. However, this does not apply to countries with flat topographies, such as Denmark, the Netherlands, or Belgium.

Additionally, to achieve the balancing capabilities of pumped storage systems, larger plants typically provide better economies of scale. Suitable locations for such larger plants are rare in Europe and some countries like Japan are considered to have used nearly all available sites [31]. This limited availability of appropriate locations drives the development of new approaches. Examples for a promising change of approach are underwater PHS, gravity energy storage and shifting the operating range of PHS to low-head applications.

Underwater PHS is a novel technology under development based on submerging a rigid tank in the ocean and using the static pressure difference for energy storage [32, 33]. The surrounding sea acts as the upper reservoir and the sphere as the lower which can be filled to generate electricity or emptied to store it. Initial model-scale tests have been successful; it is a freely scalable technology without issues regarding land use and considered cost competitive with PHS and compressed air storage [34]. Using seawater in general for PHS is so far an uncommon practice, but has been investigated as a solution for isolated grids [35]. If technical, environmental, and economic challenges are overcome, utilising seawater could be another promising expansion of PHS's potential deployment.

Gravity energy storage similarly reduces the reliance of PHS on the topographic restrictions. Storage is done via gravitational potential energy. In one of the concepts, energy is stored or extracted respectively by moving a piston of large mass up and down using water powered by a pump-turbine for conversion. While still under development, initial economic evaluations show it to have a potentially attractive LCOE similar to PHS or CAES [36]. An alternative approach proposes the use of subsea weights and buoyant floaters connected to a submerged platform. Here, energy is stored by lifting the weights and retrieving the floaters. Advantages include a relatively simple mechanism, scalability and expected roundtrip efficiencies of 80% [37].

Finally, a promising alternative suiting both trends is to extend the operating range of conventional PHS to low and ultra low-head applications, while improving its capability to provide AS. Shifting the operating range of pumped storage technology to low-head and seawater applications would unlock the potential to utilise the benefits of conventional PHS in regions so far not feasible. These benefits include large and scalable energy and power capacities, flexible operation and high performance. Additionally, by deploying pumped storage plants in coastal environments or shallow seas, these plants can be strategically placed in the proximity of offshore renewable generators such as wind farms or integrated with energy islands. Shorter distances between large-scale renewable generators and storage plants reduce transmission losses but also allow for the shared use of civil structures reducing the high required upfront cost [38].

1.1.3. THE CHALLENGES OF LOW-HEAD PUMPED HYDRO STORAGE

Low-head PHS, typically defined based on a head range of 2 – 30 m [39], has not yet seen deployment on a significant scale within our grids. This is largely due to two factors. The first is the increased upfront cost combined with long investment cycles. The second factor is a lack of proven and appropriate technologies for low-

and ultra-low head applications.

While highly dependent on the individual project and site, the major contributor to the initial capital expenditure of PHS projects, with up to 70%, are civil structures, including the reservoir, conduit, and lining [40, 41]. Due to larger volumes of water being stored in the reservoir and flowing through the conduit when it comes to low-head applications, their contribution to the overall economic viability can only be assumed to be significant. The LCOS of new high-head PHS systems ranges from 50 €/MWh to 80 €/MWh [42]. Initially, low-head plants may not be able to compete with this. However, changing demand characteristics of the electricity markets, as well as further development and improvement of technological aspects, can significantly influence economic viability and thereby the potential of large-scale deployment [43, 44]. The increase in renewables in world-wide grids will lead to rising demands, not just for short- and long-term balancing but also the provision of AS, increasing the value of both. Additional revenue from the provision of AS could hence increase economic viability. A further driver making PHS economically more attractive are growing interconnections to other grids opening up additional markets [31].

As aforementioned, technological advances do not just improve the capability of low-head PHS to contribute to grid stability but with that also drive its economic potential as a grid-scale solution. One of the primary objectives is an increased roundtrip efficiency over the full storage cycle. Aside from regulatory changes such as carbon taxation, electricity price margins have been identified as one of the major drivers toward PHS utilisation. Improved roundtrip efficiencies directly correlate with higher revenues for the operator and therefore result in increased deployment [45]. The overall efficiencies of pumped storage systems are mostly determined by the utilised pump-turbines. Compared to conventional high-head applications, low-head systems experience larger relative head changes. Consequently, to maintain a stable power in- or output, large variations in flow rates are also required. Designing hydraulic machinery capable of maintaining high efficiencies over such a large operating range is a key challenge.

To improve the capability of low-head pumped storage systems to provide AS such as frequency regulation, a highly flexible operation with fast power ramp rates is desired. Variable speed operation, unlocking the capability to adjust the rotational speed of the pump-turbine, as well as innovation in machine- and grid-side control can help reach faster power ramp rates. For a given power capacity, low-head system are characterised by larger flow rates though and, consequently, enlarged machinery. Larger mass flow rates and the associated increased inertia can lead to a higher risk of transient pressure effects, commonly known as water hammer. These effects occur when a steady flow of water is suddenly accelerated or decelerated. Significant effects can be caused by the opening or closing of valves, but also rapid changes in the rotational speed of the pump-turbine. On the contrary, the increased inertia of the hydraulic and electrical machinery may inhibit fast response times.

To address these challenges, novel technologies are required and their performance in energy balancing and the provision of ancillary services must be thoroughly evaluated. Given the limited deployment of low-head pumped storage systems

and the inherent difficulties of accurate on-site measurements [46], small-scale experimental testing and numerical simulations become crucial. However, scaling down experiments introduces its own set of challenges, particularly scaling effects. These effects arise from discrepancies in viscous forces, variations in geometry and test setup, and differences in surface roughness compared to full-scale power plants [47]. Despite these challenges, experimental testing remains a valuable tool for validating numerical models, which can then be applied to assess the performance of full-scale systems.

1.1.4. LOW-HEAD PUMPED HYDRO STORAGE UTILISING CONTRA-ROTATING REVERSIBLE PUMP-TURBINES

To tackle the aforementioned challenges and advance technologies for low-head pumped hydro storage, various pump-turbine concepts have been explored. Among these, the Archimedes screw, one of the oldest pump designs, has been adapted for turbine use, offering a broad range of applications [48]. Another approach involves bulb turbines, traditionally employed in low-head settings such as the La Rance Tidal Power Plant [49, 50]. Notably, a novel concept proposed by the ALPHEUS project stands out, designed specifically for the challenges of low-head applications and aimed for deployment in shallow seas and coastal environments [51].

The proposed system consists of several units of newly developed contra-rotating reversible pump-turbines, axial-flux permanent magnet synchronous machines (AF-PMSM) and a dedicated machine- and grid- side control. This novel approach of using two adjustable speed runners per RPT is chosen with the goal to achieve distinct advantages for low-head applications. The main objectives include increased efficiencies in pump and turbine mode due to a reduction of non-axial flow components as well as a wider operating range at these high efficiencies enabled by the additional control degree of freedom.

A schematic of the system can be found in Figure 1.3. Similar to conventional pumped storage plants, two reservoirs are needed. In the proposed application in shallow seas, the sea acts as the upper reservoir. A ring dike is deployed encapsulating a basin that serves as the lower reservoir. To store energy, the seawater is pumped out of the inner, lower reservoir to the sea using several sets of RPTs. Conversely, to recoup the stored energy, the reservoir is filled, using the same RPTs in turbine mode. To scale the energy capacity of the plant, the size of the inner reservoir is adjusted. Similarly, to scale the power capacity of the plant the number of RPT sets is varied. Each set of RPT and coupled axial-flux electric machines has an initial design power rating of 10 MW. The RPT has a diameter of 6 m and is designed for a head range of 2–20 m [51, 52].

The initial design of the pump-turbine has been described by Prasasti et al. [53] and computational fluid dynamics (CFD) simulations investigating its steady and unsteady performance was conducted by Fahlbeck et al. [52, 54, 55].

An initial economic analysis for peak load shifting operation of a potential low-head PHS plant based on German electricity prices in 2021 has shown that a maximum profit from energy arbitrage of 32.95 M€ per 100 MW of installed capacity can be achieved per year. Taking estimates for capital and operational expenditure

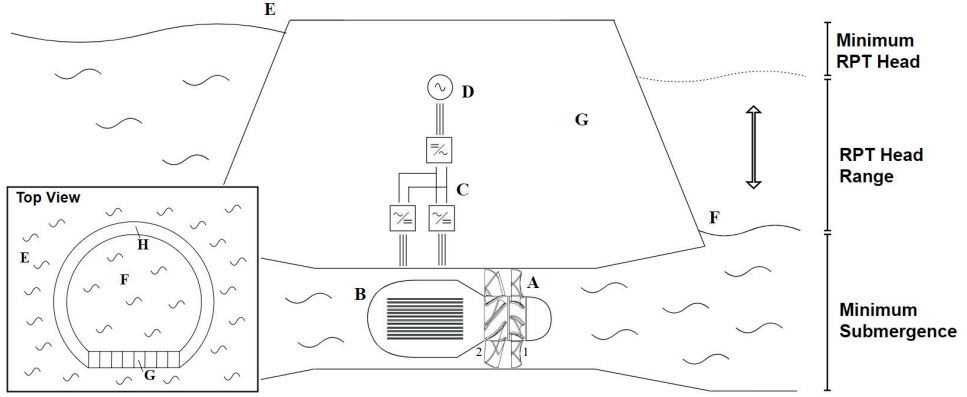


Figure 1.3.: Top view and cross-sectional schematic of the proposed low-head pumped storage system showing the contra-rotating runners **A**, axial-flux PMSMs **B**, AC-DC-AC coupling **C**, the electrical grid **D**, the sea as the upper reservoir **E**, the enclosed lower reservoir **F**, the powerhouses **G** and the ring dike **H**.

into account, a grid-scale system would be profitable with an interest rate of 5% assuming lifetimes of 75 to 100 years. Considering a 50 year lifespan the system would be profitable for an interest rate below 4.4% [56]. Additional revenue can be achieved by the operator through frequency regulation services.

1.2. RESEARCH SCOPE AND OBJECTIVES

As part of the development of the low-head pumped storage system introduced in section 1.1.4, novel technologies for the individual system components have been developed and numerical investigations into their performance, notably the contra-rotating RPT, have been carried out. However, the interaction of the components and the performance and dynamic behaviour of the integrated system, as well as low-head pumped storage systems in general, is not yet known. Aside from research related to the proposed system, existing literature on low-head pumped hydro storage is limited to conceptual work and numerical investigations focusing on potential pump-turbines, i.e. [57–59]. Overall there is a lack of evaluations of full-scale integrated low-head pumped storage systems as well as experimental testing of novel RPT technologies.

This study aims to assess the potential and technical viability of low-head pumped hydro storage as a future contributor to grid-scale energy storage, filling a current gap in literature and aiding to increase the technology readiness level (TRL) of the system proposed in section 1.1.4 from 2 to 4 (TRL 2 corresponds to the formulation of a technology concept and application, where basic principles are identified, while TRL 4 represents the validation of the technology in a laboratory environment, demonstrating its feasibility through experimental testing). To achieves

this, an experimentally verified numerical modelling approach, capable of accurately evaluating the steady-state performance and dynamic behaviour of low-head pumped storage systems, is required. Based on this motivation, the following research questions are guiding this work:

- What technologies are applicable to low-head pumped hydro storage?
- How can a novel reversible pump-turbine with two contra-rotating runners be integrated with hydraulic, mechanical, and control dynamics into a mid-fidelity numerical model?
- How can the developed integrated numerical model be experimentally benchmarked, and what insights can be gained from comparing the numerical predictions with experimental results?
- What are the potential performance outcomes and operational capabilities of low-head pumped hydro storage in supporting grid stability, particularly for energy balancing and frequency regulation services?

In order to assess existing technologies and technological advances that are applicable to low-head PHS, this study includes a review focusing on pump-turbine design, electric machines, control systems, and grid integration. After this review, the majority of the work is based on the low-head pumped storage system introduced in section 1.1.4.

To investigate the interaction of the individual components as well as the resulting steady-state performance and dynamic behaviour of the whole system, a medium fidelity time-domain system model is developed and implemented. The model integrates a steady-state pump-turbine model, which is based on a range of existing CFD simulations, with the pertinent dynamics of the system including the hydraulic, mechanical, electrical and control components. The modelled RPT and its unique approach of utilising two independent runners, poses a novel challenge of modelling their interaction and coupling to the other system components. For the conduits hydraulic model, a 1-D approach considering the compressibility of water is chosen to cover potential transient effects caused by the increased inertia of the water column. This approach has a lower fidelity compared to CFD simulations and therefore also requires significantly reduced computational resources. However, it also allows the coupling to other system dynamics and control. With this flexibility and computational efficiency, a wide range of operating conditions and scenarios can be simulated. This approach, integrating two independent RPT runners with the hydraulic, mechanical and control dynamics, tailored to the specific characteristics of low-head systems, fills a current gap in literature.

While this approach promises to offer a versatile tool to assess low-head pumped storage technology, the integrated model as well as the characterisation of the RPT, based on CFD simulations, require experimental validation. Experimental data provides a benchmark to verify and refine the numerical model, ensuring accuracy and its predictive capability. For this purpose, a 1:22 scale model of the RPT is constructed within an experimental setup at the TU Braunschweig in Germany.

Notably, the setup consists of two open-surface tanks, solely relying on gravity to provide the required head. By avoiding the need for ancillary pumps, typically used in experimental setups to provide head, the goal is to provide more realistic in- and outflow conditions by reducing the risk of non-axial flow components and pressure pulsations. With that experimental setup, both steady-state and dynamic tests are performed. The obtained experimental results are used to evaluate the performance of the newly designed and untested RPT and crucially compare them to the steady-state and dynamic modelling approaches.

Finally, to investigate and evaluate the potential of a full-scale low-head PHS plant, the integrated system model is then applied to such a grid-scale plant to investigate the performance over a full storage cycle while analysing the influence of the system components on key performance indicators. Furthermore, the dynamic behaviour of the plant is simulated to evaluate its capability to provide ancillary services, in particular frequency regulation. The results of these simulations give new insights into the technical capabilities of low-head pumped storage to contribute to grid-stability and thereby facilitate the ongoing energy transition.

1.3. DISSERTATION OUTLINE

The dissertation is structured as follows, depicted in Figure 1.4. In section 2, a review of technologies is conducted to assess their applicability to low-head pumped storage systems. This includes an analysis and comparison of pump-turbine designs, electric machines, control strategies and grid integration. This review provides the contextual background for this study and the motivation behind the novel system introduced in section 1.1.4, tackling the first research question.

Following, section 3 delves into the chosen numerical modelling approach and its rationale. The steady-state model of the RPT, the dynamic modelling approaches for the hydraulic, mechanical, electrical and control components as well as their integration and coupling are detailed answering the second research question. Additionally the relevance of the chosen modelling approach to low-head applications is discussed.

With the numerical approach aimed at investigating the performance of low-head systems outlined, section 4 focuses on the experimental approach and the benchmarking of the numerical model. This chapter provides a detailed overview of the experimental setup, instrumentation, and procedures, followed by the presentation and analysis of experimental results. A critical comparison between these results and the numerical model's predictions is conducted to evaluate the model's accuracy and reliability, addressing the third research question.

The model is then applied to a potential grid-scale plant in section 5. A case study is performed to evaluate the systems performance over a full-storage cycle and a sensitivity analysis conducted on the effect of a key system component on performance and plant footprint. Further, dynamic simulations are carried out to assess the plants potential to provide frequency regulation services. This section aims to answer the last research question by evaluating the potential performance of the novel low-head pumped storage system.

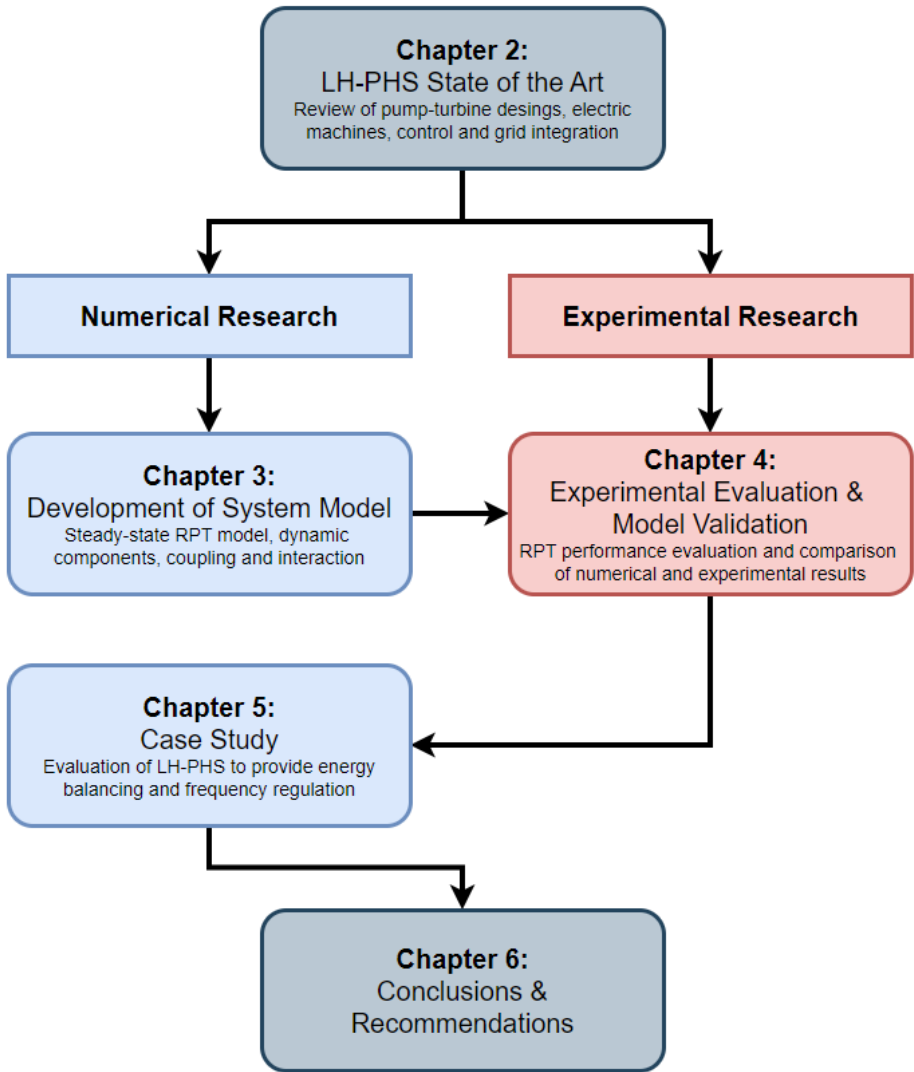


Figure 1.4.: Dissertation Outline.

2

LOW-HEAD PUMPED HYDRO STORAGE: STATE OF THE ART

Existing literature on low-head pumped hydro storage is limited. Additionally, no implementation of integrated systems has taken place. This chapter therefore delves into the state of the art of low-head pumped hydro storage, giving the contextual background to this work. It aims at giving a multi-disciplinary insight on technologies that are applicable for low-head applications, in terms of pump-turbine design, electric machines, control and grid integration. Civil structure designs are not within the scope of this review but have been, together with environmental and legal aspects, discussed by Ansorena-Ruiz et al. [60].

2.1. PUMP-TURBINE DESIGN

THE choices when selecting the type of reversible pump-turbine unit, or evaluating using a pump as turbine (PAT), are governed by a number of factors. The first thing to evaluate is the power of the hydropower plant, which is a function of head and flow rate and the general formula is given by Eq. (2.1).

$$P = \rho g H Q \eta \quad (2.1)$$

Here, ρ is the density of water, g is the gravitational acceleration, H is the head, Q is the volumetric flow rate, and η is the overall efficiency of the power plant. The gravity acceleration and water density can be regarded as constant. The equation shows that if the head is low, the flow rate must be large in order to produce high power [61]. With a large flow rate, the diameter of pipelines and the runner need to be large as well to limit the flow velocity, and thus hydraulic losses in the system. High-head conditions are usually preferable to build pump storage hydropower plants. However, low-head solutions with high volumetric flow rate are also regarded

Parts of this chapter have been published in J. P. Hoffstaedt et al. Low-head pumped hydro storage: A review of applicable technologies for design, grid integration, control and modelling. Renewable and Sustainable Energy Reviews. 2022.

as having great potential to unleash new opportunities for pumped hydro storage [50].

The definition of low-head is not unanimous among different countries and researchers. For example, the U.S. Energy Information Administration (EIA) considers low-head when the head is less than 30 meter and Okot [62] classifies it as when $5 < H < 15$ meter. In this work, the European Small Hydropower Association (ESHA) classification defines low-head, and states that low-head hydropower plants have a head of 2-30 meter [39].

The overall efficiency of a low-head power plant is more sensitive to head losses than a high-head alternative, and low-head PHS requires that the pipelines are short to be economically feasible [63]. This is because head losses are proportional to the pipeline length and the flow velocity squared, which is a further incentive for not using ternary units in a low-head case since they require more pipelines and would thus decrease the plant's overall efficiency. With the higher flow rate of high-power low-head PHS, larger reservoirs are required to store the same amount of energy as a corresponding high-head application [61]. This is because the energy storage capacity is a function of the water mass and head. Apart from that, other conditions such as the type of machine (radial-, mixed-, or axial-flow), operation (variable or fixed speed), and reservoir configuration may apply when choosing the best reversible pump-turbine configuration [64]. Chapallaz et al. [65] stated that, in practice, almost any hydro pump can also be used as a turbine. The reverse is, however, not the case. As an example, impulse turbines (Pelton or Turgo) cannot be used as pumps.

The design and characteristics of any hydro pump and turbine are determined by its conditions of operation. In turbomachinery, the specific speed is one key parameter to select the most appropriate reversible pump-turbine or using a pump as turbine (PAT). In this paper, it is defined in accordance with Dixon and Hall [66] as Eq. (2.2), and Table 2.1 shows ranges of specific speeds for various machines.

$$\Omega_s = \frac{\Omega Q^{1/2}}{(gH)^{3/4}} \quad (2.2)$$

Here, Ω_s is the specific speed and Ω is the runner rotational speed. Stepanoff [67] explained in 1948 that a higher specific speed results in a smaller, and thus cheaper, machine. With a higher flow rate, the blade design differs significantly, as illustrated in Figure 2.1. On the other hand, machines with low rotational speeds and small shear forces (e.g. Archimedes screw and positive displacement machines) are more fish-friendly [68, 69]. Radial- or mixed-flow machines are preferable for pumps with a specific speed of $\Omega_s < 2.7$, and as the specific speed increases ($2.6 < \Omega_s < 11.6$), an axial configuration is more suitable [70].

Carravetta et al. [71] postulate that axial-flow pumps can be used as PAT for heads between 1-5 m and flow rates up to 1000 l/s. They also claim that mixed-flow PATs can be used for heads in the region of 5-15 m and flow rates of 50-150 l/s. Bogenrieder [72] stated that radial pump-turbines are suitable to use for heads that are above 60 meter, with a power exceeding 50 MW. Typically, radial- or mixed-flow machines work best for high heads and low flow rates. For example, regular

Francis-like pump-turbines (mixed-flow) are the common choice when it comes to mid- to high-head applications, but the head variations at low-head operation would greatly affect efficiency [73]. Mixed-flow machines can be used as low-head PHS if the flow rate is low. However, according to Eq. (2.1), this implies that the power will also be low. Multiple machines could be used in parallel to increase the total power. Breeze [73] suggests that a Deriaz, mixed-flow machine can be used for heads between 20-100 m. This is because its design is closer to an axial machine compared to a conventional Francis-like pump-turbine and the Deriaz design also presents adjustable blades [73, 74]. Breeze further expresses the necessity of variable speed drives to extend the operational region at high efficiency.

Table 2.1.: Ranges of specific speed for various machines [70].

Technology	Specific speed Ω_s
Axial ^a	2.6 – 11.6
Mixed	0.6 – 2.7
Radial	0.1 – 0.8
Archimedes screw ^b	0.03 – 0.39
Positive displacement ^b	0.01 – 0.13

^a The contra-rotating reversible pump-turbine is classified as an axial machine.

^b Values should be regarded only as a reference number, since it is not common to indicate a specific speed for these machines.

The reason why an axial machine is preferable in a low-head application is that it allows for a higher flow rate, which is necessary for a machine with high power at low heads. An axial machine also allows for cheaper civil structures. In turbine mode, the runner rotates due to the torque that is generated by the flow-induced runner blade pressure and suction sides. The electric generator extracts power by a balancing counteracting torque at the particular rotational speed. In pump mode, an electric motor adds power to the runner in the form of torque at the particular rotational speed. A flow is developed due to the rotating runner blade pressure and suction sides, causing a balancing counteracting torque. The pressure change is in an axial machine primarily due to the change of relative flow velocity [70]. This is because the tangential velocity of the runner and the cross-sectional area are constant along a streamline in an axial machine. In a centrifugal machine, the flow must change direction from axial to radial (pump mode), or radial to axial (turbine mode), as shown in Figure 2.1. The principles for the head rise in a centrifugal machine are here described in pump mode for brevity. As the flow goes through the machine, the cross-sectional area and the tangential velocity of the runner increase with the radius through the machine. The absolute flow velocity will decrease as the cross-sectional area increases, due to continuity. According to Bernoulli's principle, the static pressure will increase with the change of absolute velocity squared [75]. The main cause of the static pressure rise is, however, due to centrifugal effects caused by the increase of the runner's tangential velocity, and passage diffusion, due to a reduction in the relative flow velocity, through the machine [70]. The result is

that the exit blade velocity needs to be small in order to limit the pressure rise in a low-head application. This means that the machine needs to be small and that the entrance-to-exit diameters decrease with the decreasing head [76]. The smaller size further limits the flow rate and thus the power.

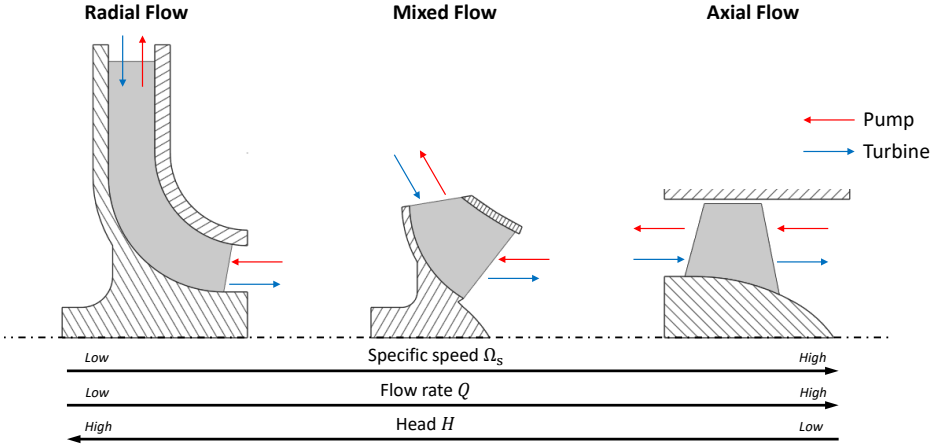


Figure 2.1.: Principle view of bladed pump-turbine configurations, note that the term "centrifugal" refers to both the radial- and mixed-flow. The drawing is based on principles shown in [65–67, 71].

In general, pump-turbines are worse at part-load conditions compared to a pure pump or turbine since the pump-turbine design is often a trade-off to reach acceptable performance at design conditions [77, 78]. Delgado et al. [79] reported that it is hard to predict part-load performance for PATs, especially in turbine mode since pump manufacturers usually do not supply any data of this. Stepanoff [67] stated that centrifugal machines have preferable efficiency as a function of flow rate; however, axial machines have a flatter efficiency curve as a function of head. This further suggests that an axial machine is preferable in a low-head scenario due to the fact that part-load operations will be less influenced by the large variation in head of a low-head PHS application.

Lately, axial-flow pump-turbines with two runners, rotating in opposite direction from one another, have been proposed as an alternative for low-head PHS. They are usually referred to as counter-rotating pump-turbines (CR-RPT) due to the rotation of the individual runners, as illustrated in Figure 2.2. According to Furukawa [80], the advantages of those machines are that they can be of smaller size, have a more stable head-flow rate characteristic curve, and have a wider range of high efficiency with individual speed control of the runners when compared to a single runner axial machine. Several numerical studies predict that a well designed low-head counter-rotating pump-turbine may achieve efficiencies of up to 80-90% in both pump and turbine mode [55, 81, 82]. Fahlbeck et al. [52] showed numerical results for a prototype counter-rotating pump-turbine in pump mode with a peak efficiency of 91%, heads up to 12 meter, flow rates between 60-160 m³/s, and a maximum

power of almost 14 MW.

Additional non-conventional machines have also been studied as low-head PHS. The Archimedes screw, depicted in Figure 2.2, is a viable option for heads between 2-10 m, discharge ranges up to 15 m³/s, and power output of up to 355 kW [62, 68, 83]. The Archimedes screw enables lower installation and maintenance costs compared to other conventional pump-turbines and can reach efficiencies of up to 90% in turbine mode [48, 84]. An additional benefit is that the Archimedes screw presents better conditions for fish-friendliness when compared to conventional bladed pump-turbines [68, 84, 85].

Positive displacement (PD) pumps are usually chosen when the system requires low specific speeds [70]. Some PD pumps can also represent a good alternative when reversible flows must be taken into account, thus resembling a PAT [86]. Positive displacement pumps are self-priming, typically produce low flow rates, can handle big variations in head without significantly changing their efficiency, and are often regarded as a good choice for viscous fluids or fluids with the presence of solids or precipitates that need to be handled [70, 75]. Rotary positive displacement machines have already been studied as micro hydro turbines in water supply pipelines with pressures up to 5 bar (hydraulic head equivalent to 51 meter) and presented efficiencies between 60-80% [87–90]. From all the available PD alternatives, the lobe and gear pump configurations – illustrated in Figure 2.2 – are the most suitable options to handle reversible flow. Given the low specific speed, PD pumps could most likely be regarded as a fish-friendly technology [69]. On the other hand, only the lobe design seems to handle fish and solid without extra mitigation measures. A few small-scale projects have tested PD RPTs [86]. However, further investigations and real-scale prototypes are still needed to validate the use of PD RPTs in low-head pumped storage application.

Pump-turbines in PHS applications can operate at fixed or variable rotational speed. Variable speed machines take advantage of a wider operating range at high efficiency and can thus produce power in a wider spectrum [63, 91]. Moreover, variable speed units ensure greater penetration and bring more flexibility to PHS operations, especially for smaller machines [92]. Despite the technical advantages, this technology is about 30% more expensive than fixed speed units. Thus, the choice between the two speed control options relies on both techno-economic and demand aspects [63, 92].

2.2. ELECTRIC MACHINES AND CONTROL

2.2.1. ELECTRIC MACHINES

IN traditional high-head, high-power PHS, synchronous machines with excitation winding and direct grid connection are used. However, doubly-fed induction machines have been adopted in Europe since 2006 for lower power applications. Doubly-fed induction machines are coupled to a partially rated converter with rotor winding to increase the operating range, which increases turbine efficiency at lower speeds [93]. As can be seen from Eq. (2.2), RPT operation at low head and high power reduces the nominal rotational speed for a fixed specific speed. Therefore, the power

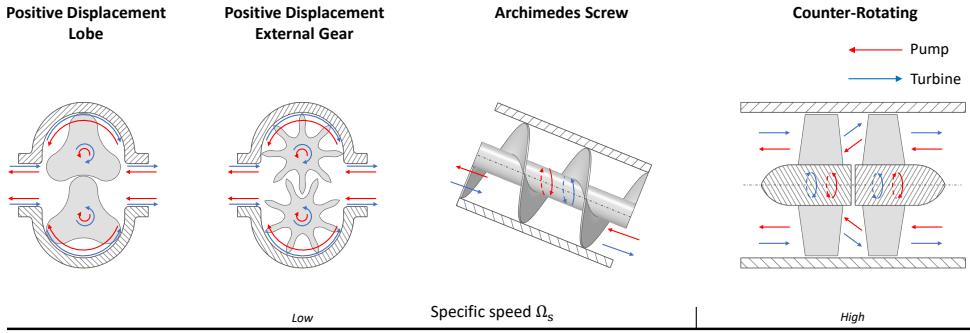


Figure 2.2.: Principle view of non-conventional pump-turbine configurations. The drawing is based on principles showed in [55, 70, 80].

take-off (PTO) in low-head PHS needs to be designed to operate at high efficiency for low rotational speeds. Furthermore, variable speed RPTs require a highly efficient PTO over a wide operating range. Doubly-fed induction machines with a gearbox were the classical choice for such low-speed applications. However, with the recent decrease in cost of power electronics, permanent magnet synchronous machines (PMSM) with a fully rated converter are opted for instead [94–101]. Advantages include a high power density, high efficiency, and controllability over a wide operating range [102, 103]. Furthermore, PMSMs with a large pole number avert the use of reduction gearing, which reduces energy losses and increases reliability [104, 105]. However, the increased cost of permanent magnets (PM) and converter losses limits its application for high-power installations.

A more recent development in PMSMs is the axial flux PMSM (AF-PMSM), which has a magnetic flux direction parallel to the axis of rotation, in contrast to their radial counterparts. These disc-type machines have a high diameter-to-length ratio, can accommodate high pole numbers, and are suitable for high-torque low-speed applications [106–108]. They have a higher power density and use less core iron, leading to a lower weight [107, 109, 110], which in turn results in a higher torque-to-weight ratio. The possible topologies are single-stator single-rotor (SSSR), double-stator single-rotor (DSSR), or single-stator double-rotor (SSDR). Furthermore, different concepts can be differentiated on the use of surface mounted or interior PMs, slotted or slotless armature, presence or absence of stator core, concentrated or distributed windings, etc. [111].

Single-stator single-rotor topologies [112] are simple in design and compact. However, there is a strong imbalanced axial force between the stator and rotor. Therefore, the rotor disc width needs to be increased to avoid twisting [107]. Double-stator single-rotor topologies [113] are a valuable alternative to SSDR topologies. Double-stator single-rotor uses fewer PMs, but experiences more copper losses due to poor winding utilisation [107]. A DSSR machine with integrated permanent magnets has a high power-to-inertia ratio, since the rotor disc serves no magnetic purpose and is eliminated [111]. The reduced inertia is a significant

benefit in a grid-supporting low-head PHS system. In a slotted stator AF-PMSM, cogging torque results from the interaction between the PMs and the stator slots. This undesired torque can be significantly reduced by changing the angle between both stators [114]. However, this also reduces power output. Finally, SSDR is deemed the most favourable AF-PMSM topology. Next to decreased copper losses, the use of a stator yoke and the corresponding iron losses can be averted. This can be achieved by using a north-south PM arrangement of the rotors. Then, the flux path is completely axial, obviating the magnetic function of the yoke. The single-stator double-rotor topology has already been adopted in wind and tidal turbine applications [115, 116]. An SSDR with coreless stator maximises efficiency, while averting cogging torque and torque ripple [117–119]. Since the flux path is axial, grain-oriented material - which has greater magnetic permeability in one direction - can be used in the stator slots. This results in significantly lower iron losses compared to non-oriented material [120], while reducing PM use compared to coreless alternatives [111].

Especially in high-voltage electric machines, the vast majority of occurring faults are stator faults, followed by rotor and bearing faults [121]. Therefore, AF-PMSMs with concentrated windings can offer a significant advantage by adopting a Modular Machine Drive (MMD) design. If a fault arises in one of the stator windings, the MMD can compensate this with the other modules and remain functional albeit the maximum power is reduced [122, 123]. This fault-tolerant design improves the reliability of the electric machine, which is a considerable advantage for a low-head PHS system providing grid support. The reliability can be further increased by means of condition monitoring techniques and fault or anomaly detection methods [124, 125]. Thanks to the drastic increase in computational power in the past years (both local and in the cloud), these techniques have become more data-driven, relying on, e.g., machine learning [126, 127], including artificial neural networks [128], support vector machines [129], and deep learning [130, 131]. The use of digital twins for predictive maintenance of mechanical components [132] or the full drivetrain [133] shows promising results and offer a perspective for the future of condition monitoring [134]. These techniques can be applied on the electric machine, and in extension on the whole drivetrain. Current, voltage, magnetic flux, speed, temperature, and vibration signals can be captured on the electric machine and serve as inputs for the condition monitoring system.

It can be concluded that the PMSM is currently the most sensible electric machine technology for modern low-head PHS due to its high efficiency and direct-drive capability, although the use of rare earth materials is a drawback. The principles of axial flux design, modularity for fault tolerance and data-driven condition monitoring are likely to play a role in the further improvement of the PMSM.

2.2.2. TORQUE AND SPEED CONTROL

In variable speed PHS, the machine speed is altered to reach a power setpoint as fast and precise as possible, both in pump and turbine mode. Therefore, the machine torque must be precisely controlled. Field oriented control (FOC) is a vector control method that has been widely used in low-head micro-hydropower

installations [94–100]. The main advantage is an independent control of the machine torque, and thus, highly dynamic performance. This is beneficial to PHS to increase its capability to provide frequency regulation services. The general principle of FOC is to regulate the i_d and i_q currents in the rotating reference frame. The electrical dynamics of a PMSM can be modelled by Eq. (2.3) and Eq. (2.4) with the d- and q-axis voltages v_d and v_q . $\Omega_e \Psi_{PM}$ is the back-EMF of the permanent magnets. R is the stator resistance. L_q and L_d are the q and d axis inductances, respectively. $\Omega_e Li$ is the armature reaction EMF, through which the q and d schemes are coupled.

$$v_d = R i_d + L_d \frac{di_d}{dt} - \Omega_e L_q i_q \quad (2.3)$$

$$v_q = R i_q + L_q \frac{di_q}{dt} + \Omega_e (L_d i_d + \Psi_{PM}) \quad (2.4)$$

By regulating the d- and q-axis currents, the torque T can be regulated as shown in the general torque Eq. (2.5) of the PMSM.

$$T = p \frac{3}{2} [\Psi_{PM} i_q + (L_d - L_q) i_d i_q] \quad (2.5)$$

Here, p is the pole pair number and Ψ_{PM} is the constant flux of the permanent magnets. Figure 2.3 shows the control scheme of a field oriented controlled PMSM. On the bottom right, the stator currents are measured and transformed to the rotating q, d reference frame. These signals are compared with the setpoints on the left and controlled by two proportional-integral (PI) controllers. These controllers determine the duty ratios resulting in the Pulse-Width Modulated (PWM) signals for the converter. In FOC, \hat{i}_d is set to zero. The circumflex ' \wedge ' indicates a setpoint for a certain variable. Eq. (2.5) shows that the machine torque is directly proportional to i_q , resulting in a highly dynamic control. To achieve decoupled control of both currents, the coupling terms in Eq. (2.5) are used as a feedforward. Furthermore, a back-EMF estimator can be implemented in the q current control.

Although FOC is highly dynamic and easy to implement, setting $i_d = 0$ is not the most efficient way to reach a desired torque setpoint for a PMSM with saliency, like an interior magnet PMSM. Therefore, maximum torque per ampere (MTPA) control can reduce copper losses and increase overall efficiency in low-head hydropower applications. The MTPA accomplishes this by minimising the stator current $i_s = \sqrt{i_q^2 + i_d^2}$ for every torque setpoint [135]. Applications with interior magnet PMSMs in wind turbines found a reduction in Joule losses (heat losses due to the resistance of the stator windings) of up to 4.2%, while maintaining a dynamic response to changing torque setpoints [135, 136].

The position sensor plays a critical role in FOC. However, a position sensor is costly and its signal can contain noise. Therefore, saliency-based sensorless rotor position estimators [99, 100, 137, 138] are proposed for low-power systems, since they can increase reliability and reduce cost [100]. For low rotational speed runners, as in low-head PHS, the saliency-based approach is the most suitable [100]. Here, a high pulse frequency is injected, while the current response, which depends on the rotor magnetic flux position, is observed.

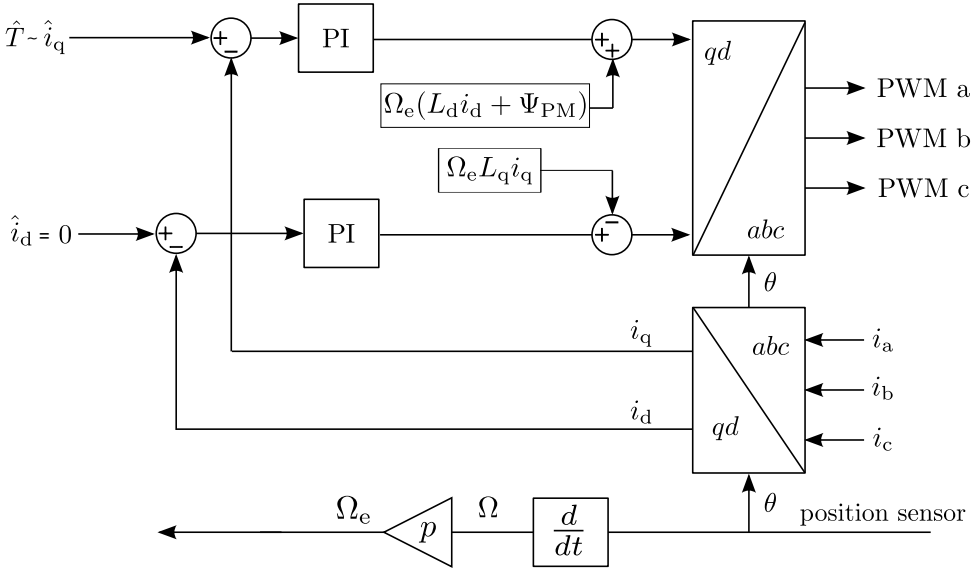


Figure 2.3.: Decoupled field oriented control of a PMSM with estimated back-EMF feedforward.

Active distribution rejection control (ADRC) is used in torque and speed control to account for known and unknown electrical, hydraulic, or mechanical disturbances in the system, increasing performance and robustness. Guo et al. [95] applies a first order ADRC for a PMSM in a hydropower application, where the known disturbances are mechanical friction and hydraulic torque. A second order state observer is used to estimate the rotational speed and hydraulic torque. ADRC is especially useful in low-head high-power PHS, since any change in the system tubes has a significant influence on the head losses, because of the high flow rate at low head.

Direct torque control (DTC) is an alternative control method to FOC. In DTC, the electromagnetic torque and stator flux (Φ) are controlled by switching between a discrete number of stator voltage vectors, which in turn form the stator flux vector interacting with the rotor flux. Based on the torque and flux linkage reference and the current flux vector position, a lookup table is consulted to select the optimal voltage vector. If e.g. the torque must be increased, a voltage vector is selected so that the angle between stator and rotor flux is increased. Figure 2.4 visualises the control schematic. To find the torque and stator flux, an estimator based on phase voltages and currents is used (bottom). These estimated values are compared to torque and flux setpoints. Hysteresis controllers then determine the proper voltage vector from a lookup table, resulting in the switching signals. Direct torque control has a slightly better torque response compared to FOC and does not require a position sensor [139, 140]. However, DTC relies on an accurate estimator. Especially at low speeds, an estimator based on phase voltages and currents cannot accurately estimate the stator flux [141], which makes it less suitable for low-head

PHS. Although some improved estimator algorithms have been studied [141], this drawback is best averted by using a position sensor in the estimator. Disadvantages of DTC include variable switching frequency, high harmonic current distortion, and torque ripple [139, 140, 142]. To achieve a smoother dynamic response and thus less torque and flux ripple, space vector modulation (SVM) is used instead of the lookup table [139, 140, 143].

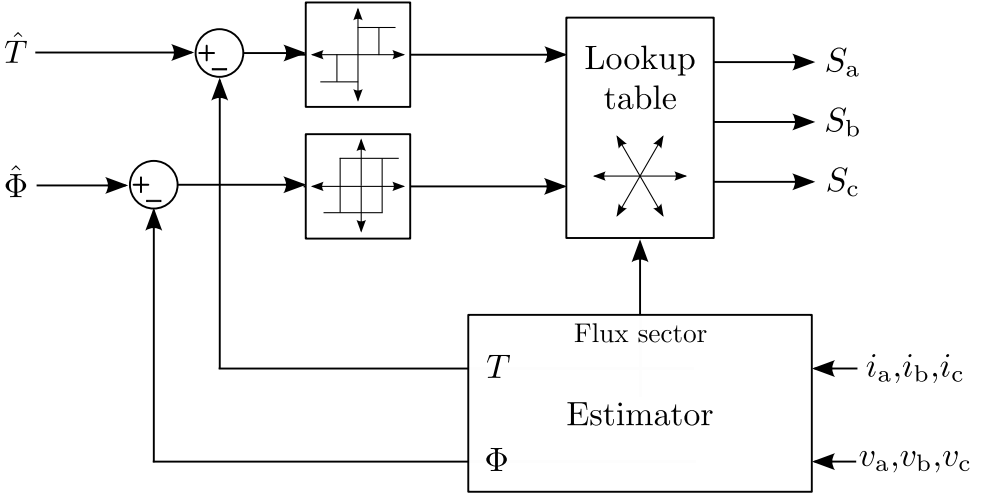


Figure 2.4.: Control schematic of DTC.

2.2.3. POWER CONTROL

In the power control of low-head PHS, the goal is to reach a power setpoint as fast and efficiently as possible. Three main control parameters are determined: the pump/turbine rotational speed Ω ; the inlet vane angle α ; and the blade pitch β . An RPT with only Ω as control parameter is defined as a non-regulated RPT. A single- and double-regulated RPT further include, respectively inlet vane control, and inlet vane and blade pitch control. In low-head PHS, a regulated RPT is recommended, because it allows the RPT to be operated at high efficiency in a large operating range of heads, flow rate, and power setpoint.

MAXIMUM POWER POINT TRACKING ALGORITHMS

Maximum power point tracking (MPPT)-based algorithms are used to find the optimal speed setpoint for a certain power setpoint in turbine mode. In a low-head turbine, this power setpoint is the maximum available power, hence the name MPPT. In grid-supporting PHS, this may not be the case, as the power setpoints depend on grid frequency. Therefore, adjustments need to be made to the existing algorithms. The MPPT algorithms can be divided into direct and indirect methods. Direct MPPT algorithms are based on iterative extremum-seeking control algorithms.

These algorithms require limited knowledge of the system, but are inherently slow due to their iterative behaviour, making them less suitable for grid-supporting PHS. However, they can still be used in storage systems with lower dynamic requirements because of their simplicity. Indirect methods are based on a model of the system, making them more dynamic but less flexible. Most of the existing MPPT control methods rely on flow rate measurements. However, a flow rate sensor is costly and has a certain error. In low-head RPTs, the accuracy can further decrease due to a non-uniform flow, a short intake, and high turbulence [144]. To evade these drawbacks, Borkowski and Dariusz [101] presented a flow rate estimator. The estimator is based on an artificial neural network (ANN), which is trained by experimental data.

Among direct MPPT control methods, the perturb and observe algorithm has been investigated for non-regulated low-head turbines. The principle operation consists of altering or perturbing the rotational speed Ω , i.e. accelerating or decelerating, and analysing the change in output power P , measured at the electric machine or converter. If the power has increased, the sign of $d\Omega$ is maintained and the procedure continues. Otherwise, $d\Omega$ is reversed [94]. Eq. (2.6) shows how the speed setpoint $\hat{\Omega}$ is altered after each iteration. Note that $\delta(t)$ implies the sign of $d\Omega$.

$$\hat{\Omega} = \int_{t_{k-1}}^{t_{k-1}+T_s} K\delta(t) dt \quad (2.6)$$

$$\delta(t) = \text{sgn}(P_k - P_{k-1}) \text{sgn}(\Omega_k - \Omega_{k-1}) \quad (2.7)$$

Inherent to this method is that the system will still perturb Ω when the MPP is reached, resulting in an oscillation around the MPP. Step size K is an adaptive value that increases when the power is continuously rising and decreases when the power is fluctuating [94]. However, the dynamic behaviour of this method is not optimal. If K is too low after oscillations and the MPP shifts, the dynamic response is poor. To allow both dynamic response and minimal power fluctuation around the MPP, K can be taken proportional to the power gradient $\frac{\Delta P}{\Delta \Omega}$ [145]. Due to the parabolic nature of the turbine characteristics, K is high when far away from the MPP and gradually decreases when the MPP is neared. Note that using this gradient-based step size cannot be used to reach a lower power setpoint \hat{P} . However, the step size here can be proportional to $|\hat{P} - P|$. In wind turbine applications, fuzzy logic is recently used to find the value of K , where the perturbed variable is the generator voltage, which is proportional to the generator speed [146–148].

Gradient descent control is a direct maximum efficiency point tracking (MEPT) algorithm that allows multiple control variables, opposed to the perturb and observe algorithm. However, to derive the efficiency, an accurate flow sensor is necessary, which was discussed to be a challenge in low-head PHS systems [144]. On every operating point, the control variables are incremented with the direction of their partial derivatives of efficiency at the current operating point, multiplied by a step size k [149]. In Eq. (2.8), α is the vane opening and β is the blade pitch.

$$\Delta\alpha = k \frac{\partial\eta}{\partial\alpha} \quad \Delta\beta = k \frac{\partial\eta}{\partial\beta} \quad \Delta\Omega = k \frac{\partial\eta}{\partial\Omega} \quad (2.8)$$

If the time constants of the control parameters are known, k can be chosen differently for each control parameter. Furthermore, k can be adaptive and defined by a line search algorithm at every iteration [150]. Although this control algorithm shows great potential, any disturbances on the gradient estimation due to measurement error or mutual influence between control parameters has a great impact on the convergence [149]. Therefore, a moving average filter and a Kalman filter can, respectively, be used to increase robustness [101, 151]. Furthermore, Borkowski [101] accounts for the time delay of flow rate settlement after a change in turbine control parameter further reduce risk of a non-converging control.

Indirect MPPT algorithms rely on prior knowledge of the system in order to determine the optimal torque or speed reference to achieve a power setpoint. Recently, this system knowledge is mostly captured in the form of empirical equations, hill charts, or lookup tables, which are derived from measurements or numerical analysis like computational fluid dynamics. Márquez et al. [96] derived an empirical formula for a propeller turbine, which is a modified Kaplan turbine, designed for low-heads and low flow rates. Eq. (2.9) relates the non-regulated turbine efficiency to flow rate and turbine speed.

$$\eta_h(\Omega, Q) = 3.33 \ Q \left[\frac{1}{2} \left(\frac{90}{\lambda_i} + Q + 0.78 \right) e^{\frac{-50}{\lambda_i}} \right] \quad (2.9)$$

$$\lambda_i = \left[\frac{1}{(\lambda + 0.089)} - 0.0035 \right]^{-1}, \quad \lambda = \frac{RA\Omega}{Q}$$

Although this model can be used in low-head control models, it is important to note that flow rate Q is a function of head and rotational speed $Q = f(H, \Omega)$ for a non-regulated RPT. Therefore, changing Ω will affect flow rate Q as well. Zhang et al. [152] proposes a polynomial empirical equation for the efficiency of a turbine $\eta_h(\Omega, Q)$, where the coefficients can be derived from experimental data. Borkowski and Dariusz [153] used an ANN to compose and validate an efficiency equation $\eta_h(\Omega, Q)$ together with a flow rate characteristic $Q(\Omega, \alpha)$ for a regulated turbine. The control system based on these characteristics requires no flow rate sensing. However, the Q characterisation is for a constant head and the flow rate is approximated by a linear function of speed. This limits its application under varying head at low rotational speeds.

Similarly, ANN has also been used to form lookup tables [154]. Lookup tables can be constructed over a large operating range during on-site measurements or by using an existing dataset. Pérez-Díaz and Fraile-Ardanuy [154] use two ANNs to train the head and efficiency for input parameters Q , Ω , and α . A possible application of the resulting lookup tables is to find reference $\hat{\Omega}$ and $\hat{\alpha}$ to reach the optimal efficiency for a given head. In this control system, no flow sensor is necessary, thus reducing cost and increasing reliability, especially for low-head systems.

Hill charts define the relation between flow rate Q , rotational speed Ω , inlet vane angle α , and efficiency η for a constant head H . Therefore, if Ω and α are known, Q and η can be read from the graph. Furthermore, α and η are plotted versus the so-called unit quantities¹ such as the unitary rotational speed Ω_{11} and unitary flow

¹Unit quantities refer to the characteristics of a turbine with a runner diameter of 1 m, operating at

rate Q_{11} in Eq. (2.10), making hill charts scalable for different heads. However, in a real system, the losses $H_L(Q)$ have to be taken into account, making it difficult to estimate the net head across the turbine without a flow rate measurement. Especially in a low-head high-power system, where the flow rate is high, these losses have a significant influence on the efficiency.

$$\Omega_{11} = \frac{\Omega D}{\sqrt{H}}, \quad Q_{11} = \frac{Q}{D^2 \sqrt{H}} \quad (2.10)$$

Q_{11} and Ω_{11} can also be compensated when the Reynolds number of the real system differs from the design [155]. Fraile-Ardanuy et al. [156] applied a hill chart to a control system in order to find the optimal efficiency speed for given α and measured Q . For a reduced-scale RPT [157], a lookup table is trained based on measurements. The lookup table is used to find $\hat{\Omega}$ for given measured H and \hat{P} . However, the speed is controlled by α , while it was shown in the paper that $Q_{11} = f(\alpha, \Omega)$. However, the proposed control system is promising for low-head hydropower if both Ω and α are controlled separately. Then, the RPT could be controlled to reach \hat{P} at the highest efficiency for a certain measured H .

One drawback of using turbine characteristics is that the electrical machine and converter losses are not included. Therefore, the overall MPP may differ from the turbine MPP [98]. De Kooning et al. [158] found that the MPP displacement in wind turbines was greater for low wind and thus lower rotational speeds. In direct MPPT methods, these losses are included if the power is measured on the converter side. Another drawback of indirect MPPT methods is that they do not account for system performance deterioration over a long time period. However, reinforcement learning, as proposed for wind turbines [159, 160], can solve this problem at the cost of a higher real computational intensity.

MODEL PREDICTIVE CONTROL

An important factor in RPT operation and control that is often overlooked in traditional MPPT strategies is the transient effect of the water supply system caused by a control action. Fang et al. [161] stated that increasing the control action magnitude actually decreased the output power, while the settling and maximum turbine pressure deviation increased. Therefore, it can be seen how using an MPPT control that does not account for these effects can have poor dynamic behaviour when applied to a real system. In some studies on MPPT control, the water inertia time T_w is incorporated as a time delay on the control action [101] or as an extra mechanical inertia on the RPT [162]. However, this does not fully capture the transient effects. Therefore, model predictive control (MPC) is applied to PHS systems [163–165]. In MPC, a detailed model of the full PHS system, including hydraulic transients, losses, and an RPT model, are used. Based on a certain operating state setpoint, an internal optimisation algorithm simulates control actions and observes the predicted outcomes of the model. The outcomes are then given a

¹ m net head. They are commonly associated with units of speed and velocity, however their actual dimensions are quite different and have no physical meaning.

cost value based on the power response. These predictions are made for multiple future time samples. Each time sample, this process is repeated. Therefore, MPC is an accurate control method that can work on complex systems, at the cost of a significantly high computational intensity. Furthermore, MPC can also incorporate system constraints, such as maximum pressure deviation and mechanical rate limits. Chaoshun et al. [163] proposed using a nonlinear MPC, which includes the elastic water hammer effect in a high-head PHS plant. Liang et al. [164] used MPC to define the optimal switching time between pump and turbine mode for a multi-RPT PHS plant. However, these studies did not include pressure constraints, which are especially important in systems with long pipelines. The MPC for a 40 meter PHS plant by Mennemann et al. [165] included this effect. MPC is currently mostly investigated for high-head PHS. However, the benefits of adapting MPC for low-head PHS could be substantial, because of the potentially increased influence of transient effects, as described in section 1.1.3. For a dynamic system providing frequency support, the MPC's computational intensity increases even further, which might slow down the optimisation algorithm. However, with the recent advancements made in parallel computing with, e.g., multi-core processors (CPUs) and many-core processors such as graphical processing units (GPUs), the MPC process can be accelerated [166], making it suitable for complex dynamic systems like low-head PHS.

2.3. GRID INTEGRATION

A reliable electrical power grid is a balanced system. As generation and demand fluctuate perpetually, transmission system operators (TSO) and distribution system operators (DSO) have to keep the system balance everywhere in the electrical grid. This balance ensures that the grid operates at its nominal frequency (50 or 60 Hz) and that voltage and power load remain within a certain limit at all times. However, the higher the penetration of intermittent renewable energy sources, the more insecure this balance. Thus, the increasing penetration of IRES is a challenge that TSO and DSO have to handle [167, 168].

As discussed in section 1.1.1, power systems currently rely on conventional thermal power plants and the rotational inertia of their synchronous generators to stabilise the grid. IRES, however, typically are connected to the grid via converters and therefore do not provide that inherent grid inertia. As of today, the grid-connected converters for IRES follow the grid frequency by using a phase locked loop (PLL). This tracks the grid frequency in order to keep the IRES converters synchronised to the grid. The PLL control concept is known as grid-following control [4, 169].

To tackle the challenge of increasing IRES and decreasing natural system inertia without affecting the system stability, two approaches are feasible. The first is to maintain a minimum number of rotating machines. Among other purposes, the contribution of short-circuit power and voltage support can provide the necessary inertia to the transmission system in a case of disturbances in the grid [170, 171]. The second solution is through IRES itself. This is possible by using the capabilities of the power electronics, or energy storage systems (ESS), to provide and ensure a

stable grid frequency without any synchronous rotating machines. For this purpose, a grid-forming control mode is currently being developed and tested in many research projects. Here, the controlled converter acts as an AC voltage source with stated voltage, phase, and frequency. By controlling the voltage magnitude and frequency, the converter behaves very similar to a synchronous generator. The fundamental difference between grid-following and grid-forming is the way of synchronisation. By applying the swing Eq. (2.11) and Eq. (2.12) [172], the grid-forming control strategy calculates the voltage angle and amplitude deviation, using current power transfer. It is thus self-synchronising. Therefore, a converter using grid-forming control coupled with an ESS is currently being discussed as a viable alternative to imitate the synchronous generator's behaviour regarding frequency control, especially its ability to provide synthetic electrical inertia [4, 169, 173]. In power plants with rotating mass and consequent inertia that are decoupled from the grid frequency, an additional control loop is required that gives a power reference proportional to the derivative of grid frequency. To provide the additional power requested by the synthetic inertia, the plant may still rely on the physical inertia present but due to its decoupled nature depends on said synthetic inertia control.

$$P_m - P_e = J\omega_0 \frac{d\omega}{dt} \quad (2.11)$$

$$\omega = \frac{d\vartheta}{dt} \quad (2.12)$$

Here, P_m is the mechanical power, P_e is the electrical power, ω_0 is the nominal angular frequency, ω is the output angular frequency, ϑ is the rotation angle, and J is the total moment of inertia of the rotor mass.

Figure 2.5 shows a simplified block diagram for a synthetic electrical inertia control system. As illustrated, ESS are needed along the grid-forming control to provide the necessary synthetic electrical inertia. This shows that ESS are an important factor in the energy transition and will play a key role in the future. Energy storage systems will provide inertia for local grid stability as well as other necessary AS, such as steady state voltage control, fast reactive current injections, short-circuit current, black start capability, and island operation capability [174].

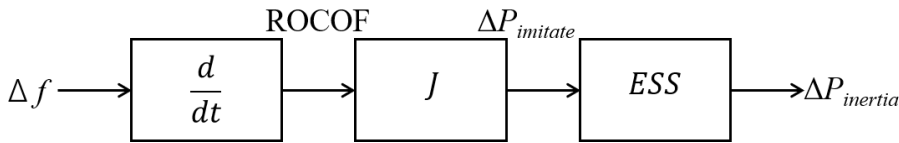


Figure 2.5.: Simplified block diagram for synthetic electrical inertia control [175, 176]. Here, Δf is the deviation of system frequency, ROCOF is the rate of change of frequency, J is the virtual inertia control constant, $\Delta P_{imitate}$ is the active power of the converter, and $\Delta P_{inertia}$ is the emulated virtual inertia power that could be imitated into the system.

SUMMARY

This review of technologies applicable to low-head pumped hydro storage, highlights both the opportunities and challenges inherent in developing viable solutions for pumped hydro storage at low-head sites. While conventional high-head PHS has long been a proven technology, adapting pumped storage to low-head conditions requires a reevaluation of pump-turbine design, electrical machines, control strategies, and grid integration. The literature underscores the growing interest in alternative pump-turbine configurations such as counter-rotating reversible pump-turbines, which offer advantages regarding operational flexibility and efficiency. Additionally, the integration of suitable power electronics, variable-speed operation, advanced control algorithms and grid-support services are crucial in improving the capabilities of low-head PHS to facilitate an increased renewables penetration in our grids. Despite these advancements, a significant gap remains in the modelling and simulation of such systems, particularly in capturing the interactions between hydraulic, mechanical, electrical, and control components.

3

LOW-HEAD PHS SYSTEM NUMERICAL MODEL: COUPLING THE HYDRAULIC, MECHANICAL, ELECTRICAL AND CONTROL COMPONENTS

To understand the steady-state performance and transient behaviour of novel pumped storage technology, both numerical and experimental methods can be employed [177]. Computational Fluid Dynamics simulations and small-scale experimental testing can give insightful results, but also have limitations. High-fidelity CFD models are a key tool when developing new hydro-machinery. They are capable of delivering accurate results on turbomachinery performance and predict complex flow patterns both in steady-state conditions and for transient simulations in time-domain[178]. Their major disadvantage is the computational expense, which can limit the size of the computational domain and transient effects that are included. Inherently, this leads to limitations in the amount of different operating conditions and cases that can be evaluated [179, 180]. Additionally, CFD simulations focus on the flow behaviour and typically do not include other relevant system dynamics resulting from the interaction or coupling with the drivetrain, electric machines or control subsystems. Experimental setups can provide reliable results for both steady-state and dynamic investigations but are costly, complex for the reduced

Parts of this chapter have been published in J.P.Hoffstaedt et al. Low-head pumped hydro storage: An evaluation of Energy Balancing and Frequency Support. IET Renewable Power Generation. 2024. & J.P.Hoffstaedt et al. System model development and numerical simulation of low-head pumped hydro storage. Trends in Renewable Energies Offshore. 2022. & are currently under review as J.P.Hoffstaedt et al. Analysis of a Contra-Rotating Pump-Turbine for Low-Head Applications: An Experimental Study and Numerical Comparison. Energy Conversion and Management.

scale fabrication of pump-turbine sets and time-consuming. Furthermore, they present challenges regarding the accuracy of measurements and scaling issues among others. Using low and medium fidelity numerical approaches have the advantage of a drastic reduction in the computational resources required. Additionally, these versatile approaches allow for the integration of other system dynamics and control algorithms, enabling the simulation of a wide variety of scenarios. The trade-off of this efficiency and versatility is a decrease in accuracy compared to higher fidelity models. Nonetheless, if an appropriate modelling approach is chosen to consider all relevant effects to the desired simulation cases, adequate accuracy can be reached. Once validated, such a model can be applied to simulate the steady-state performance and transient behaviour of a full-scale storage plant. In this chapter, a time-domain numerical modelling approach is developed and presented. The system model includes the most relevant dynamics of the novel low-head pumped storage system introduced in section 1.1.4. By integrating the RPT with the conduit, reservoir, valve, drivetrain, and control subsystems, the model aims to provide a comprehensive analysis of the system behaviour. The objective is to create a versatile and efficient numerical tool capable of evaluating the system's performance in energy balancing, its transient response during dynamic operations, such as frequency regulation services, and the interaction between the individual system components.

3.1. OVERVIEW AND MODELLING APPROACH

A schematic overview of the main model components and their coupling is shown in Figure 3.1, representing the physical system components as illustrated in Figure 1.3. At the core of the coupled system model, is the steady-state characterisation of the newly designed RPT consisting of two individual runners. This RPT model is coupled to hydraulic conduits on either side of it as well as to the two individual drivetrains. The flow dynamics are included through a discrete conduit model, assessing the temporal and spatial changes of flow rates and pressure heads. The hydraulic conduit is divided into two sections: the high-pressure section on one side of the RPT and the low-pressure section on the other. The high-pressure conduit takes the static head of the upper reservoir, denoted as H_{ur} , and the high-pressure RPT head H_{rptl} as inputs. This produces the flow rate to the upper reservoir Q_{ur} and the RPT flow rate Q_{rpt} . Notably, the RPT's flow rate remains constant and is used as an input for the low-pressure conduit. Contrary to the high-pressure conduit, it uses one flow rate and one pressure head, the one of the lower reservoir H_{lr} , as inputs. The outputs are the flow rate into the lower reservoir Q_{lr} and the head of the valve H_v . Depending on the flow rate and valve opening angle, driven by the opening angle command γ_{com} , the valve provides the low-pressure RPT head H_{rptr} to the RPT characterisation. The tip speed ratios of both runners are calculated from the flow rate and both rotational speeds, which are obtained from the individual drivetrain models. With the tip speed ratios, the head coefficients, efficiencies and hydraulic torques of both runners are obtained. Finally, the hydraulic torques of both runners and the machine torques $\tau_{m1,2}$ set by the control algorithm are given to the drivetrain models.

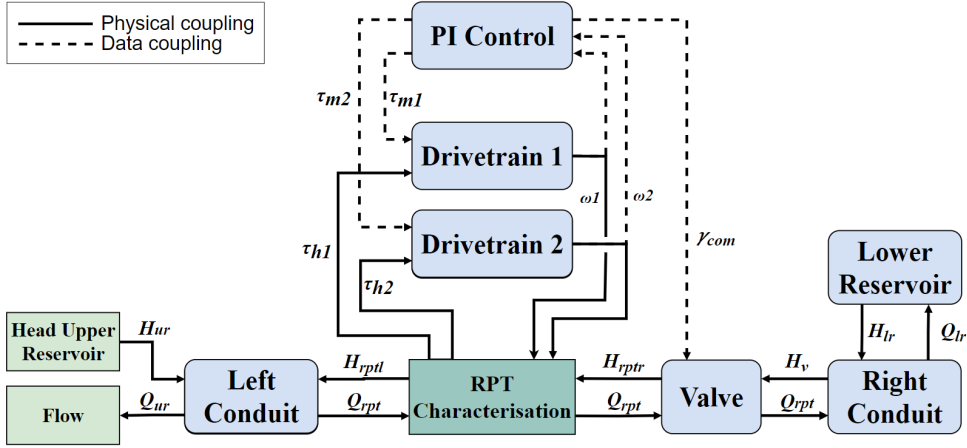


Figure 3.1.: Schematic overview of the system model showing the numerical interactions and coupling between components. In blue are model components with dynamic effects, in dark green steady-state components, and in light green the inputs/outputs.

The resulting set of coupled algebraic and ordinary differential equations (ODE) that represent the behaviour of the main components, are implemented and solved numerically in the time-domain using a standard ODE solver, following the so-called Method of Lines [181]. Following, the numerical approach for each component is given.

3.2. CHARACTERISATION OF THE REVERSIBLE PUMP-TURBINE

To model the hydraulic behaviour of the newly developed contra-rotating RPT, it is first characterised across its operating range. The two contra-rotating runners of the RPT are shown in Figure 3.2. Runner 1, shown in red, is the downstream runner in turbine mode. Conversely, runner 2, indicated in blue, is the downstream runner in pump mode. In both turbine and pump modes, runner 1 rotates clockwise, while runner 2 rotates counter-clockwise relative to their respective flow directions.

The characterisation is based on 180 steady-state CFD simulation results as per Fahlbeck et al. [52], covering the operating range in both pump and turbine modes. The simulation's computational domain included one blade passage per runner with an infinitely long hub. Since the system can vary the rotational speeds of both runners, resulting in adjustable speed ratios between them, the runners were characterised individually using their tip speed ratios. The tip speed ratios are defined in Eq. 3.1 as the ratio between the tangential speeds of the tips of the runners, calculated from the corresponding rotational speeds $\omega_{1,2}$ and runner radius R , and the average axial flow velocity u .

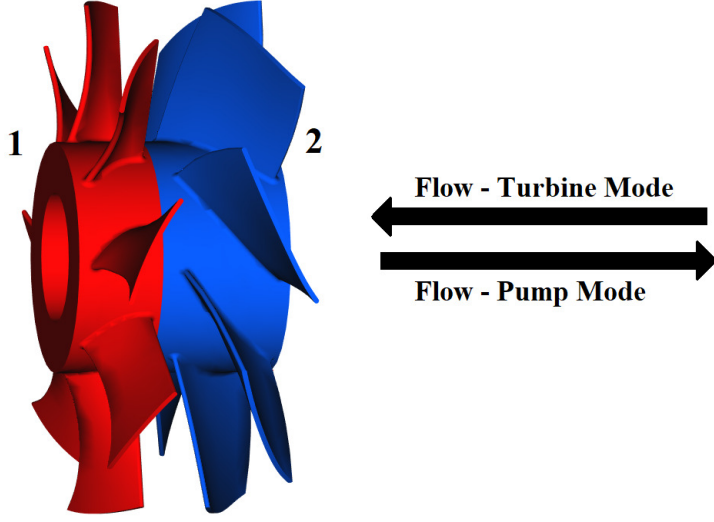


Figure 3.2.: Low-Head RPT consisting of two contra-rotating runners with a full-scale diameter of 6 m, a design power rating of 10 MW and design flow rate of 130 m³/s. Runner 1 is shown in red and runner 2 in blue. The flow direction is indicated for both turbine and pump operation.

$$\lambda_{1,2} = \frac{\omega_{1,2}R}{u} \quad (3.1)$$

The tip speed ratio can also be interpreted as the inverse of the dimensionless flow coefficient which is commonly used in turbo-machinery literature. Using a non-linear polynomial regression, the CFD results are translated into dimensionless head coefficients $C_{h1,2}$ and efficiencies $\eta_{1,2}$ as a function of both runners' tip speed ratios $\lambda_{1,2}$, covering most of the operating range of the RPT in pump and turbine modes. The head coefficients are defined as the pressure difference across each runner, with the runner heads $H_{r1,2}$, the fluid density ρ and the gravitational acceleration g , divided by the dynamic pressure, given in Eq. 3.2.

$$C_{h1,2} = \frac{\rho g H_{r1,2}(\lambda_1, \lambda_2)}{\frac{1}{2} \rho u^2} \quad (3.2)$$

The hydraulic efficiencies of the runners are defined for turbine mode in Eq. 3.3, as the mechanical power of the runners given by the rotational speeds and hydraulic torques $\tau_{h1,2}$ divided by the available hydraulic power to each runner with the runner heads, the volumetric flow rate Q , the fluid density and the gravitational acceleration.

$$\eta_{1,2} = \frac{\omega_{1,2} \tau_{h1,2}(\lambda_1, \lambda_2)}{\rho g Q H_{r1,2}(\lambda_1, \lambda_2)} \quad (3.3)$$

For pump mode, the hydraulic efficiency is defined as the inverse of Eq. 3.3. The average axial flow velocity is calculated using the volumetric flow rate and the entire cross-sectional area of the conduit at the runners location. By rearranging Eq. 3.3, the hydraulic torques of each runner can be obtained from the runner mechanical power divided by their rotational speed.

Finally, a polynomial regression is performed on the calculated dimensionless coefficients to create 3-D performance maps that are used in the coupling with the other components of the integrated model. The process of obtaining the RPT characterisation in the form of the 3-D maps from the CFD simulations is illustrated in figure 3.3.

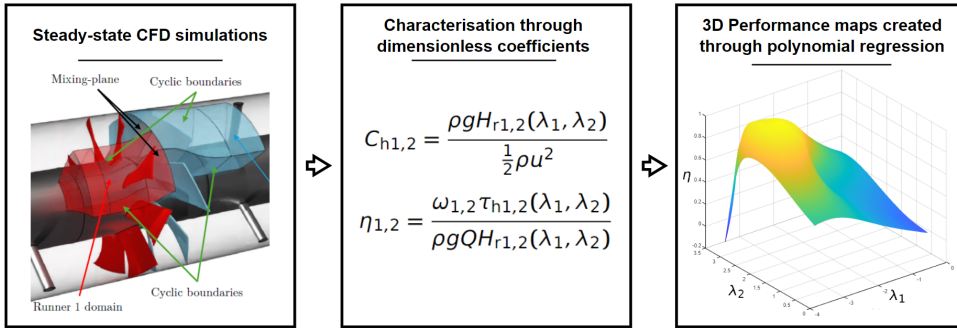


Figure 3.3.: Illustration showing the conversion of the steady-state CFD simulations to the RPT characterisation based on dimensionless coefficients.

The characterisation results in turbine mode for runner 1 and 2 are given in Figure 3.4. Figure 3.4a and Figure 3.4c show the head coefficients of runner 1 and 2 respectively as a function of the tip speed ratio of runner 1. The different curves in the graph represent different proportions between the runners' tip speed ratios. Figure 3.4b and Figure 3.4d show the corresponding efficiencies of the runners. As evident from all graphs, the speed ratios between the two runners affect the performance of each one individually. Runner 1 sees a fairly consistent increase in head coefficient as the tip speed ratios decrease. However, its efficiency clearly shows a range of maximum performance that is shifting slightly as the ratio between the runners is adjusted. This highlights the benefit of the individual variable speed control of each runner resulting in a wider operating range at high efficiencies. In the range of tip speed ratios between 2.5 and 3.25, efficiencies above 0.9 and a maximum value around 0.95 are achieved. Runner 2 has a much wider operating range with more constant head coefficients and high efficiencies with an overall maximum of around 0.97 and a maximum of 0.9 within the operating range that is ideal for runner 1. It is important to note that in turbine mode, runner 2 serves as the upstream runner, benefiting from less disturbed inflow. As a result, it operates more efficiently across a broader range of tip-speed ratios. In contrast, runner 1 is subjected to more disturbed flow conditions, particularly outside of the design operating range. This may include flow separation caused by the wake effects from

runner 2 at lower tip-speed ratios.

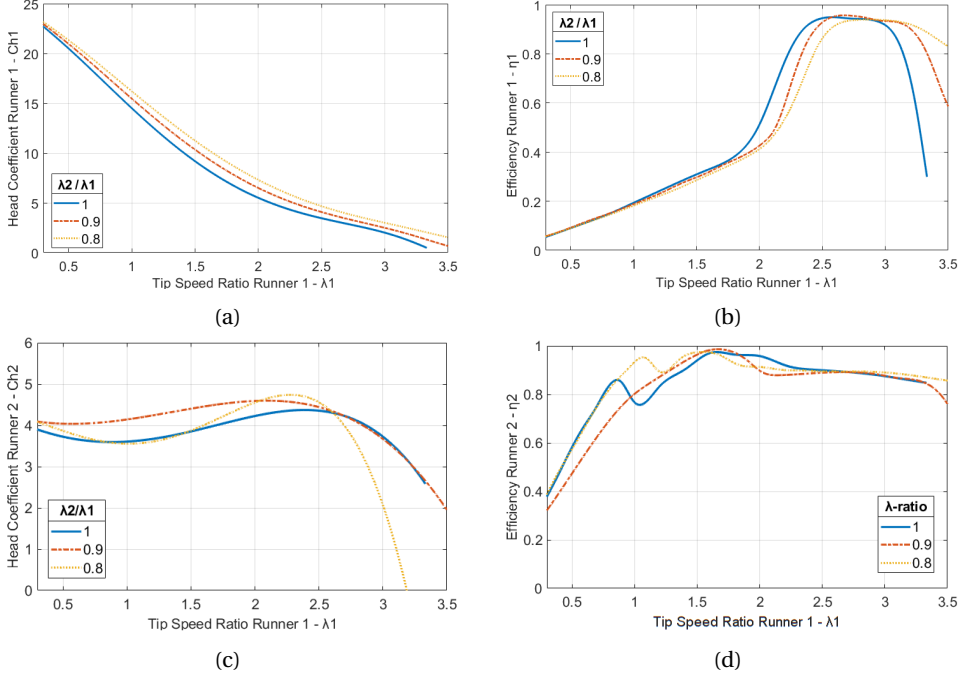


Figure 3.4.: Characterisation of runners 1 and 2 in turbine mode as a function of the tip speed ratio of runner 1 for different operational speed ratios between the runners. a) Head coefficient runner 1. b) Efficiency runner 1. c) Head coefficient runner 2. d) Efficiency runner 2.

The corresponding characterisation curves in pump mode are shown Figure 3.5. The range of tip speed ratios in which the RPT operates in pump mode differs from turbine mode. Both runners show fairly linearly increasing head coefficients with increasing tip speed ratios. However, the dependency of runner 2, the downstream runner in pump mode, on the ratio between the rotational speeds, is more significant. Above tip speed ratios of around 5, less stable trends for the head coefficients and a performance dropoff can be observed. Both runners show high efficiencies of around 0.9, with runner 1 peaking at 0.92. The downstream runner 2 also shows a steep dropoff in efficiency below tip speed ratios of 3–3.5 depending on the ratio between the rotational speeds of the runners.

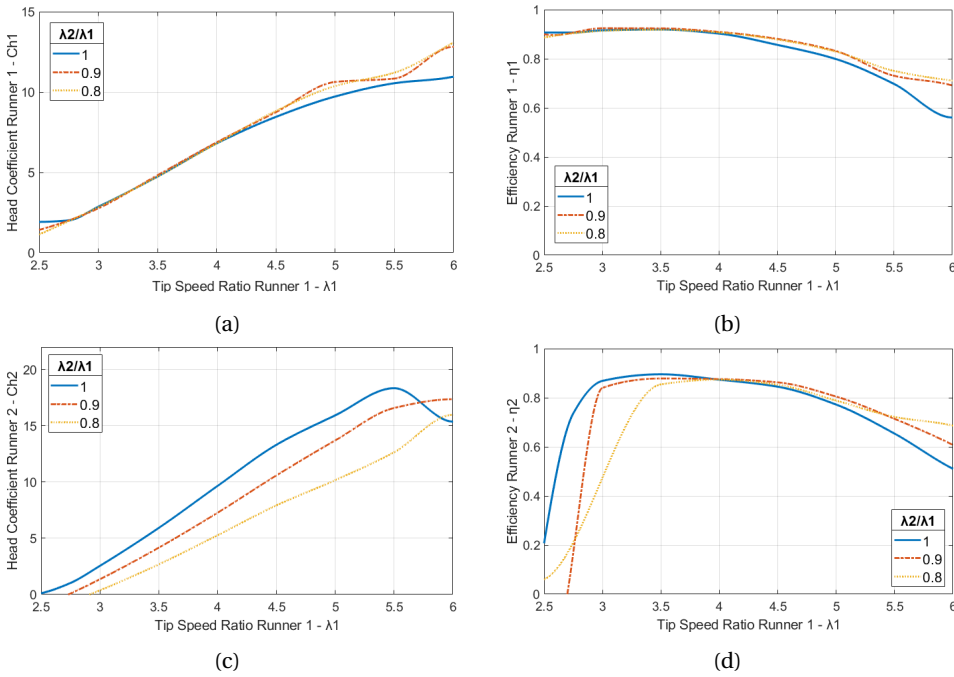


Figure 3.5.: Characterisation of runners 1 and 2 in pump mode as a function of the tip speed ratio of runner 1 for different operational speed ratios between the runners. a) Head coefficient runner 1. b) Efficiency runner 1. c) Head coefficient runner 2. d) Efficiency runner 2.

3.3. HYDRAULIC MODEL

3.3.1. 1-D COMPRESSIBLE FLOW MODELLING IN PUMPED HYDRO STORAGE CONDUITS

Different approaches are used to model the flow behaviour inside the conduits of PHS plants depending on the required accuracy and computational performance. Approaches that neglect the compressibility of water are computationally efficient, however, if transients are to be investigated, compressibility effects have to be considered [182]. Additionally, a choice can be made between only considering the axial flow direction or employing a two or three-dimensional approach. It needs to be considered though, that the computation gets exponentially more complex with added dimensions. For this model, a one-dimensional compressible flow approach is therefore chosen. Due to the enlarged mass flow rates of water in low-head applications and desired fast changes of operating points, compressibility effects are covered though. To obtain the pressure and fluid axial velocity along the conduit, the coupled coupled partial differential equations shown in Eq. 3.4 and Eq. 3.5 are chosen [183–185]. These are based on the fundamental equations of conservation of mass and momentum and are commonly known as water hammer equations.

$$\frac{\partial H}{\partial t} = -U \frac{\partial H}{\partial x} - \frac{a^2}{g} \frac{\partial U}{\partial x} \quad (3.4)$$

$$\frac{\partial U}{\partial t} = -U \frac{\partial U}{\partial x} - g \frac{\partial H}{\partial x} - S \quad (3.5)$$

Here H is the pressure head, U the fluid velocity, a the effective pressure wave velocity in the fluid, g the gravitational acceleration, D the conduit's inner diameter and S represents a term to account for friction losses. If the pressure wave velocity in the pipe is much greater than the fluid velocity and the conduit is cylindrical, the convective terms given by $-U \frac{\partial H}{\partial x}$ and $-U \frac{\partial U}{\partial x}$ can be neglected [186]. The speed of pressure waves within the conduit depends on the stiffness of the pipe and the compressibility of the liquid [187]. In a stiff conduit of a hydroelectric power plant with potentially some gas bubbles forming due to cavitation caused by pressure transients, the pressure wave velocity is typically between 700 and 1200 m/s [188]. For all applications of the model considered in this work, the fluid velocity will not exceed 8 m/s.

While only considering steady friction is sufficient to estimate the initial magnitude of a pressure transient in the system, an additional unsteady friction term will improve the simulated dissipation of such a pressure wave over time [189]. The equations resulting from these changes and adapted to represent flow rates rather than fluid velocities are shown in Eq. 3.6 and Eq. 3.7.

$$\frac{\partial H}{\partial t} = -\frac{a^2}{gA} \frac{\partial Q}{\partial x} \quad (3.6)$$

$$\frac{\partial Q}{\partial t} = -gA \frac{\partial H}{\partial x} - S_s - S_u \quad (3.7)$$

The additional Q , A , S_s and S_u are volumetric flow rate, cross-sectional area of the conduit, and the representative terms for steady and unsteady friction losses. The steady friction losses can be approximated using the Darcy-Weisbach formulations using the friction factor f as shown in Eq. 3.8 [190]. For the unsteady friction losses, a one-coefficient model, k , of an instantaneous acceleration-based method is used as shown in Eq. 3.9 [189]. The fluid accelerations that induce these losses, are calculated from the averaged cross-sectional values. With values between 0.015 and 0.06 m/s² the coefficient k has been shown to closely match experimental results [189].

$$S_s = \frac{fQ|Q|}{2DA} \quad (3.8)$$

$$S_u = \frac{k}{g} \left[\frac{\partial Q}{\partial t} + \text{Sign}(Q)a \left| \frac{\partial Q}{\partial x} \right| \right] \quad (3.9)$$

NUMERICAL SOLUTION METHOD

To solve the fluid equations, the partial differential equations are discretised in space and converted to ODEs using a central scribed finite difference method. The pressure and flow rates are solved along the spatial dimension and consecutively

for the temporal steps. The resulting grid of nodes is illustrated in figure 3.6. The temporal increments are indicated by the subscript i and the spatial by j .

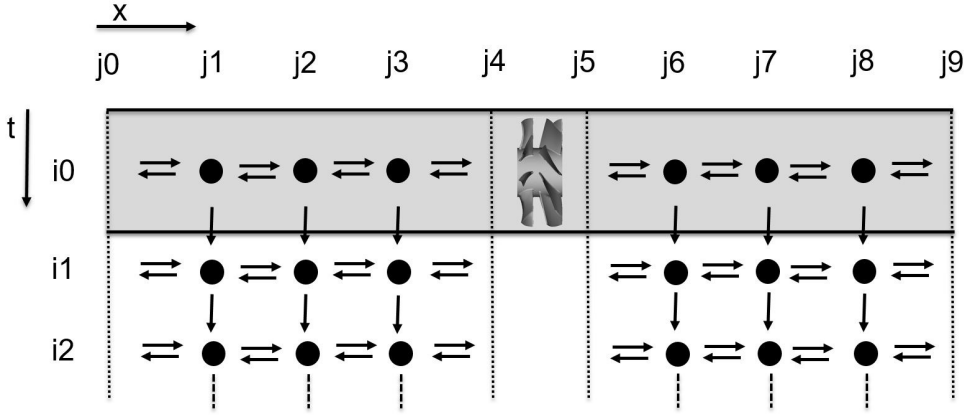


Figure 3.6.: Node grid used for spatial and temporal discretization.

Using the central finite difference method the spatial derivatives $\frac{\partial Q_{i,j}}{\partial x}$ and $\frac{\partial H_{i,j}}{\partial x}$ are replaced by the second-order approximations $\frac{Q_{i,j+1} - Q_{i,j-1}}{2\Delta x}$ and $\frac{H_{i,j+1} - H_{i,j-1}}{2\Delta x}$ with Δx referring to the spatial distance between nodes. The finite difference method is chosen due to its simplicity and ease of implementation when applied to sets of coupled equations with one of the disadvantages being the requirement of a regular node grid [191].

BOUNDARY CONDITIONS

To solve for the pressure head and flow rate at the boundaries of the chosen computational domain, the method of characteristics is used resulting in algebraic equations describing the relationship between pressure head and flow rate. The basic characteristic equations for upstream and downstream boundaries are given in Eq. 3.10 and Eq. 3.11 [189].

$$Q_{i,j} = Q_{i,j+1} - \frac{gA}{a} H_{i,j+1} - \frac{f}{2DA} \Delta t Q_{i,j+1} |Q_{i,j+1}| + \frac{gA}{a} H_{i,j} \quad (3.10)$$

$$Q_{i,j} = Q_{i,j-1} + \frac{gA}{a} H_{i,j-1} - \frac{f}{2DA} \Delta t Q_{i,j-1} |Q_{i,j-1}| - \frac{gA}{a} H_{i,j} \quad (3.11)$$

If the reservoir is assumed to be large enough that travelling pressure waves would be entirely absorbed, non-reflecting boundaries can be implemented. To do so, the terms accounting for the pressure difference between the boundary and the neighbouring node are removed. In a friction-less system, this leaves the boundary flow rate to be equal to the flow rate at the neighbouring node.

When using characteristic equations, the spatial and temporal steps have to be chosen correctly to ensure a stable solution and hence accurately represent a

pressure wave propagating through the conduit. Neglecting non-linear terms, the Courant condition shown in Eq. 3.12 can be used to determine the appropriate spatial distance between nodes for a given time step or vice versa [185]. E.g. assuming a maximum wave velocity of 1480 m/s combined with a spatial distance between nodes of 0.148 m would result in 0.1 ms timesteps. To reach a sufficient level of accuracy a minimum node density is required. In an iterative process the spatial distance can be reduced until no further improvements are achieved.

$$\Delta x \geq a \Delta t \quad (3.12)$$

Lastly, hydraulic losses outside the computational domain, H_l , are included at the boundaries via minor loss coefficients k according to Eq. 3.13 and Eq. 3.14 with H_{res} as the reservoir pressure head and $H_{i,j}$ as the pressure head at the boundaries.

$$H_l = \sum k \frac{u^2}{2g} \quad (3.13)$$

$$H_{i,j} = H_{res} - H_l \quad (3.14)$$

3.3.2. RESERVOIR AND VALVE MODEL

When modelling the proposed low-head pumped hydro storage plant, the lower reservoir will empty and fill and consequently cause slow changes in the water level based on the conservation of mass. The changing height in the reservoir H_{res} is calculated as in Eq. 3.15 by the in- or outgoing flow rate and the reservoir area A_{res} , which is assumed uniform along the reservoir's height.

$$\frac{dH_{res}}{dt} = \frac{Q}{A_{res}} \quad (3.15)$$

The valve actuator response is modelled using a first-order linear ordinary differential equation as given in Eq. (3.16) with γ as the valve opening angle, γ_{com} as the valve opening angle command and T_v as the valve time constant.

$$\frac{d\gamma}{dt} = \frac{1}{T_v}(\gamma_{com} - \gamma) \quad (3.16)$$

The valve is coupled to the conduit model via a minor hydraulic loss coefficient for the valve, k_v , as a function of its opening angle. This function is adapted depending on the application of the model and the valve used. For modelling the full-scale plant, a gate valve is assumed with the relationship between opening angle and loss coefficient shown in Eq. 3.17 and Figure 3.7 as per [192]. Here, the opening angle ranges from $0 \leq \gamma < 1$, with zero corresponding to a fully open valve.

$$k_v = \frac{\frac{1348}{75}\gamma^3 - \frac{41}{5}\gamma^2 + \frac{128}{75}\gamma}{(1 - \gamma)} \quad (3.17)$$

Different valve configurations can also be included in the model, such as the use of a butterfly valve as an alternative. The relationship between loss coefficient and

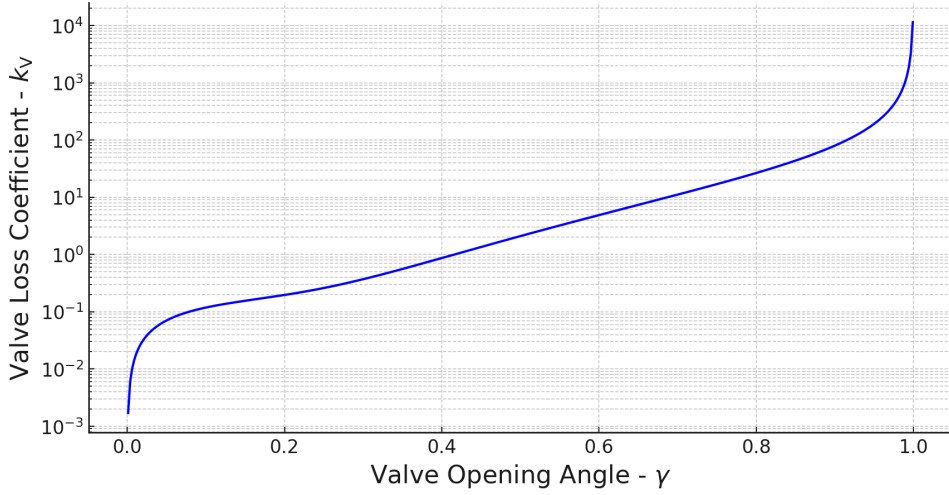


Figure 3.7.: Valve loss coefficient k_v as a function of the valve opening angle γ for the gate valve of the full-scale system.

valve angle is shown in Eq. (3.18) and Figure 3.8. Here, an opening angle of 90° corresponds to a fully open valve and 0° to a fully closed one.

$$k_v(\gamma) = \exp(-4.2351 \ln(\gamma) + 18.1149) \quad (3.18)$$

3.4. DRIVETRAIN MODEL

The proposed system employs a variable speed direct drive without a gear-ratio between the two runners and their respective axial-flux PMSM. The electric machines are situated in bulbs directly adjacent to the runners. Neglecting flexibility in the drivetrain components, the rotational speeds can be assumed constant along the driveshaft between runners and motor-generators. This allows to model each drivetrain as an individual rigid body with an equivalent rotational inertia to account for the different rotating parts leading to Eq. (3.19) and Eq. (3.20) [193].

$$J_1 \frac{d\omega_1}{dt} + \tau_{f1} = \tau_{h1}(\lambda_1, \lambda_2) - \tau_{m1} \quad (3.19)$$

$$J_2 \frac{d\omega_2}{dt} + \tau_{f2} = \tau_{h2}(\lambda_1, \lambda_2) - \tau_{m2} \quad (3.20)$$

Here $J_{1,2}$ denote the rotational mass moments of inertia, $\omega_{1,2}$ as the rotational speeds, $\tau_{h1,2}$ as hydraulic torques, $\tau_{m1,2}$ as the electric machine torques and $\tau_{f1,2}$ as the friction torques. The conduit model is coupled to both of these drivetrains via the hydraulic torques which are obtained from the RPT characterisation as described

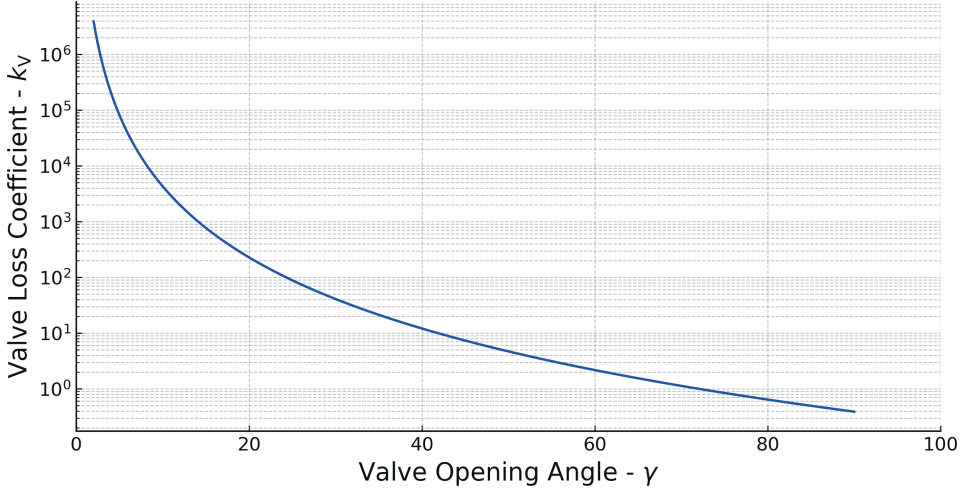


Figure 3.8.: Valve loss coefficient k_v as a function of the valve opening angle γ for a butterfly valve.

in section 3.2. The electric machines and control are coupled via the machine torques.

To facilitate a general description of the drivetrain's friction, an empirical non-linear model is considered to give the most convenient representation of the friction torques $\tau_{f1,2}$ as a function of the rotational speeds according to Eq. 3.21 and Eq. 3.22.

$$\tau_{f1} = B_1 + C_1 \omega_1^{D_1} \quad (3.21)$$

$$\tau_{f2} = B_2 + C_2 \omega_2^{D_2} \quad (3.22)$$

Here, $B_{1,2}$ are the static friction coefficients, $C_{1,2}$ the linear dynamic coefficients and $D_{1,2}$ the non-linear dynamic coefficients. For the full-scale system no empirical data is available. The friction torque model is therefore simplified to only contain the linear dynamic coefficient determined as a percentage of the nominal torques at the nominal rotational speeds.

3.5. ELECTRIC MACHINES AND CONTROL

3.5.1. CONTROL OVERVIEW AND TOPOLOGIES

Due to the RPT configuration utilising two individual runners integrated in separate drivetrains, a total of three control degrees of freedom are available to reach a desired operating point. These are the two rotational speeds of the runners and the opening angle of the flow control (inlet) valve. By adjusting these control parameters,

varying power setpoints can be reached for a given available gross head. To evaluate if all three control degrees of freedom are required, four control topologies are assessed. These are shown in Figure 3.9.

		Speed ratio (ζ)	
		Fixed	Variable
Inlet valve (k_v)	No	Topology 1	Topology 2
	Yes	Topology 3	Topology 4

Figure 3.9.: Overview of the four different control topologies based on the three control degrees of freedom - the rotational speeds of both runners and the opening angle of the valve. [194] ©2024 IEEE

The inlet valve can either be used to adjust the head-flow conditions over the RPT or kept fully open. Additionally, the ratio between the rotational speeds can either be chosen to be adjustable or fixed. Out of the four options, only topology 4 offers the use of all three degrees of freedom. To evaluate if this more complex control approach is required and to obtain the combination of these parameters, rotational speed of runners 1 and 2 as well as the valve opening angle, that reach the highest efficiency for all possible power setpoints at any given head, the steady-state RPT characterisation is used in combination with approximations of the hydraulic and drivetrain losses of the system. A detailed description of this assessment is given by Truijen et al. [194].

Based on these calculations, it is concluded that topology 4 offers an improved efficiency in parts of the operating range compared to the other control topologies. The resulting rotational speeds and valve opening angles to reach the operating points offering the highest efficiency are stored in lookup tables. The highest efficiency for each possible operating point and their corresponding control parameters are given in Appendix A.1.

When conducting energy balancing simulations, the choice of power setpoint for any given head during the storage cycle is based on the setpoint offering the highest efficiency. In turbine mode, this correlates with the maximum power available. Conversely, in pump mode, the highest efficiency points lie between the minimum and maximum power. However, if the efficiency difference between two operating points is under one percent, roughly the error margin of the RPT characterisation, the point with the highest power is preferred.

3.5.2. AXIAL-FLUX PMSMs AND CONTROL ARCHITECTURE

The axial flux PMSMs are modelled in the rotating dq reference frame (Figure 3.10), where the stator inductances, the armature reaction, the stator losses and the iron losses (comprising eddy current and hysteresis losses) are included [158]. Figure 3.11 visualises the applied control architecture. Here, the circumflex ' \wedge ' indicates a setpoint for a certain variable. From the lookup table discussed in section 3.5.1, the rotational speed setpoints $\hat{\omega}_{1,2}$ and valve angle $\hat{\gamma}$ can be found that reach the power setpoint at the current head with the highest efficiency. For each machine, the speed setpoint is fed to a cascaded speed controller. Based on the difference between the speed setpoint $\hat{\omega}$ and the measured speed ω , a first PI-controller defines the torque setpoint τ_m . Next, this machine torque is controlled using field oriented control. Here, the i_d current is regulated to zero, resulting in a directly proportional relation between the i_q current and the machine torque. Therefore, a torque setpoint $\hat{\tau}_m$ from the speed PI-controller directly translates to a current setpoint \hat{i}_q . Based on the difference between the $\hat{i}_{d,q}$ current setpoints and the measured current $i_{d,q}$, PI-controllers define the applied voltages $v_{d,q}$.

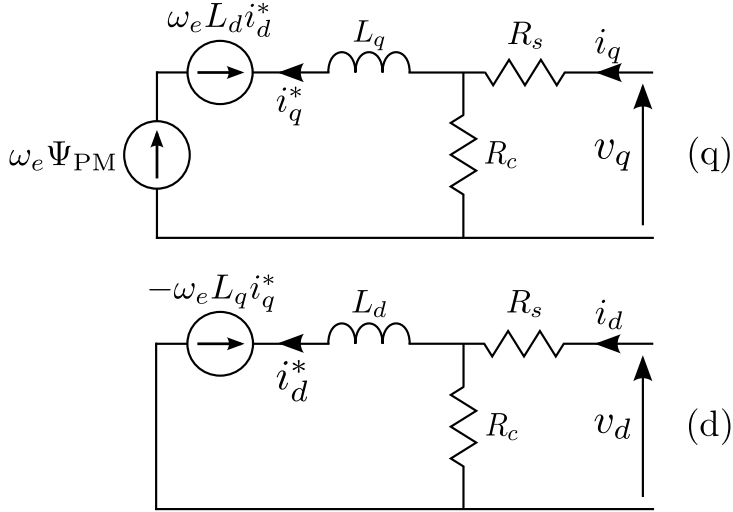


Figure 3.10.: Equivalent scheme of an axial-flux PMSM in the rotating dq reference frame.

These cascaded PI-controllers are tuned by shaping the step response in terms of rise time, settling time and overshoot of the torque and speed setpoints. Additionally, in order to ensure stability and robustness, the parameters are tuned to have a gain and phase margin of respectively > 10 dB and $> 45^\circ$ over the operating range. Although this guarantees a fast power response, it can cause fluctuations during the power response rise time. This is due to how the speed PI-controller uses the torque as a means to control the speed. If a new power setpoint (and thus new speed setpoints) is applied, the PI-controller outputs a torque that scales with the error between the new speed setpoint and the current speed. As this error is high initially,

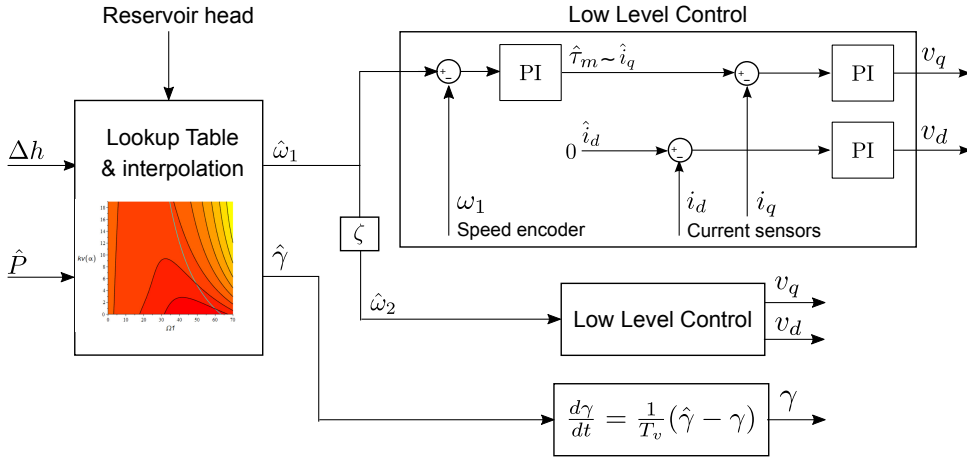


Figure 3.11.: Schematic overview of the applied control architecture.

the output torque setpoint is either very low or very high. As the power is a product of speed and torque, this means that the higher the torque actuation, the higher the power fluctuation during transition periods. As an example, if a power setpoint is increased in turbine mode and this corresponds to an increase in rotational speeds, the machine torques will decrease to allow the hydraulic torque to speed up the RPT, resulting in an initial power decrease before increasing to the higher power setpoint once the rotational speeds are reached. Therefore, a dynamic torque constraint is designed to limit the fluctuation of the power response to a predefined value P_{fl} . On a power setpoint \hat{P} change on time t_0 , the measured individual powers at this time $P_{1,2}(t_0)$ are saved. Next, the stored data in the lookup tables is addressed to find the individual powers $\hat{P}_{1,2}$ for the new power setpoint. Then the machine torque setpoints are constrained until the power setpoint is reached according to Eq. 3.23.

$$\frac{\min(P_{1,2}(t_0), \hat{P}_{1,2}) - P_{fl}}{\omega_{1,2}(t)} < \tau_{m1,2}(t) < \frac{\max(P_{1,2}(t_0), \hat{P}_{1,2}) + P_{fl}}{\omega_{1,2}(t)} \quad (3.23)$$

SUMMARY

Chapter 3 established the foundation for the numerical modelling of the low-head pumped hydro storage system, integrating a medium-fidelity time-domain model that captures the dynamic behaviour of key system components. This model incorporates the hydraulic conduit, the reversible pump-turbine with contra-rotating runners, and the independent drivetrain systems, allowing for detailed performance analysis under various operating conditions. The chapter detailed the development of a numerical framework to predict steady-state and transient responses, utilising CFD-derived performance characteristics for the RPT. Additionally, it addressed key modelling challenges and trade-offs. Following, as part of the experimental evaluation, the developed model is benchmarked against experimental results.

4

EXPERIMENTAL EVALUATION AND MODEL COMPARISON

This chapter presents a 50 kW experimental setup featuring a 1:22 scaled model of the previously introduced reversible pump-turbine. Unlike conventional pump-turbine technologies, the design utilises two contra-rotating runners, each integrated into fully independent drivetrains. This unique configuration, which allows for individual variable speed control of each runner, enables a wide range of operating conditions. The experimental setup serves to benchmark both, the steady-state RPT model, based on CFD simulations and the medium-fidelity time-domain numerical model developed in chapter 3. The latter captures the dynamic behaviour of the main components, integrating the flow inside the hydraulic conduits, the reversible pump-turbine, and the dual drivetrain system. A series of steady-state and dynamic experiments are conducted, with their results compared against the numerical predictions. Validating these numerical modelling approaches is a crucial step in the development of the technology for full-scale deployment. Lastly, the extended model is used to simulate transient dynamics during a shutdown sequence in turbine mode, offering new insights into the operational behaviour.

4.1. EXPERIMENTAL SETUP AND METHODS

4.1.1. HYDRAULIC FACILITIES WITH OPEN SURFACE TANKS

The experimental setup was constructed at the Leichtweiß-Institute for Hydraulic Engineering and Water Resources of the Technische Universität Braunschweig in Germany. Figure 4.1 provides a schematic overview of the setup, which includes two open surface tanks [195]. The tanks model the upper and lower reservoir found in pumped hydro storage applications. The lower tank features an adjustable spillway and both tanks are connected via two pipes; the first incorporating the reduced scale

Parts of this chapter are currently under review as J.P.Hoffstaedt et al. Analysis of a Contra-Rotating Pump-Turbine for Low-Head Applications: An Experimental Study and Numerical Comparison. Energy Conversion and Management.

contra-rotating reversible pump-turbine. The water level of the elevated tank is 9.7 m above the centre line of the RPT, whereas the level in the lower tank is between 1.25 and 2.25 m above the centre line. This results in a gross head of the system between 7.45 and 8.45 m. The pipes have a diameter of 50 cm, tapering to 27.6 cm via two contraction/expansion sections which are designed at a 4-degree angle to prevent flow separation. The total conduit length is 19.85 m. This configuration allows for a maximum flow rate of approximately 400 l/s. A butterfly valve is positioned between the elevated tank and the RPT, with the aim to enable manual control of the discharge flow, nevertheless, it can also alter the net head over the RPT. The setup is designed to enable testing in both turbine and pump modes. In turbine mode, the flow goes from the elevated tank to the lower tank through the RPT in pipe 1, while pipe 2 remains closed. In pump mode, pipe 2 is opened, which allows a flow from the elevated tank to maintain a stable water level in the lower tank. In both modes, water is pumped from an underground reservoir to the elevated tank via the laboratory's supply system. The elevated tank is equipped with a sharp-edged weir to maintain a consistent water level when sufficiently supplied with water discharge. This ensures a constant static pressure throughout the experimental runs.

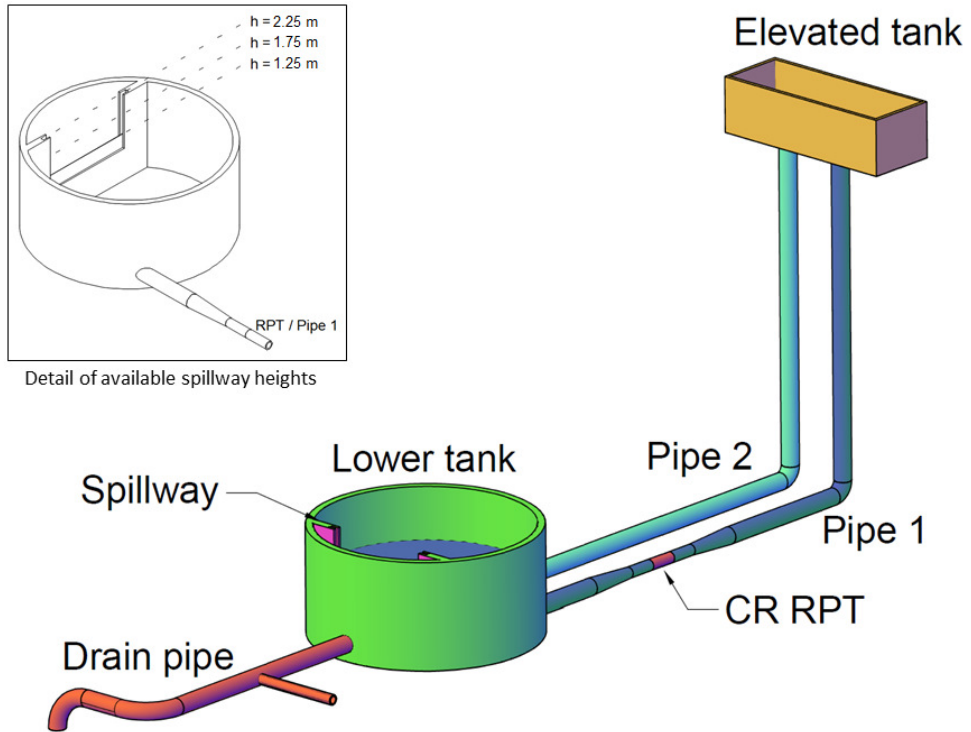


Figure 4.1.: Schematic overview of the experimental setup including the upper and lower reservoir, spillway, piping and contra-rotating RPT.

This experimental design is notable for its use of free surface tanks, solely relying

on gravity to provide the required hydraulic head, distinguishing it from other pump-turbine test configurations that predominantly utilise pumps to achieve this [196, 197]. The gravity-based system was chosen with the aim of reproducing more realistic in- and outflow conditions, assuming a reduced risk of swirl and pressure fluctuations typically induced by pump systems.

4.1.2. CONTRA-ROTATING REVERSIBLE PUMP-TURBINE

The scaled 1:22 contra-rotating RPT is geometrically nearly identical to the full-scale version described in section 3.2 and shown in Figure 3.2. Aside from scaling the diameter from 6 m to 27.6 cm, the only modification is the reinforcement of the runner blade roots to prevent deformation during testing. Akin to the full-scale version, the rotational speed of each runner can be controlled individually. The adjustable speed ratio between the runners allows an operating range encompassing ratios between 0.7 and 1.0. The additional degree of freedom emerging from the ability to control each of the runners individually means that for any given RPT net head, a variety of operating points can be achieved. In turbine mode, the RPT has a design flow rate of around 283 l/s and a mechanical power of 16.7 kW, with an expected efficiency of 90.3%. In pump mode, the design flow rate is about 375 l/s with a power rating of 55.4 kW at an efficiency of 88.5% [54].

To compare the experimental results with the numerical approach developed in chapter 3, the scaled-down RPT is characterised. For this purpose, a similar methodology as introduced in section 3.2 for the full-scale RPT is applied. Since no pressure probe can be placed in between the runners, a single stage RPT head coefficient is obtained instead of individual ones for each runner. Additionally, rather than relying on individual runner efficiencies, hydraulic torque coefficients are used for each runner. In the numerical model this is possible since the efficiencies of the runners are defined as the mechanical power, obtained from the rotational speeds and hydraulic torques, divided by the hydraulic power or vice versa, as given in Eq. 3.3. The head and hydraulic torque coefficients are calculated as shown in Eq. 4.1 and Eq. 4.2.

$$C_h = \frac{\rho g H_{\text{RPT}}(\lambda_1, \lambda_2)}{\frac{1}{2} \rho u^2} \quad (4.1)$$

$$C_{\tau 1,2} = \frac{\tau_{h1,2}(\lambda_1, \lambda_2)}{\frac{1}{2} \rho A R u^2} \quad (4.2)$$

Here, C_h is the head coefficient calculated from the stage RPT head, which is a dimensionless parameter that represents the ratio of the net head of the RPT to the dynamic head of the fluid. $C_{\tau 1,2}$ are the hydraulic torque coefficients - dimensionless parameters representing the ratio between the hydraulic torques of the runners, $\tau_{h1,2}$, and the available hydraulic reference torque. This coefficient allows for the assessment of the hydraulic performance of each runner independently of specific operating conditions.

The scaled runners are manufactured via 3D-printing using the aluminium alloy AlSi10Mg. After the printing process, both runners have undergone a process of

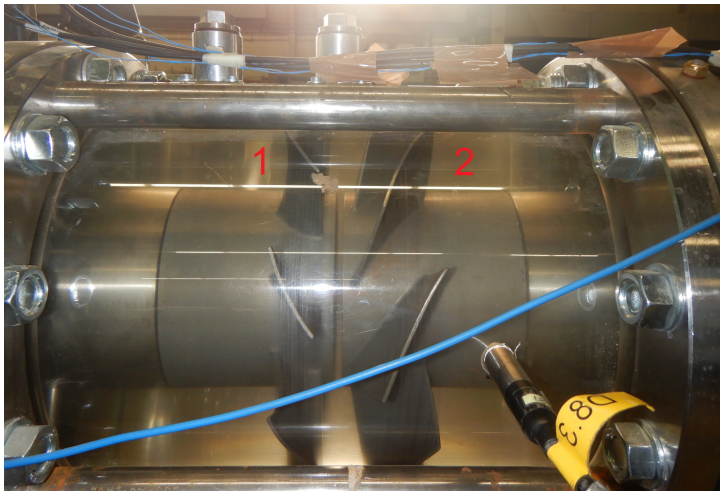
vibratory finishing, reducing the surface roughness to $3.58\mu\text{m}$ for runner 1 and $2.32\mu\text{m}$ for runner 2. A smooth runner surface is desirable due to an improved hydraulic performance.

4.1.3. DRIVETRAIN ASSEMBLY

Each runner of the RPT is powered by a set of power-electronic drives and electrical machines with a rated power of 37 kW each. To connect the runners to the electric machines, two sets of bevel gears with a gear ratio of 1:1 are included in the hubs to either side of the RPT. Due to the diameter of these bevel gears being constrained by the inner hub diameter, the maximum torque of each drivetrain is limited to around 200 Nm. A photograph of the RPT and drivetrain assembly is shown in Figure 4.2a. In the lower part of the image, the two electric machines and their drive shafts leading to the bevel gears can be seen. The RPT is mounted in a transparent piece of pipe made of acrylic tube. This has the advantage that the physical integrity of the runners and potential cavitation can be visually assessed. A drip feed lubricator is used to provide a constant flow of oil to the bevel gears and shaft seals. The out-flowing oil can be inspected for metal particles indicating excessive wear of the gears, which could be caused by the initial alignment of the drivetrain assembly having moved. The alignment of the electric machines, driveshafts, gears and runners is crucial to avoid such wear and the resultant friction torques but also to minimise vibrations. Additionally, the RPT was manufactured and assembled with a tip clearance of 0.5 mm, further necessitating very low tolerances on the whole assembly. Figure 4.2b shows a close-up image of the RPT within its acrylic tube.



(a)



(b)

Figure 4.2.: (a) Assembly of the RPT and drivetrains including the electrical machines (1), the RPT surrounded by an acrylic tube (2), hidden bevel gears (3), contraction and expansion tubes to either side (4), lower tank (5) and not visible flow meter, butterfly valve and elevated tank (6). (b) Close-up of the RPT, showing runner 1 (1) and runner 2 (2).

4.1.4. INSTRUMENTATION AND DATA ACQUISITION

The setup is equipped with a series of sensors to record data on the flow characteristics and machine operation. The instrumentation is listed in Table 4.1 and the location of the pressure probes and torque sensors illustrated in Figure 4.3 [195]. The 12 pressure probes, denoted p1–12, are located in six different axial locations. For each of these locations, the values given by the respective pair of probes are averaged. The difference between probes p7/p8 and p5/p6 is used to obtain the RPT net head. Additionally, probes are located just before (p3/4 and p9/10) and after (p1/2 and p11/12) the contraction and expansions tubes. An electromagnetic flow meter is located between the butterfly valve and the RPT. The electromagnetic flow meter was chosen due to its minimal disturbance of the flow. The torques are measured for each drivetrain using two torque transducers positioned next to the electrical machines. The variable frequency drives provide an estimation of the rotational speeds as well as the machine torques based on an internal machine model.

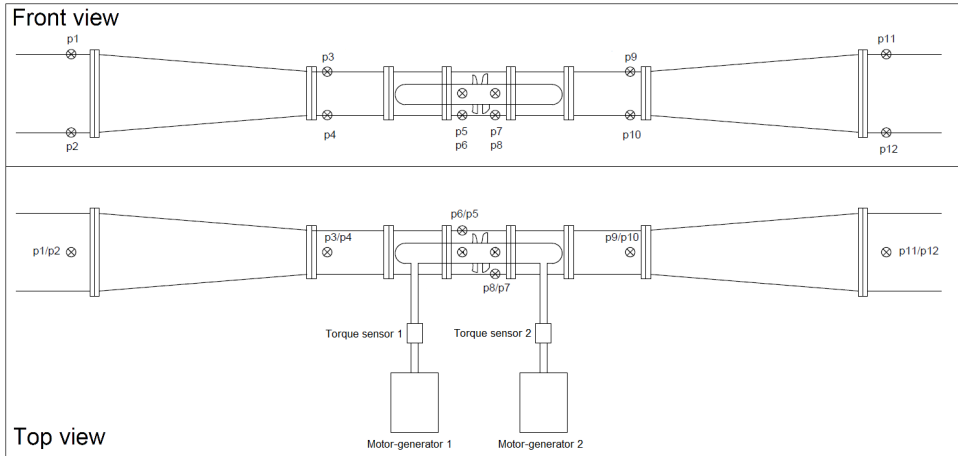


Figure 4.3.: Overview of the experimental instrumentation including 12 pressure probes (p1–12) and 2 torque sensors. Not depicted is an electromagnetic flow meter. Sketch not to scale.

The setup is operated to perform both steady-state and dynamic tests. During steady-state tests, a sampling frequency of 10 Hz is selected and each steady-state point is measured over at least 60 s. Dynamic cases are recorded at 1000 Hz. To minimise the potential error on the pressure measurements, all probes are (re-)calibrated at a maximum of one week prior to the tests. To account for a potential drift in the measured pressure data in between probe calibrations, each testing day a static pressure measurement is conducted with all probes, allowing to correct with the known height of the water column relative to the position of the individual probes.

Table 4.1.: List of the instrumentation used in the experimental setup.

Measurement	Instrumentation	Type	Nr	Meas. Range	Accuracy
Flow - Q	Krohne OPTIFLUX 2000	Electromagnetic flowmeter	1	0 – 600 l/s	$\pm 0.312\%$
Pressure - p1–6	Druck Limited PDCR 1830	Piezoresistive sensor	6	-0.5 – 0.35 bar	$\pm 0.1\%$
Pressure - p7,9,10,12	BD Sensors DMP 321	Piezoresistive sensor	4	0 – 2.4 bar	$\pm 0.25\%$
Pressure - p8,11	Druck Limited PDCR 830	Piezoresistive sensor	2	-0.5 – 5 bar	$\pm 0.1\%$
Torque - $\tau_{1,2}$	HBM T22	Strain gauge torque-transducer	2	0 – 500 Nm	$\pm 0.5\%$
Rotational Speed - $\omega_{1,2}$	Siemens Sinamics S120	Motor-Generator Drive	2	–	$\pm 0.04\%$

4.1.5. TESTING PROTOCOL AND OPERATING RANGE

There are two main limitations to be considered in this experimental setup. The first is the maximum torque caused by the limited diameter of the bevel gears. The second is the risk of cavitation due to the low hydraulic head at the low pressure side of the RPT. Within these limitations, a wide range of operating conditions have been tested with the experimental setup to evaluate the steady-state performance of the RPT. During these tests, the range of Reynolds numbers at the RPT is between $0.6 - 1.0 \times 10^6$. An overview of all tests is given in Table 4.2.

In turbine mode, a total of 92 operating points have been tested. Since the rotational speed of each runner can be adjusted separately, tests are conducted incrementally across the whole speed range of each runner and for varying speed ratios (ω_2/ω_1) between them. Additional operating conditions were reached by closing the butterfly valve to an angle of 45° (half-closed) and 22.5° (three-quarters closed) as well as by adjusting the spillway, situated in the lower reservoir, to vary the net pressure head over the RPT. However, by reducing the height of the spillway to 1.25 m, and with that the static head on the low-pressure side of the RPT, significant cavitation was audibly and visually observed on the runners. Therefore, the number of cases under these conditions was limited to avoid damage to the pump-turbine. It was also observed that for rotational speeds below 500 RPM, flow separation occurred, rendering the pressure measurements of the probes directly downstream of the RPT unusable. Consequently, no reliable RPT net head could be obtained for these operating points.

In pump mode, a total of 29 operating points were obtained. Pump mode testing is constrained due to several factors. Firstly, it is necessary to create a sufficient RPT net head to overcome the gross head, requiring a minimum rotational speed of both runners. Additionally, the torque limitations of the bevel gears limit the upper end of the operating range. For these reasons, the butterfly valve was not used in pump mode testing. Furthermore, akin to turbine mode testing, the risk of cavitation did not allow for a reduction in the spillway height.

In addition to the flow rate, the rotational speeds and the RPT net head measurements, the individual hydraulic torques of both runners are measured to characterise the RPT behaviour under different operating conditions. Torque measurements for both drivetrains are taken outside of the RPT assembly, adjacent to their respective electric machines. This means that the measured torques include the friction torques, mainly induced by the bevel gears. These have to be accounted in order to obtain the required hydraulic torques of the runners. Therefore, the friction torques between the instrumentation and the runners were characterised separately across the speed range of the runners. To gather the required data, the entire setup is drained and both runners incrementally accelerated in 100 RPM steps. At each step, the torque is recorded for a short period of time. In the absence of hydraulic forces, these measurements are used to obtain the friction torques under steady-state conditions.

The friction torque measurements required a lower and narrower range. Consequently, they were obtained from the power electronic drives instead of the dedicated torque sensors. The purpose of this is to reduce the noise of the

Table 4.2.: Overview of steady-state experimental tests. A total of 121 operating points, 92 in turbine and 29 in pump mode, were recorded.

Mode	ω_2/ω_1	ω_1 [RPM]	ω_2 [RPM]	Valve Angle [°]	Spillway Height [m]	Nr. of Points
Turbine	1.000	100-1100	100-1100	90	2.7	15
Turbine	0.900	100-1100	90-990	90	2.7	12
Turbine	0.900	800-1100	720-990	90	1.7	4
Turbine	0.800	100-1100	80-880	90	2.7	13
Turbine	0.800	500-1100	400-880	90	1.7	7
Turbine	0.752	100-1100	75.2-827.2	90	2.7	13
Turbine	0.752	842	632	90	1.7	1
Turbine	0.752	500-1100	376-827.2	45	2.7	7
Turbine	0.752	300-900	225.6-678.8	22.5	2.7	7
Turbine	0.700	100-1100	70-770	90	2.7	13
Pump	1.000	950-1100	950-1100	90	2.7	4
Pump	0.900	1050-1250	945-1125	90	2.7	7
Pump	0.800	1050-1250	840-1000	90	2.7	6
Pump	0.752	1100-1337	827.2-1005	90	2.7	6
Pump	0.700	1146-1350	802-945	90	2.7	6
Total Number of Points:						121

measurements and improve reliability. The measured friction torques were in the range of 1–6.5 Nm for runner 1 and 1–9.5 Nm for runner 2. This is within 2% of the measurement range of the torque meters (500 Nm).

4.2. FRICTION TORQUE CHARACTERISATION

The steady-state characterisation of the friction torques of each runner was performed through a regression analysis based on the dry friction test data as described in section 4.1.5. Figure 4.4 illustrates the range of the recorded raw data points at each rotational speed, their average and the corresponding regression curves for both runners. An empirical non-linear model was considered to give the most convenient representation of the friction torques $\tau_{f1,2}$ as a function of the rotational speeds according to Eq. 4.3.

$$\tau_{f1,2} = B_{1,2} + C_{1,2}\omega_{1,2}^{D_{1,2}} \quad (4.3)$$

Here, B_i are the static friction coefficients, C_i the linear dynamic coefficients, D_i the non-linear dynamic coefficients and ω_i the rotational speed of either runner 1 or 2. For runner 1, the spread of data for each rotational speed point is comparably low with the standard deviations ranging from 0.25 to 0.63 Nm for the individual rotational speeds. During the steady-state performance tests of the RPT, the torques for runner 1 range from a minimum of around 40 Nm to a maximum of 190 Nm. For the worst case scenario, applying the maximum deviation of the friction torque characterisation to the minimum torque, this leads to an error in the calculated

hydraulic torques of below 4%. For runner 2, there is a much larger spread due to noise and inaccuracies in the torque approximations by the drives. The standard deviations here range from 0.35 to 2.88 Nm. The torque range of runner 2 during the experiments is between 60 Nm and 180 Nm. For the worst case, this may cause an error below 7%. While the average expected error is much lower, the resulting uncertainty must be considered when comparing the experimental and numerical results.

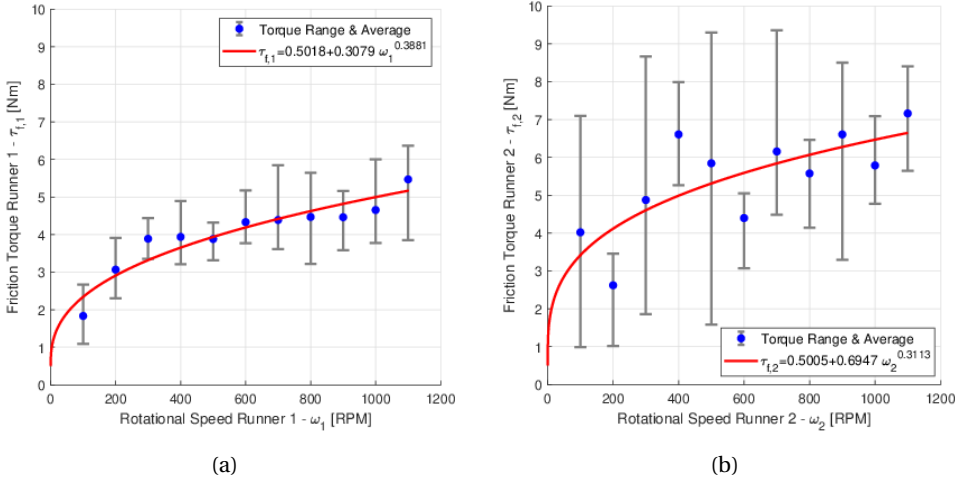


Figure 4.4.: Measured friction torques for runner 1 in (a) and runner 2 in (b) as well as their respective characteristic regression.

With the friction of both drivetrains characterised, the hydraulic torques of each runner are obtained by correcting the torques measured adjacent to the electric machines with the presented friction torque regression curves as a function of their rotational speed. In turbine mode, the respective friction torques are added to the measured torque and in pump mode subtracted.

4.3. STEADY-STATE RESULTS

During turbine mode testing, a maximum flow rate of 360 l/s was measured and a maximum mechanical power of 22 kW. The highest hydraulic efficiency measured during the experiments was 89%. In pump mode, a maximum flow rate of 370 l/s at a mechanical power of 42 kW was measured. The highest hydraulic efficiency measured in pump mode was 92%. The efficiencies and mechanical powers over the operating range of the RPT in turbine and pump mode are given in Appendix B.1. The significant differences in mechanical power between turbine and pump mode are mostly attributed to the hydraulic losses of the experimental setup. The hubs and struts adjacent to the RPT introduce considerable losses that reduce the generated power in turbine mode and increase the required power in pump mode. The

maximum efficiencies between turbine and pump mode for the proposed RPT are comparable. However, efficiencies for RPTs generally differ between operating modes since the hydraulic geometry is typically designed and optimised for either turbine or pump mode operation. In turbine mode, energy is extracted from the flow while in pump mode energy is introduced. This leads to differing flow characteristics which is a major challenge when designing a RPT capable of a high performance in both modes [197, 198]. The contra-rotating RPT in this experimental setup has been designed specifically for pump mode, tested in turbine mode and then optimised for both [56]. At the best efficiency points, a hydraulic roundtrip efficiency of 82% is achieved. When accounting for additional hydraulic, mechanical, and conversion losses, this performance is still favourable compared to conventional pumped hydro storage plants, which commonly have roundtrip efficiencies ranging from 70% to 80% [21].

It should be noted though, that there are scaling effects to be considered when using scaled-down experiments to evaluate the performance of full scale hydraulic machinery. These stem from differences in viscous effects, the geometry and general layout of the test setup as well as variations in the surface roughness compared to a full-scale power plant [47]. However, on-site measurements of full-scale plants are difficult and can be inaccurate [46]. Scaled-down experimental testing is therefore an efficient and useful tool to compare numerical and experimental results and use the numerical modelling approaches, once validated, to evaluate the performance of potential full-scale systems. The comparison of the experimental and numerical results is based on the RPT heads and hydraulic torques of runner 1 and 2. These are given for turbine and pump modes in Figure 4.5. It should be noted that for the purpose of visual clarity these graphs include the results for the incrementally increasing rotational speeds for varying speed ratios. The additional results obtained by changing the opening angle of the valve and adapting the static head at the lower reservoir are not depicted. However, in the following comparison with the numerical results all operating points are used.

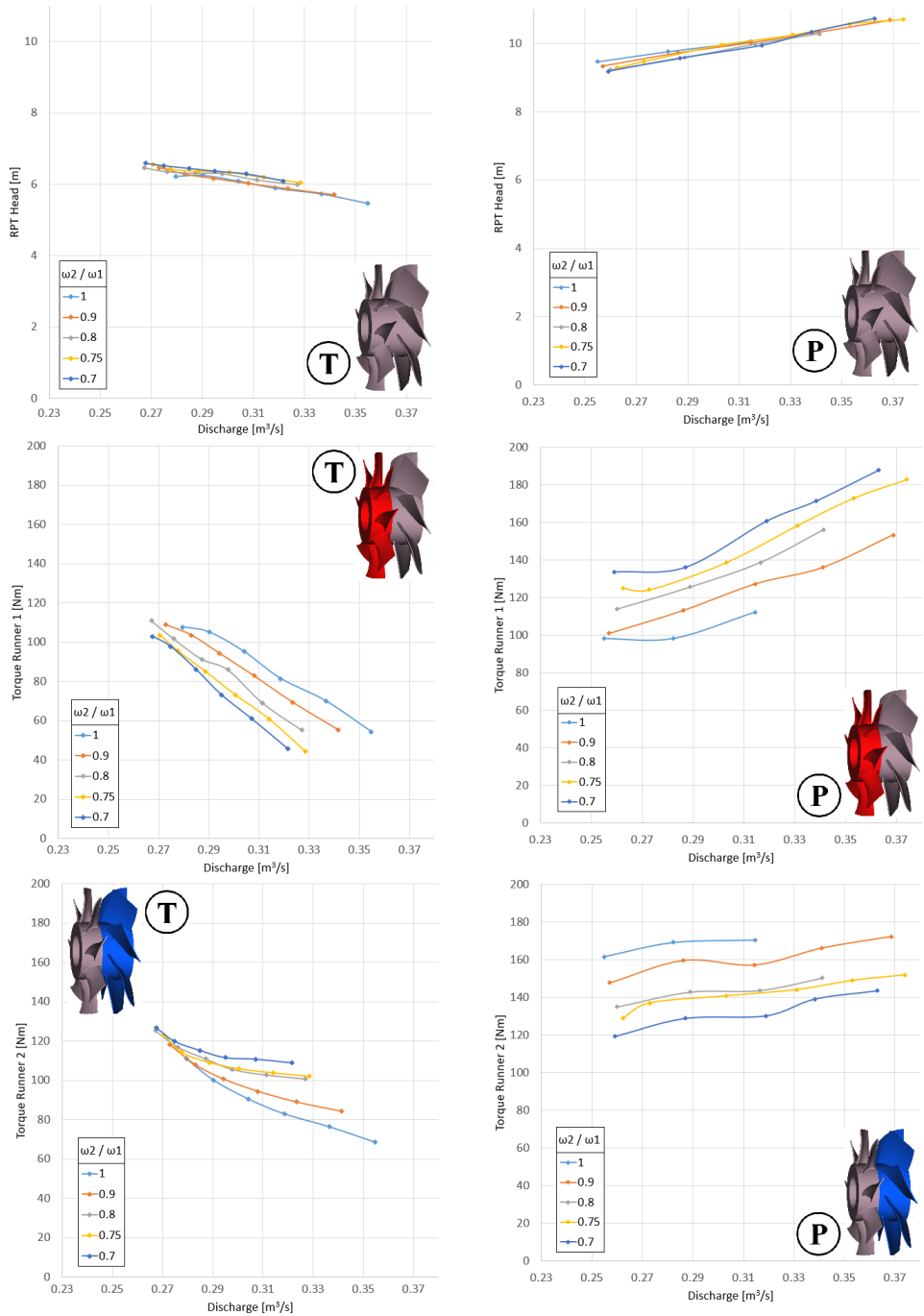


Figure 4.5.: Steady-state experimental results for the RPT heads and torques of runner 1 and 2 in turbine and pump modes. Turbine and pump operation are depicted with a T and P respectively, while runner 1 is in red and runner 2 is in blue.

The results for turbine mode are given on the left side of the figure and the pump mode results on the right. The different lines in the graphs represent the different speed ratios between runner 2 and runner 1.

The variations in RPT head are primarily determined by changes in hydraulic losses, which are largely attributed to the hubs and struts adjacent to the RPT. Since these hydraulic losses are directly proportional to the discharge, the RPT head decreases as discharge increases in turbine mode. Conversely, in pump mode, the RPT head must increase to overcome these rising hydraulic losses. While this relationship is non-linear, this is only partially visible here due to the relatively minor changes in RPT head. The curves for different speed ratios align closely, which is expected, as the relationship is governed by the discharge-to-head correlation.

The hydraulic torques of runner 1 and runner 2 in turbine mode are shown in the bottom left two sub-figures. Several interesting trends can be noted. Overall, it can be seen that runner 2 experiences higher torques compared to runner 1. While it rotates slower for the majority of the operating range, it is designed with a larger axial length compared to runner 1 and therefore experiences these higher torques with the aim to have a fairly even split in terms of power. Furthermore, it can be observed that lower discharges and their associated lower rotational speeds correspond to higher torques for both runners. Another clear observation is that the torques of runner 1 and 2 are closer to one another as they get closer to a speed ratio of one. In turbine mode, runner 1 is the downstream runner and its performance is heavily influenced by runner 2 upstream.

The hydraulic torques of both runners are shown on the right side for pump mode. Here it can be clearly seen that for the maximum rotational speeds and consequent discharges, the maximum torque of the bevel gears (200 Nm) is almost reached. The minimum torque occurred for runner 1, a speed ratio of 1 and the minimum discharge and RPT head. For the majority of the operating points, runner 2 contributes larger torques than runner 1. Contrary to turbine mode though, the fraction of torque that runner 1 contributes increases with decreasing speed ratios between the runners. This is to be expected since a reduced speed ratio reflects a reduced rotational speed of runner 2 and consequently reduced runner head. For speed ratios of 0.7 and partially for 0.75 and 0.8, runner 1 contributes a larger portion of the torque.

4.4. COMPARISON OF STEADY-STATE RESULTS TO THE RPT MODEL

Based on the hydraulic torque and RPT head data of the measured operating points, the head and torque coefficients are calculated. With the tip speed ratios of these operating points, the corresponding numerical coefficients are obtained from the RPT model. Figure 4.6 shows the comparison of the coefficients obtained experimentally and numerically.

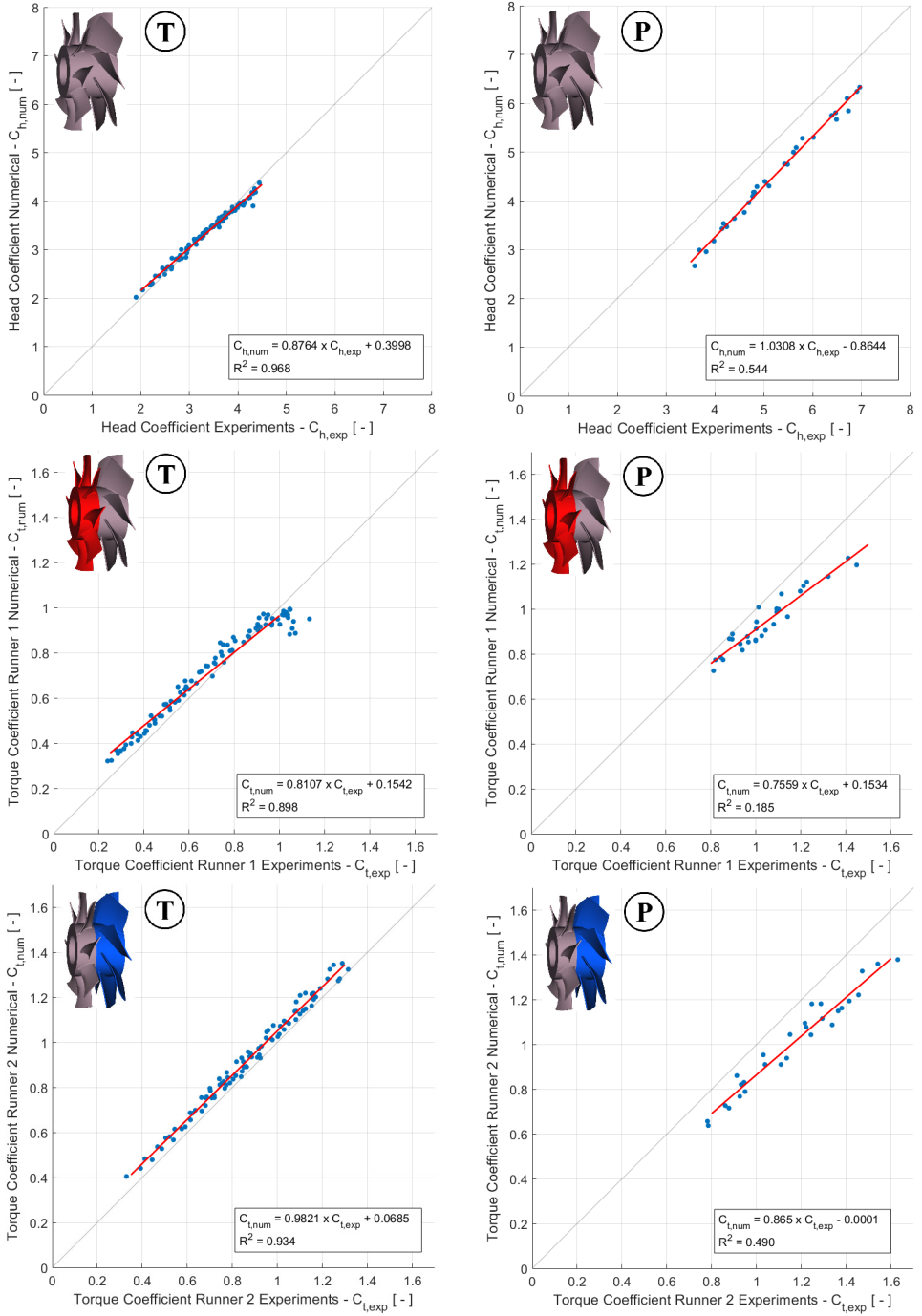


Figure 4.6.: Comparison of the steady-state head and torque coefficients of the experimental and CFD numerical results. Turbine and pump operation are depicted with a T and P respectively, while runner 1 is in red and runner 2 is in blue.

The three sub-figures on the left show the comparison of experimental and numerical head and torque coefficients in turbine mode. For the head coefficient there is a very good match between experimental and numerical results with correlation coefficient values R^2 of 0.968. A minor trend can be observed, changing from a numerical to an experimental head coefficient overestimation as it increases. Generally, higher head coefficients correspond to the lower end of the rotational speed range of the runners. As previously discussed, at these lower speed operating points, flow separation starts to occur which affects the pressure measurements and with that the measured RPT net head. The effect of flow separation can be observed more clearly for the comparison of the torque coefficients for runner 1. While the results show an overall good match up until torque coefficients of about 0.95, the compared points are less accurate above that value. These higher torque coefficients similarly correspond to lower rotational speeds and tip speed ratios at which flow separation affects the hydraulic torque. Notably, this effect is only visible for runner 1 as it is the downstream runner in turbine mode. The observed flow separation was only present at operating points far from the design range of the RPT though and is therefore not considered significant for evaluating its overall performance. Leaving out the deviation towards the higher end of the torque coefficient, there is a minor overestimation of the numerical torques compared to the experimental results. A similar trend can be observed for runner 2. Aside from potential inaccuracies in the CFD simulations, another likely cause of this overestimation may be an inaccuracy in the static component of the friction characterisation. However, with R^2 -values of 0.898 and 0.934, the numerical model can still provide sufficient representation over the operating range.

In pump mode, shown in right three sub-figures, the correlations are not as evident compared to turbine mode. For the head coefficients, a consistent offset of approximately 0.75 can be observed, although the slope of the correlation between experimental and numerical data remains highly accurate. Both comparisons of the torque coefficients in pump mode also show a worse correlation with both an offset and a linear deviation in the trend. Several factors likely contribute to these discrepancies between the numerical and experimental results. During the pump mode experiments, cavitation was observed throughout the operating range, which can lead to performance degradation in hydraulic machinery. This could explain the higher experimental torque values compared to the numerically predicted values needed to reach equivalent operating points. Additionally, the less accurate correlations in pump mode could be attributed to the proximity of RPT to the water inlet. In turbine mode, the flow reaches the RPT after a long straight section and the downwards pipe which reduces the risk of significant non-axial flow components being present. In contrast, the flow in pump mode may be more prone to disturbances due to the shorter upstream length. The CFD simulations, which assume uniform inflow conditions and use a relatively short computational domain, may not fully capture these non-uniformities in the experimental setup. This could cause discrepancies between the simulated and experimental flow behaviour. Although the friction torque characterisation might introduce inaccuracies, these should affect both turbine and pump modes similarly and therefore it is unlikely

that friction alone can account for the mismatch observed in pump mode. Finally, the proximity of the pressure probes to the RPT could introduce errors in measuring the experimental RPT head values.

4.5. COMPARISON OF DYNAMIC RESULTS WITH THE INTEGRATED SYSTEM MODEL

To evaluate the transient response of the system and benchmark the dynamic components of the numerical modelling approach, notably the hydraulic conduit and drivetrains, dynamic cases have also been tested with the experimental setup. The dynamic response of the flow rate is mainly driven by the balance between gross head, RPT net head and head losses of the experimental setup as well as the conduit water inertia. This inertia is defined by the dimensions of the conduit. Similarly, the dynamic response of the drivetrain is determined by the balance between the torques and the rotational mass moments of inertia of the individual drivetrains. To obtain accurate values for the rotational inertias of both drivetrains in the experimental setup, a characterisation test is performed. Both runners are accelerated in dry conditions to their maximum operating rotational speeds and then both motor torques are set to zero. Setting the hydraulic and generator torques in Eq. 3.19 and Eq. 3.20 to zero, the inertias are calculated based on the characterised friction torques and the change in rotational speed over time. Both inertias and all other relevant system parameters used in the simulations are given in Table 4.3.

Table 4.3.: Overview of simulation parameters.

Conduit length	L	19.85	m
Conduit diameter at RPT section	D_1	27.6	cm
Conduit diameter piping	D_2	50	cm
Pressure wave velocity	a	1000	m/s
Darcy friction factor	f	0.0127	-
Unsteady loss coefficient	k	0.04	m/s ²
Rotational inertia drivetrain 1	J_1	0.116	kg m ²
Rotational inertia drivetrain 2	J_2	0.145	kg m ²
Minor loss coefficients			
- Entrance	k_{en}	0.45	-
- Exit	k_{ex}	1.0	-
- Bend	k_{be}	0.2	-
- Bulbs (incl. expansion/contraction)	k_{b}	2 x 5.21	-
- Butterfly valve (fully open)	k_{v}	0.39	-
- Safety valve (fully open)	k_{v2}	0.4	-

The dynamic case chosen for the model validation starts in steady-state with runner 1 at 764 RPM (80 rad/s) and runner 2 at 611 RPM (64 rad/s). Both runners are then accelerated over the course of about one second to 1250 RPM (131 rad/s) and 1062.5 RPM (111 rad/s) respectively. Finally, both runners are decelerated to

their original operating points. The rotational speeds are shown in Figure 4.8. The valve remains fully open during the sequence. To simulate this case with the numerical model, the measured generator torques of both drivetrains are used as inputs to the drivetrain model. Additionally, the pressures recorded just outside the contraction and expansion tubes (see probes p1/2 and p11/12 in Figure 4.3) are used as inputs to the boundaries of the computational domain. The corresponding generator torques are shown in Figure 4.7. A moving average filter with a window size of 0.1 s has been applied to the data series.

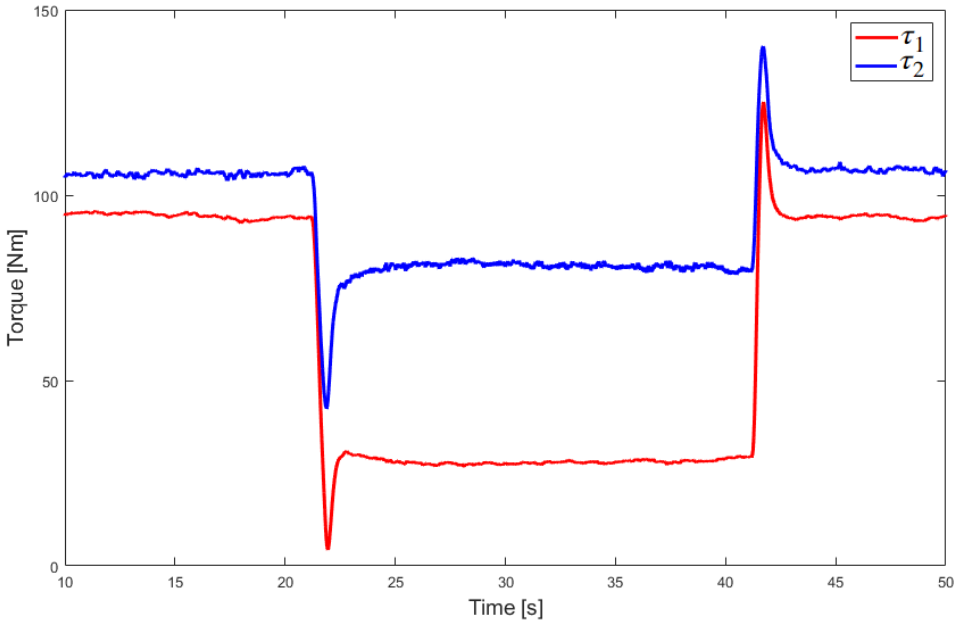


Figure 4.7.: Generator torques of both drivetrains. These are used as an input to the simulation of changing the operating point.

At the timestep $t = 21$ s, both generator torques are rapidly reduced to achieve the desired acceleration of the runners before increasing again to stabilise the rotational speeds at the new operating point. At $t = 41$ s, the reverse happens to decelerate the runners back to their original operating point. The resulting rotational speeds of runner 1 and 2 in the experimental test ($\omega_{1,Exp}$, $\omega_{2,Exp}$) and the simulation results ($\omega_{1,Sim}$, $\omega_{2,Sim}$) are shown in Figure 4.8.

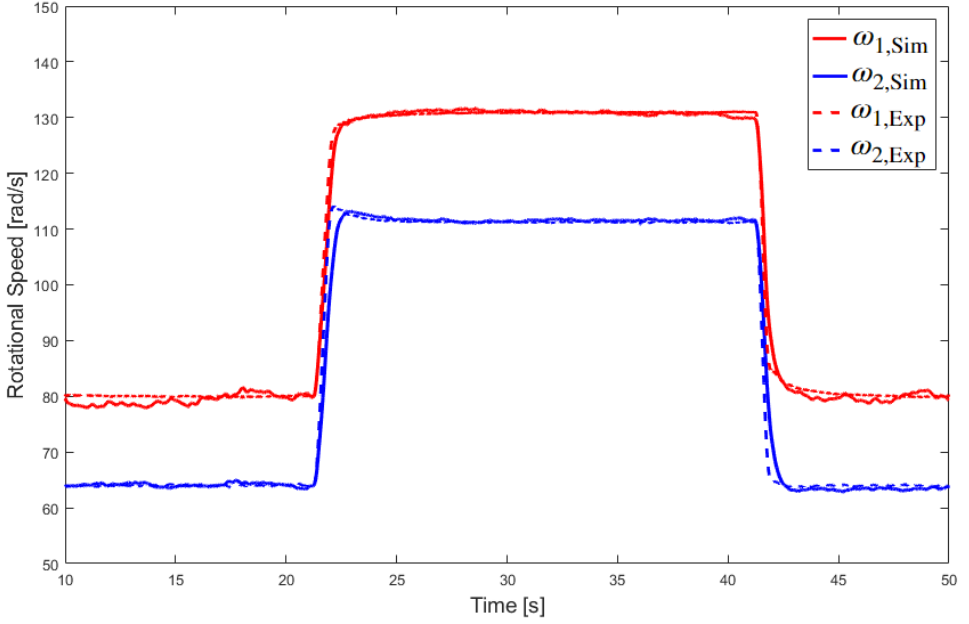


Figure 4.8.: Comparison of the rotational speeds of both runners during the experimental test and the simulation.

In order to focus on the validation of the dynamics, the friction torque coefficients were tuned in the numerical model to have the same conditions in steady-state for both rotational speeds. In steady-state conditions, minor deviations in the simulation results can be observed compared to the experimental results. The rotational speeds in the experiments are kept constant by the control algorithm of the drives, which adjusts the generator torques in response to load fluctuations caused by the turbulent flow around the hubs and struts adjacent to the RPT. These complex flow patterns are not captured in the 1-D modelling approach, resulting in the slight variations of rotational speeds. The dynamic response of the rotational speeds to the changes in generator torques show a close match between experiment and simulation. For both runners, a slightly slower response can be observed in the simulation. This indicates that the drivetrain inertias are marginally overestimated, likely caused by the uncertainty on the friction torque characterisation that is used to calculate the inertias of the drivetrains in the experimental setup.

The results for the flow rate of the experiment (Q_{Exp}) and simulation (Q_{Sim}) are

shown in Figure 4.9. At both operating points the steady-state values are closely matched with a difference at the higher operating point of $< 3\%$, reflecting the close match of the steady-state RPT model with the experimental results. The remaining difference is likely caused by a minor overestimation of the hydraulic losses. The dynamic response also shows the simulated flow reacting slightly faster than the experimental one. It is important to mention that the electromagnetic flow meter used to record the data uses a filter with a time constant of 0.1 s which effect also contributes to the slower response shown in the experimental data.

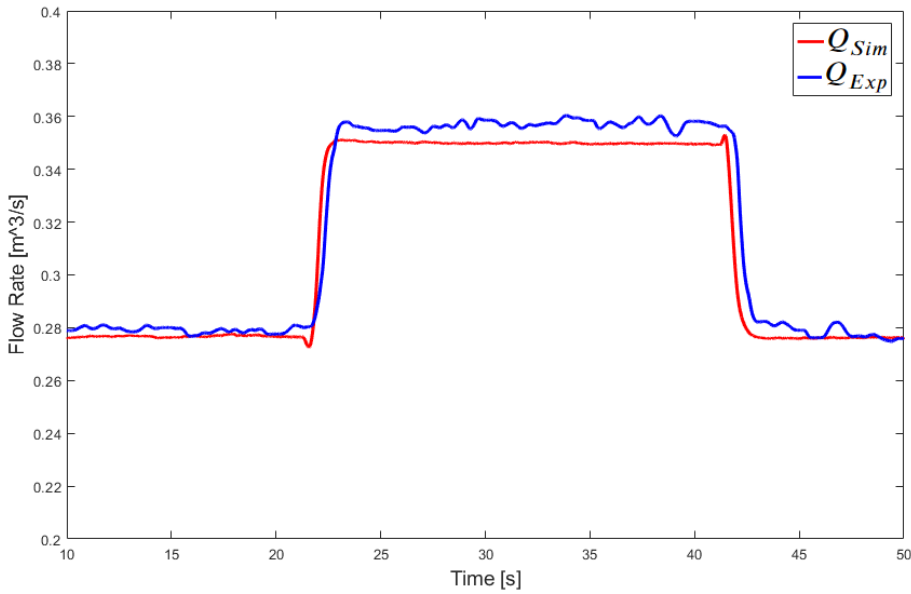


Figure 4.9.: Comparison of the flow rate during the experimental test and the simulation.

Overall, both major dynamic components of the numerical model show a close match compared to the experimental results. With the numerical approach partially validated, the model can be applied to a full scale system in order to simulate its dynamic behaviour when rapidly changing operating points. These changes in operating points correspond to adjusting its power setpoints and with that its capability to react so sudden grid demand fluctuations by providing frequency regulation services.

4.6. TURBINE SHUTDOWN SEQUENCE SIMULATION

Aside from changing its power setpoints, changing quickly between turbine and pump modes also improves the storage systems ability to react to changes in supply and demand of the grid. Such a mode switching sequence involves the deceleration and acceleration of both runners, reverting their direction of rotation and the closure

and opening of the flow control valve. As previously discussed, low-head systems have an increased conduit inertia compared to conventional high-head system of the same power rating and are therefore at higher risk of transient pressure effects, commonly known as water hammer. For the 1:22 scaled version of the storage system in the laboratory, a mode switching sequence has been selected. However, due to safety concerns regarding potential pressure spikes during valve closure, this sequence cannot be tested at the desired speed. The highest risk of water hammer occurs during shutdown in turbine mode, as the largest amount of water is decelerated by the valve. To evaluate the potential pressure spikes, this shutdown sequence is simulated at different rates of runner deceleration and valve closure. The selected shutdown sequence is shown in Figure 4.10.

4

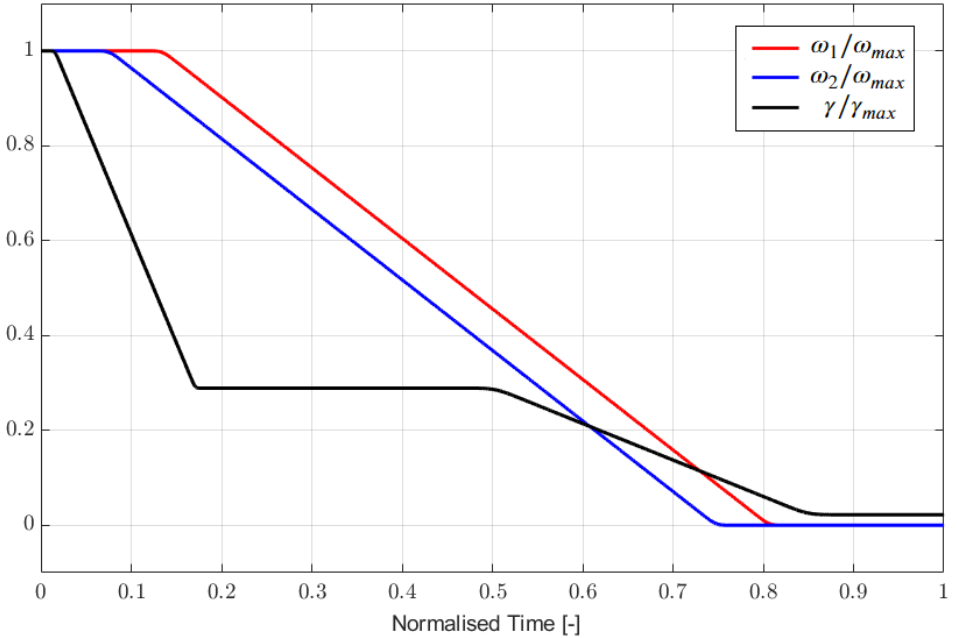


Figure 4.10.: Shutdown sequence in turbine mode including the rotational speeds of both runners and the valve opening angle.

The rotational speeds and the valve opening angle are normalised with their respective maximum values. The initial rotational speed of runner 1 is 842 RPM (~ 88 rad/s) and for runner 2 it is 633 RPM (~ 66 rad/s). This corresponds to a flow rate of 273 l/s. The time is also normalised with respect to the desired shutdown time for the whole sequence of 1.7 s. The valve is closed in two steps, starting just before both runners are decelerated and finishing after the runners are standing still. These rotational speeds and the valve opening angle are used as inputs to the numerical model. All other parameters remain unchanged as per the simulation carried out in Section 4.5. Since the experimental values of the pressures at the boundaries are not available, both upstream and downstream pipe sections are included in the computational model to account for the entire inertia of the water column. The sequence is simulated using its desired shutdown time as well as accelerated by a factor of 2, 4 and 10. The resulting pressure transients adjacent to the valve for these simulations are shown in Figure 4.11.

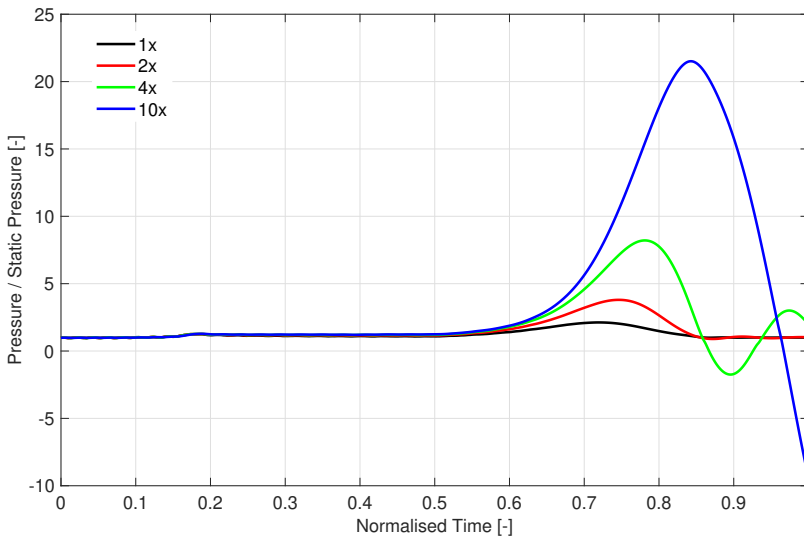


Figure 4.11.: Pressure adjacent to the valve for the shutdown sequence at original rate of change as well as accelerated by a factor of 2, 4 and 10.

The pressure head results of all simulations have been non-dimensionalised by dividing them by the expected static head, which in this case is 9.7 m. The initial two-thirds closure of the valve only results in a minor increase in pressure for all simulations. The major pressure fluctuations occur when the valve approaches full closure. At the desired sequence time, the simulation shows that the maximum pressure reaches roughly twice the static pressure. When doubling the rate of change, the maximum pressure reaches around four times the static pressure. Similarly, at four and ten times the rate of change, the pressure fluctuations have the potential to go up to eight and twenty-two times the static pressure respectively. At the desired

rate of change and even at double the speed, the maximum pressure does not appear to pose a risk to the system. Depending on the specification of the conduit and adjacent equipment, at higher rates, the maximum pressure may cause a risk to the integrity of the system. Additionally, at four and ten times the rate of change, a significant non-physical negative pressure transient can be observed following the positive spike and consequent reversing of the flow. This indicates column separation which occurs when the pressure in a conduit drops to or below the vapour pressure of the liquid, causing the liquid column to break and form vapour cavities. When the pressure recovers, these cavities collapse, creating high-pressure surges that can lead to damage to the conduit and equipment or even catastrophic failure.

5

AN EVALUATION OF LOW-HEAD PUMPED HYDRO STORAGE'S POTENTIAL TO PROVIDE ENERGY BALANCING AND FREQUENCY SUPPORT

The goal of this chapter is to assess the low-head PHS system's potential performance and dynamic behaviour over its full operating range during energy balancing, as well as the provision of frequency regulation services. The system used for this evaluation is schematically outlined in Figure 1.3. This evaluation is based on key indicators such as roundtrip efficiencies, the size of the required reservoir as well as the time required to supply a percentage of the systems nominal power as frequency containment reserves (FCR) among others. To achieve this, time-domain simulations of a grid-scale plant operation are conducted using the numerical model developed in chapter 3 and experimentally benchmarked in chapter 4. The simulations consider a case study in which a grid-scale version of the proposed storage plant is applied to a prospective storage site in the Dutch North Sea. Although economic and environmental investigations are not within the scope of this research, the results of this work can provide a basis and give insight for further analysis of these aspects.

In order to evaluate the system's performance over a full balancing cycle, including both the complete charging and discharging processes, the modelling approach neglects short-term dynamic effects to enable longer simulations with a minute timescale resolution. A sensitivity analysis is performed to investigate the effect of scaling the design power rating of the motor-generators on the overall performance

Parts of this chapter have been published in J.P.Hoffstaedt et al. Low-head pumped hydro storage: An evaluation of Energy Balancing and Frequency Support. IET Renewable Power Generation. 2024.

and size of the required reservoir for a given desired storage capacity. While the motor-generators are scaled, all other components, notably the RPTs, remain unchanged. This analysis is motivated by the capability of RPTs to operate beyond their initial design power rating, which is equivalent to the electric machines original rating. To investigate the dynamic behaviour of the plant during the rapid changes of operating points required to provide frequency regulation services, the integrated dynamic model is used. With this approach, simulations of the plant providing FCR to the electrical grid are performed. Using different initial states of charge and consequent operating conditions, these simulations help to understand the potential capabilities and limitations of the system to provide frequency regulation services.

5.1. THE PROSPECTIVE STORAGE SITE

The site for the case study is located in the Dutch North Sea as shown in Figure 5.1. This site is selected due to the Dutch government's commitment to developing several large-scale wind farms within the Dutch Exclusive Economic Zone [199][200]. This region is characterised by its favourable wind conditions and relatively shallow waters, which not only make it suitable for offshore wind farm installations but also for the addition of a large-scale low-head pumped hydro storage system. By creating an energy hub in that location with storage capabilities adjacent to renewable generators, several benefits can be achieved. Firstly, short distances between the storage plant and generators can significantly reduce the transmission losses and cost of infrastructure [38]. Secondly, additional interconnectors can be created to neighbouring countries bordering the North Sea region, further promoting the integration of renewable energy into the wider European grid. Lastly, by sharing parts of the civil structures with offshore wind farms, some of the high upfront cost can be shared.

Aside from the proximity to energy infrastructure, one of the main factors to consider for the site assessment is the local bathymetry, since the sea depth defines the available gross head. The proposed site has a sea depth of approximately 28 metres and is assumed constant for the whole area of the reservoir. The RPT has a runner diameter of 6 metres, with a conduit inlet/outlet diameter of 10 metres and a minimum submergence depth of 2 metres. Based on these dimensions, the available head range of this site is 2–16 metres. This assumes that the RPT units are not submerged beneath the seabed. While the RPT itself is hydraulically designed for heads of up to 20 metres, the 10 MW power rating of the motor-generators severely limits the usable head range, particularly the maximum head in pump mode. The tidal range for the proposed site is around 1.5 metres [201]. For this study, the tidal influence on the gross head is neglected since the impact of a tidal cycle with a minor tidal range should average out with time when asynchronous to the storage cycle of the plant. With each set of the proposed RPT being rated at 10 MW, the whole system is initially scaled to a design power capacity of 1 GW utilising 100 RPT units with a total net storage capacity of 4 GWh. Other factors for the site assessment include the composition of the local seabed since a large clay layer is required to seal the bottom of the reservoir and avoid excessive seepage. Wave

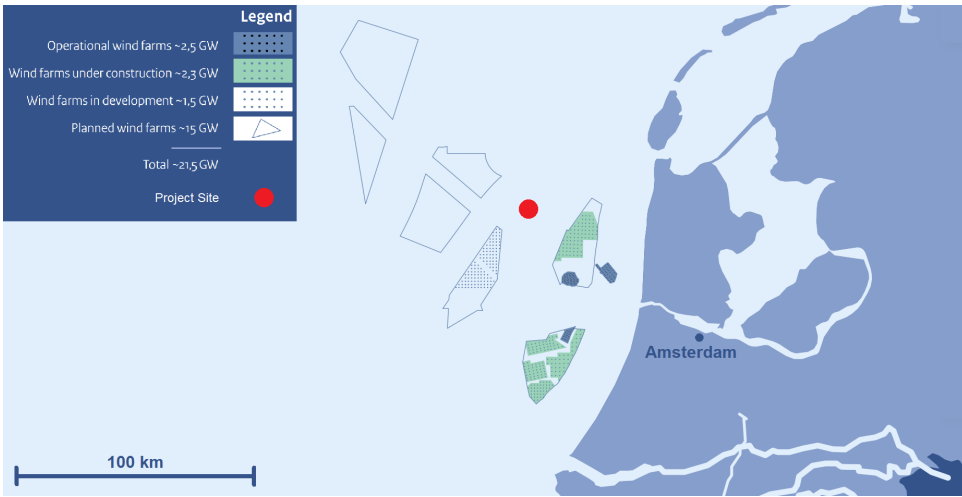


Figure 5.1.: Location of the site for the proposed low-head pumped storage plant in the Dutch North Sea, (adapted from [200]).

conditions that may restrict the construction process and type of dams used must also be considered, along with other legal and environmental aspects for which further information are given in [60].

5.2. PERFORMANCE AND SENSITIVITY ANALYSIS DURING ENERGY BALANCING

At the selected storage site, the maximum available gross head is 16 m. However, using the proposed PMSMs with a power rating of 10 MW each, the maximum achievable head in pump mode is only 9 m. The RPTs themselves have a much wider operating range though and can therefore be operated at higher hydraulic powers. Using the steady-state model, simulations of the full balancing cycle have been carried out including pump and turbine operation modes. Iteratively, the power rating of the electric machines is increased between 10 and 20 MW in 2.5 MW steps. The objective of these simulations is to evaluate the performance and operational conditions of the plant throughout the full cycle as well as the required reservoir size and cycle times. The major outputs are therefore the efficiencies of both runners, the total power output, the flow rate, the net head of the RPT unit and the water level in the lower reservoir. All simulation parameters related to major and minor hydraulic losses as well as the drivetrain losses remain consistent with those used in the dynamic simulations and can be found in Table 5.2 in section 5.3.

Increasing the power rating of the PMSMs correlates almost linearly with an increase in the maximum achievable gross head. Increasing the head range consequently results in a steep rise in storage capacity per unit area. This change in energy density as a function of PMSM power rating as well as the corresponding

change in roundtrip efficiency over the full cycle are shown in Figure 5.2. An overview of the results from the cycle simulations are also given in Table 5.1.

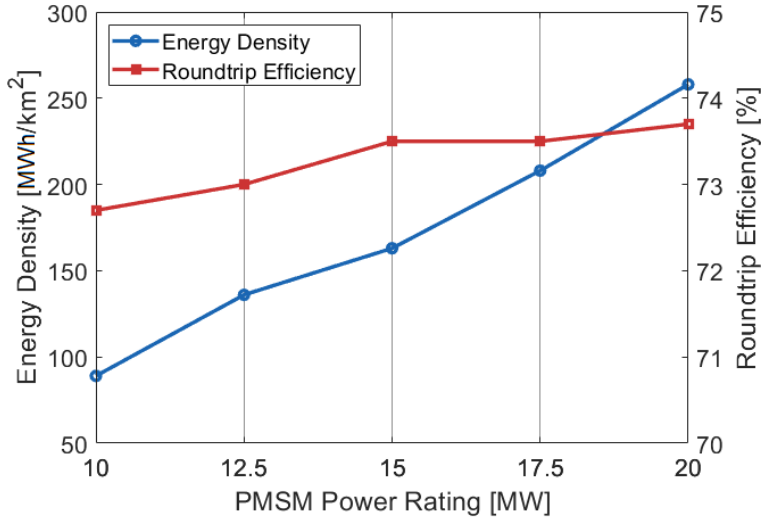


Figure 5.2.: Energy density and roundtrip efficiency of the pumped storage system as a function of the power rating of the electric machines.

By doubling the power rating of the PMSMs the energy density increases threefold while the roundtrip efficiency changes very little and even increases by about 1%. For the proposed plant with a desired net energy capacity of 4 GWh this means a reduction in reservoir area from 45.5 km² to 15.6 km². The average power per RPT unit also increases from 5.2 MW to 9.6 MW (0.52 GW and 0.96 GW for the full plant) reducing the time for a full cycle from 18 hours and 17 minutes to 9 hours and 52 minutes. Comparing the balancing cycle of the 10 and 20 MW PMSMs, the water level in the lower reservoir and the flow rate per RPT unit over the full cycle are shown in Figure 5.3. For both cases, the storage system is initially fully discharged leading to different initial water levels in the reservoir. It should also be noted that a reservoir level of zero does not correspond to a fully emptied reservoir but rather the minimum possible water level in the reservoir determined by the minimum submergence of the RPT inlets as illustrated in Figure 1.3. The reservoir levels decrease as the RPTs operate in pump mode emptying the reservoir and thereby charging the storage system. Once the reservoir reaches its minimum, the plant switches to turbine mode, indicated by the red vertical line in the graphs. As the flow rates invert, the reservoir is filled again and the storage system discharged.

The minimum flow rates are the same with both power ratings of the electric machines with around 57 m³/s in pump mode and 60 m³/s in turbine mode. The maximum flow rate is increased using the 20 MW version of the PMSMs to around 161 m³/s from 135 m³/s in turbine mode and to 141 m³/s from 123 m³/s in pump

Table 5.1.: Comparison of simulations for varying PMSM power ratings.

PMSM power rating	10	12.5	15	17.5	20	MW
Max. head	9	11	12	13.5	15	m
Reservoir area	44.8	29.4	24.5	19.2	15.5	km ²
Average power (per RPT unit)	5.2	6.6	7.3	8.5	9.6	MW
Time pump mode	9:33	7:33	6:39	5:46	5:07	hh:mm
Time turbine mode	8:44	6:54	6:14	5:24	4:45	hh:mm

mode. Generally, the change in flow rate is a direct result of the changing power setpoint and head of the RPT with the last remaining influencing factor being the slightly fluctuating RPT efficiency. This can be specifically observed towards the end of the pump cycle with the 10 MW PMSMs as the flow rate increases with the increasing power setpoint. Once the maximum power of 10 MW is reached, the increasing net head of the RPT causes a close to linear decrease in flow rate.

The charging and discharging power per RPT unit as well as the efficiency of the plant during the full cycle are shown in Figure 5.4. The efficiency includes all hydraulic as well as drivetrain losses but it excludes losses from the electrical machines and converters. Over the full cycle in both pump and turbine mode,

5

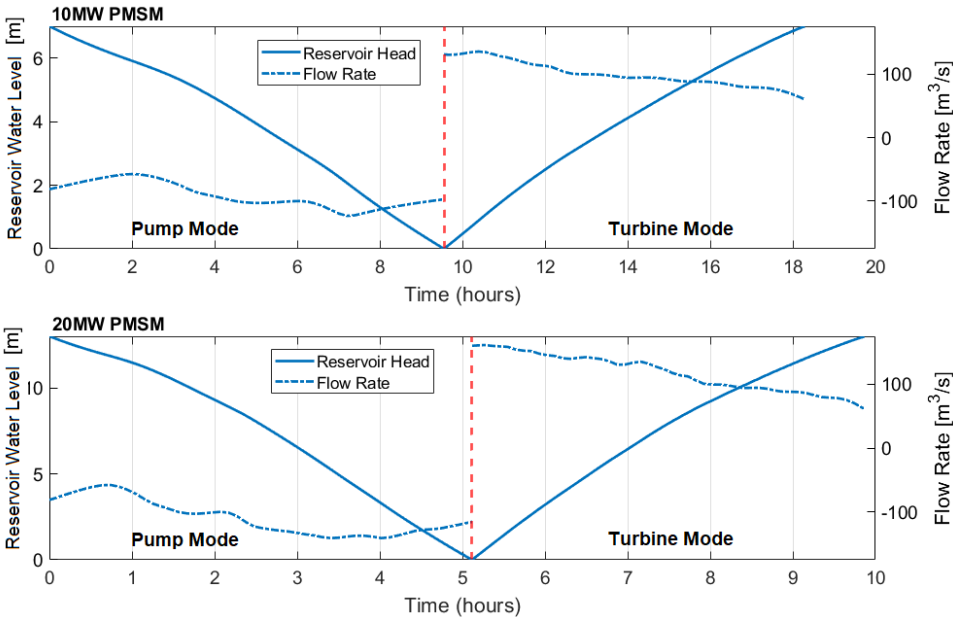


Figure 5.3.: Reservoir water level of the storage plant and flow rate of each RPT unit over a full balancing cycle compared for a 10 and 20 MW PMSM.

high efficiencies mostly in the range of 82 - 87% are achieved. The minimum efficiency appears in pump mode at the beginning of the cycle where the gross head is the smallest. No clear correlation is visible between the overall efficiency and the hydraulic losses suggesting that the efficiency is mostly determined by the RPT characteristics as the operating points change. Some of the minor fluctuations in the efficiency deviating by less than 1% are also caused by the resolution of the lookup tables and the required interpolation between the datapoints. The maximum power capacity for both cases and both modes is only reached during a small part of the cycle as the maximum head is approached.

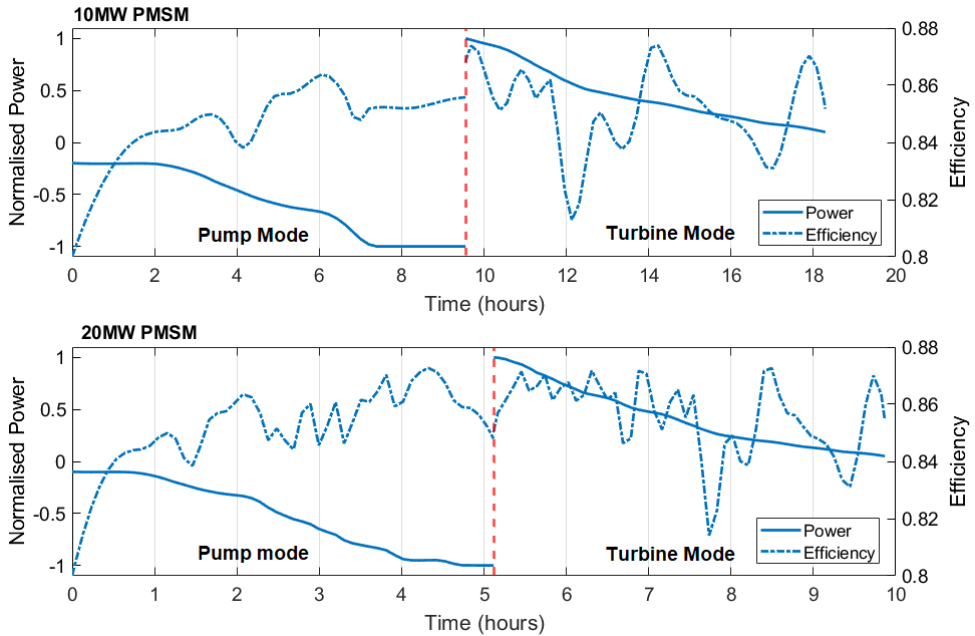


Figure 5.4.: Power and efficiency of the storage plant over a full balancing cycle compared for a 10 and 20 MW PMSM.

With no overall loss in performance and a maximum increase in flow rate of 19%, the apparent major disadvantage of using the scaled up version of electric machines is the requirement of an additional PMSM per RPT unit. Since the electric machines are located in the bulb adjacent to the runners, increasing the power capacity of the existing machines is constrained since that would result in an increase in diameter. This would, in turn, enlarge the bulb causing higher hydraulic losses. Instead, a second PMSM unit can be attached to the same drivetrain doubling the torque and power capacity. The additional cost and complexity of adding a second electric machine to each RPT should be offset by the significantly reduced reservoir size that is required for the desired 4 GWh energy storage capacity. The dam would be shortened from a total length of 95 to 56 km. Although it is worth noting that for alternative storage sites with a shallower sea depth, the larger reservoir size required

when limiting the power rating of the electric machines to 10 MW could be partially offset by a reduction in dam height of 6 metres. In addition to the economic benefits, a reduced reservoir size also alleviates environmental and legal concerns. Furthermore, the increase in average power input and output and the corresponding reduction in cycle time should further help to improve the economics.

For energy balancing, the evaluated plant demonstrates comparable performance at grid-scale to conventional high-head pumped storage plants, which are typically sized between 1 and 1.5 GW and achieve roundtrip efficiencies ranging from 70% to 80% [21]. The major disadvantage of such a low-head plant compared to high-head applications is its reduced energy density. However, in regions without suitable topography for high-head applications, alternative concepts can unlock the use of pumped storage technology. Other such amended concepts include subsea energy storage, gravity energy storage and underground pumped storage. These have theoretical roundtrip efficiencies of up to 73%, 80% and 77% respectively [202–204]. While promising, these technologies also face challenges and limitations regarding the required civil structures, suitable sites and scale that can be reached. At grid scale and balancing at similar timescales as LH-PHS, compressed air energy storage and battery energy storage are commonly discussed. Compressed air energy storage currently achieves roundtrip efficiencies of 42 to 55% and lithium-ion batteries reach over 90% [15]. Due to the high performance and scalability of lithium-ion batteries they have seen significant uptake in recent years but also face safety as well as environmental concerns regarding recycling, extraction and toxicity of the raw materials needed [205, 206].

To suit different applications, a heterogeneous pool of storage technologies is deemed necessary. While further information regarding economic and environmental assessments is required, the results presented demonstrate the technical potential of LH-PHS to contribute to that pool with grid-scale energy balancing.

5.3. POTENTIAL TO PROVIDE FREQUENCY REGULATION SERVICES

While PHS systems are widely recognised for their potential in short and long-term energy balancing, this section focuses on the capability of the proposed system to provide frequency regulation services. This system, similar to most renewable generators, is coupled to the grid via inverters and therefore does not provide inherent grid coupled inertia. It can, however, directly contribute to grid stability through frequency regulation by rapidly absorbing or injecting power into the grid. The main limitation to provide these services is how quickly the system can vary its power output, which in the case of PHS is largely determined by its mechanical and hydraulic characteristics. Key factors include the inertia of the drivetrain, power-takeoff, and the flow dynamics inside the conduits. Sudden changes in flow rate may also induce transient pressure waves previously referred to as water hammer effects, a significant concern for system stability and safety. The plant's control system design and tuning also have a considerable effect on the responsiveness of the plant.

The dynamic system model developed in chapter 3 is implemented in the commercial platform MATLAB-Simulink using a fixed step solver with a sample time of 1 ms. All simulations start in steady-state from a defined operating point and have a simulation time of 13 seconds. For the spatial discretisation, 40 nodes are used. Standard values from the literature are used for unknown loss coefficients, surface roughness etc. Table 5.2 gives an overview of all used parameters. The model includes all hydraulic and drivetrain losses, and contrary to the steady-state model also the losses in the electric machines and AC-DC-AC coupling. Excluded from the analysis are the potential hydraulic losses from the bulb used adjacent to the runners containing the PMSMs.

Table 5.2.: Overview of the model parameters for dynamic simulations.

Conduit length	L	60	m
Conduit diameter (RPT section, inlet)	$D_{1,2}$	6, 10	m
Pressure wave velocity	a	1000	m/s
Darcy friction factor	f	0.0158	-
Unsteady loss coefficient	k	0.04	m/s ²
Rotational inertia drivetrain 1	J_1	167 x 10 ³	kg m ²
Rotational inertia drivetrain 2	J_1	237 x 10 ³	kg m ²
Damping torque coefficient 1	$D_{f1,2}$	4137	Nm/rad/s
Damping torque coefficient 2	$D_{f1,2}$	6125	Nm/rad/s
Valve time constant	T_v	1.0	s
Minor loss coefficients			
Entrance	k_{en}	0.05	-
Exit	k_{ex}	1.0	-
Expansion	k_{exp}	0.04	-
Contraction	k_{con}	0.13	-

To evaluate the system's potential to provide frequency regulation services, simulations of providing frequency containment reserve are carried out. For these simulations, 20% of the plant's nominal power capacity was allocated as reserve. Such an FCR response would be triggered if the grid frequency deviates by more than 10 mHz from its nominal 50 Hz. The maximum FCR response would be fully activated for a deviation of more than 200 mHz. The following simulations assume the worst case scenario and aim to provide the full FCR provision as quickly as possible.

Since the proposed system operates over a wide range of operating conditions, the dynamic response is expected to differ, depending on the initial state. For instance, when the plant operates in turbine mode with an empty lower reservoir (indicating maximum energy capacity), the available head of the RPT reaches its maximum value. Consequently, for a specific power change, the necessary change in flow rate is less compared to scenarios where the reservoir is nearly full and the head of the RPT is lower. To assess if the plant is capable of delivering the same amount of FCR independent of its state of charge, two cases in turbine mode are compared. In the first case, the RPT experiences a gross head of 9 metres stepping from 8 to 10 MW

per RPT unit (0.8 to 1 GW for the full plant). In the second case, the RPT has a decreased gross head of 5 metres and steps from 2 to 4 MW per RPT unit. Figure 5.5 shows the simulated change of power setpoint for the first case.

When providing FCR in the Netherlands, changes in power setpoint are required to be reached within 30 seconds [207]. This is defined as the power change period, and the desired setpoint can be exceeded by up to 30%. The tolerances around the power setpoints are split into two sections. The allowed range in which 95% of the values must fall and the tolerable range in which a maximum of 5% of the values may lie. The absolute tolerance is calculated based on the power setpoint and the percentage multiplied by the FCR power provided. After the power change period, a transient period of 90 seconds starts where the allowed range gives a 20% tolerance above and below the power setpoint and a tolerable range of 30%. Finally, after the transient period, the tolerances drop to 10 and 20% respectively [208].

As can be observed from Figure 5.5, the system is able to reach its new power setpoint within around 3.5 seconds, thus easily fulfilling the requirements. To increase the power, the system accelerates both runners resulting in a higher flow rate at the given head. To achieve this promptly, the machine torques are reduced which explains the initial step-down in power. In order to fulfil the regulations while minimising the power change period, the initial torque step and minimum power are limited. In the presented simulation the initial step-down in power is limited to 20% of the provided reserve. If this step, while within the regulations,

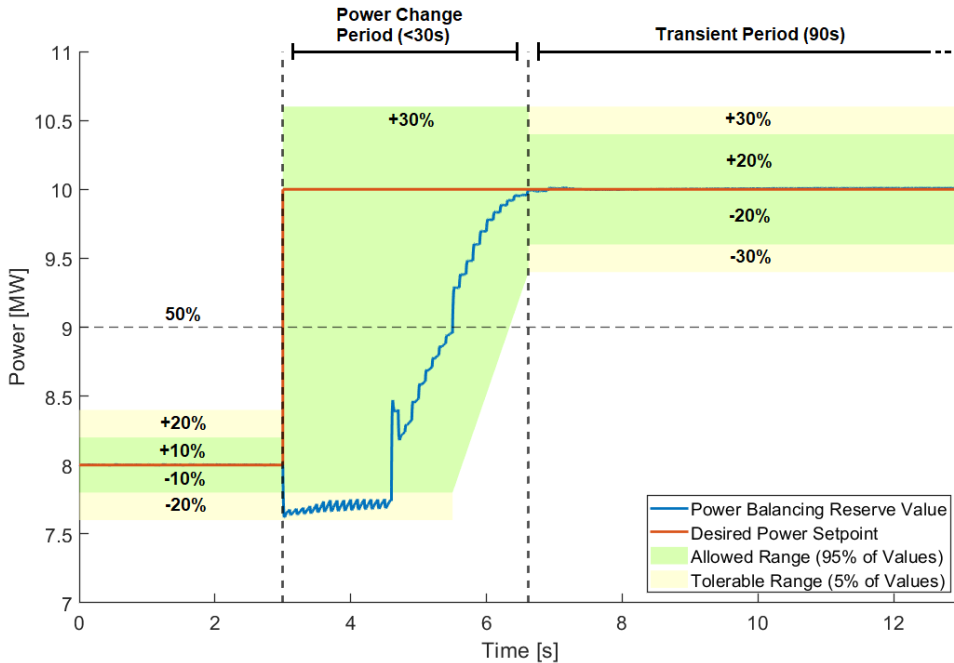


Figure 5.5.: Power per RPT unit during a FCR simulation stepping from 8 to 10 MW.

would be deemed undesirable, limiting the initial power reduction to 5% of the reserve, would only increase the power change period by about one second. The two machine torques and rotational speeds for this case are shown in Figure 5.6. Here this initial step-down in torque can be observed after which the torque is dropped further as the runners accelerate to maintain the minimum power setpoint. Once the rotational speeds approach their new desired setpoint the machine torques are increased to reduce the acceleration. The small fluctuations observed both in power and torque are caused by the speed control loop updating the current setpoint in 100 ms intervals.

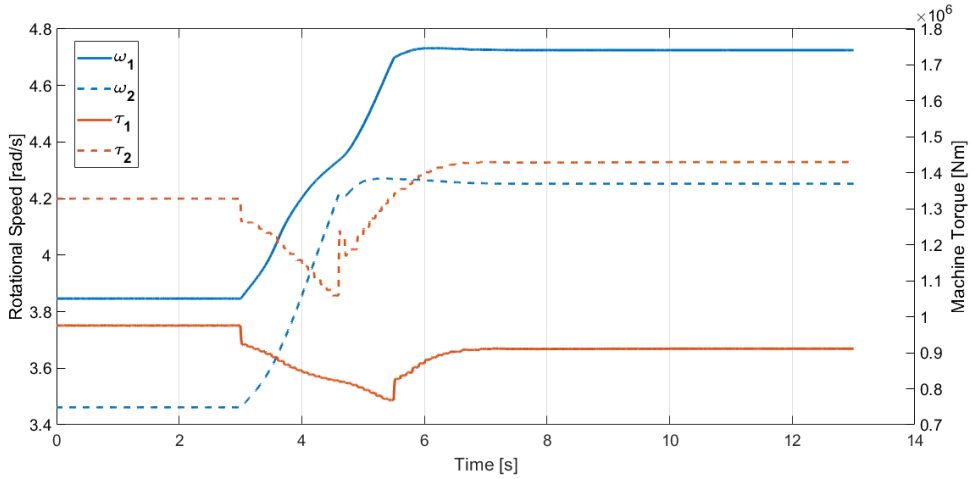


Figure 5.6.: Rotational speeds and machine torques per RPT unit during a FCR simulation stepping from 8 to 10 MW.

Figure 5.7 shows the change of power for the second case. Most notably, the power change period here takes around 5 seconds and with that 40% longer than the previous case. This is explained through the larger change in flow rate of $22.6 \text{ m}^3/\text{s}$ compared to a change of $15.4 \text{ m}^3/\text{s}$ in the first case. The angular velocities of the runners also increase by around 1.05 rad/s compared to around 0.85 rad/s .

During neither of the simulated cases, any significant transient pressure effects were observed. The rotational inertia of the runners limits their acceleration sufficiently to avoid the excitation of pressure waves in the water column. While this is the case for the assumed physical characteristics of this plant, changes in the conduit or RPT dimensions may increase the risk of such pressure transients occurring. Additionally, if the flow valve is used to achieve a new operating setpoint, there could be an additional risk of such effects as has been shown in chapter 4.

It is clear that this plant is capable to provide Frequency FCR across its entire operating range. With that, it is also equipped to offer other essential frequency regulation services, including automatic and manual frequency restoration reserves (aFRR & mFRR). Notably, these services demand a less rapid adjustment of operating points compared to FCR. Additional components that may constrain the dynamic

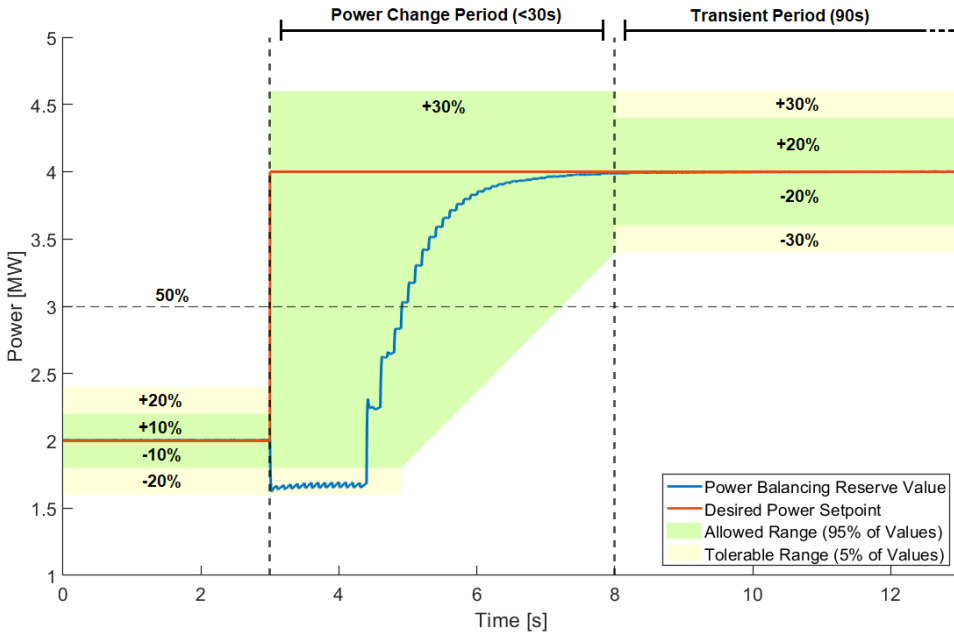


Figure 5.7.: Power per RPT unit during a FCR simulation stepping from 2 to 4 MW.

response of the system and are not covered in these results are the power electronics and grid side control. Their effect should be limited though compared to the physical inertias of the plant.

Among energy storage technologies, flywheels, supercapacitors and batteries are typically considered to have fast enough power ramp rates to provide frequency regulation services [209], i.e. capable of power change periods in the range of seconds. However, only battery storage offers large enough energy capacities to also provide balancing. With new technologies such as variable speed and hydraulic short circuit, existing conventional pumped storage plants have also been enabled to provide frequency regulation [210]. With a continuous reduction of spinning reserves in our power grids, providing ancillary services such as FCR, aFRR and mFRR is a crucial component of energy storage systems to contribute to grid stability. Accordingly, providing these services opens up another revenue stream for the operator.

6

CONCLUSIONS AND RECOMMENDATIONS

Due to the rapid rise of intermittent and inverter-coupled renewable energy sources, large-scale integration of energy storage into our electricity grids will become imperative. Shifting the operating range of pumped hydro storage to low-head applications could pave the way to utilise the storage technology in regions, where so far it had not been considered economically feasible. Further technological advancements can significantly contribute in enhancing its capability to improve grid stability while also making it cost competitive. However, no deployment on a significant scale has been attempted and research tackling the specific technical challenges arising from low-head applications is limited. This study aimed to assess the technical potential and viability of low-head pumped hydro storage as a contributor to future grid stability. For this, first a review of technologies discussing their applicability for low-head systems was conducted before a numerical model was developed to assess the performance, dynamic behaviour and component interaction of an integrated low-head pumped storage system. This numerical approach was compared to experimental results and consequently applied in a case study to assess a potential grid-scale system. Based on the research questions presented in section 1.2, the following conclusions are drawn.

6.1. CONCLUSIONS

APPLICABLE TECHNOLOGIES FOR LOW-HEAD PUMPED HYDRO STORAGE

The review of low-head technologies in chapter 2 examined various pump-turbine designs, electric machines, control strategies, and grid integration methods addressing the first research question regarding what technologies are applicable to low-head pumped hydro storage. The analysis highlighted the potential advantages of the technologies embedded in the proposed system which are numerically and experimentally assessed in the remaining chapters. The key findings from this review are as follows.

In a low-head context, the choice of pump-turbine design is highly dependent on the flow rate of the system. Axial flow pump-turbines, with variable speed drives, are the most suitable solution for high flow rates which leads to higher power inputs/outputs.

The concept of utilising two contra-rotating runners instead of a single runner as a reversible pump-turbine is aimed at reaching high efficiencies over a wide operating range. This is due to a reduction in non-axial flow components and the gained control degree of freedom stemming from the adjustability of the rotational speed of both runners.

For the power take-off, axial flux PMSMs have been considered the most suitable electric machines for low-head PHS due to their high efficiency, high power density, and suitability for high-torque-low-speed operation. The machine torque can be controlled to achieve a speed setpoint by either field oriented control or direct torque control, with the latter having a slightly better torque response if a position sensor is used, but increasing the torque ripple. Active disturbance rejection control can be used to complement the torque and speed control, increasing performance and robustness. To derive the speed setpoint, MPPT algorithms based on RPT models are suitable for low-head PHS because of their short response time and steady power output. However, it is important to include the whole system with its losses in the model to have precise control. Model predictive control is a computationally intense control method that can account for transient effects in complex systems, making it a valuable option for low-head PHS.

The discussion on grid integration has shown that, in order to compensate for an increase in intermittent generation and a reduction in spinning reserves, a combination of grid-forming control alongside bulk energy storage is necessary. To ensure grid stability, such systems are required to provide frequency regulation services next to other ancillary services, namely steady state voltage control, fast reactive current injections, short circuit currents, black start, and island operation capability.

DEVELOPMENT OF THE INTEGRATED MID-FIDELITY NUMERICAL MODEL

Chapter 3 detailed the development of the numerical model, tackling the second research question by exploring how a novel reversible pump-turbine with two contra-rotating runners can be integrated with hydraulic, mechanical, and control dynamics into a mid-fidelity numerical framework. The following conclusions are drawn from this investigation.

From a numerical modelling perspective, similar approaches of traditional PHS can be used when modelling low-head PHS. However, there are significant changes in the characteristics of low-head systems requiring more attention on certain model components' capabilities. Additionally, integrating the novel RPT technology with two individual runners requires a new approach in characterising its performance. This approach must also account for the coupling and interaction between the runners as well as to the hydraulic, mechanical, electrical and control components.

Accurately modelling the performance of the RPT is essential for low-head systems, which, unlike conventional pumped hydro storage, operate across a broader range of relative head and discharge conditions. Low-head pumped storage systems are also more likely to experience significant transient pressure effects than conventional high-head systems due to the increased inertia of the water column. To account for these effects in the hydrodynamic model, the compressibility of water is included. This has proven beneficial during simulations of rapid changes in valve opening angles, where such pressure transients were observed. However, it was anticipated that changes in the rotational speeds of the runners or the speed ratio between them might also induce such effects.

Interestingly, these were not observed in the simulated system. The rotational inertia of the runners limits rotational acceleration sufficiently and, consequently, the excitation of pressure waves. While this holds true for the assumed physical characteristics of the simulated plant, modifications to the conduit or RPT dimensions could increase the risk of pressure transients. Therefore, incorporating water compressibility into the model to evaluate transients under varying plant configurations, or to conduct simulations that account for the use of the flow valve, proves to be valuable.

Utilising a 1-D approach for the hydrodynamic model proved sufficient to capture the discharge and pressure across the conduit. One significant disadvantage is that the risk of cavitation can not be assessed. The transient pressures at the varying locations in the conduit are averaged in the cross sectional plane which may neglect localised low-pressure zones. Additionally, when coupling the 1-D hydrodynamic model to the steady-state RPT characterisation inaccuracies may be introduced when predicting the RPT performance under operating conditions where significant non-axial flow components are present. Nonetheless, implementing a multidimensional fluid model would increase the required computational resources significantly. This would limit the amount of scenarios and cases that can be simulated and hence restrict the applicability of the model beyond the desired scope.

Aside from the water column, the dynamics of the drivetrains and motor-generators are included in the model to account for the dynamic response of the entire system. This is more significant in low-head systems due to the relative larger diameter and associated rotational inertia of the runners and electric machines. The use of axial-flux electric machines may further increase their effect on the dynamic response of the systems since they often have larger diameters compared to other motor-generators. These mechanical dynamic effects are typically not included in CFD simulations.

Furthermore, the use of two independent runners per RPT unit requires each runner to be modelled individually due to their coupling with separate drivetrains and the interdependence of their performance, where the operating conditions of one runner significantly influences the behaviour of the other. The utilised medium-fidelity hydrodynamic modelling approach offers the flexibility to integrate the pump-turbine model with the other relevant system components such as the conduit, drivetrains, electric machines, and control systems. The subsystem models are grounded in physical principles, enabling insight into the relevant physics of the system response. The significantly improved computational efficiency compared to CFD allows for time-domain simulations of a wide range of operating conditions and scenarios while considering the effects of the coupled subsystems. The efficiency is largely achieved through the reduced dimensionality and resolution of the hydrodynamic model which does limit its ability to capture highly localised or multidimensional flow behaviours. Despite these constraints, the efficiency and modularity of the model allows for the exchange or coupling of further subsystems, maintaining its applicability to a broad range of analyses.

This combination of flexibility and efficiency makes it a powerful tool for the development of a technology such as low-head PHS. In this study the model was applied to performance evaluations during energy balancing operations, transient behaviour analyses for ancillary service provision, system scaling and sizing as well as the testing of coupled control algorithms. These applications were significantly aided by the mod-

els efficiency and flexibility which allowed for frequent and rapid adjustments of crucial system parameters and components.

EXPERIMENTAL EVALUATION AND COMPARISON TO NUMERICAL RESULTS

To benchmark the developed numerical approach, an experimental setup incorporating a 1:22 scaled version of a new contra-rotating RPT was constructed and used to perform steady-state and dynamic tests in both pump and turbine operation modes. Chapter 4 addresses the third research question by presenting the setup and results, exploring how the developed integrated numerical model can be experimentally benchmarked and what insights can be gained from comparing the numerical predictions with experimental results.

The used setup consists of two open-surface tanks, setting it apart from other experimental campaigns that utilise pumps to provide the required head. This allows for more realistic in- and outflow conditions, by reducing the risk of encountering swirl and pressure pulsations typically induced by pumps. For the conducted experiments, the range of Reynolds numbers at the RPT was between 0.6 – 1.0e6.

During turbine mode testing, a maximum flow rate of 360 l/s was measured and a maximum mechanical power of 22 kW. The highest hydraulic efficiency measured during the experiments was 89%. In pump mode, a maximum flow rate of over 370 l/s at a mechanical power of 42 kW was measured. The highest hydraulic efficiency measured in pump mode was 92%. At the best efficiency points a hydraulic roundtrip efficiency of 82% is achieved. It should be noted though that, when assessing the performance of hydraulic machinery in scaled-down systems, uncertainties regarding the direct applicability of results to full-scale operations arise due to scaling effects. In this case, these uncertainties would specifically arise from differences in Reynolds numbers and the relative roughness of the RPT and surrounding wet surfaces. Despite these limitations, these scaled experiments are crucial for the benchmarking of the developed numerical modelling approach.

Comparing the steady-state experimental results to the RPT model, which is derived from a series of CFD simulations, a close match is observed in turbine mode with correlation coefficient values between 0.9 and 0.97. In pump mode, the results are slightly worse, however, the overall performance is sufficiently predicted through the operational range. Challenges and uncertainties in this comparison arise from both the experimental and numerical approaches. For once cavitation and flow separation affect the pressure measurements close to the RPT. The effect of flow separation was only observed in far off-design operating conditions in turbine mode though and would not affect the performance of a full-scale system. Cavitation can lead to performance degradation for both the scaled-down and full-scale version of the technology. Full-scale systems would experience a larger static head at the low-pressure side of the RPT therefore reducing the risk of cavitation occurring. Nonetheless, this effect needs to be carefully evaluated before deployment. Further inaccuracies in the comparison may stem from the CFD simulations that were used as a basis for the RPT model. The proximity of the RPT to the inlet in pump mode introduced non-axial flow conditions that are not captured in the simulations due to the boundary conditions assuming a purely axial flow. Lastly, measuring the runner torques with the transducers placed next to the electric machines

rather than the RPT proved challenging, as it introduced additional uncertainties in the characterisation of friction torques.

In addition to benchmarking the numerical modelling approach, the steady-state experimental results have confirmed key predictions. The RPT design, which utilises two individual contra-rotating runners, is capable of delivering high efficiencies by reducing non-axial flow components. More importantly, it provides these high efficiencies around and above 85% over a wider operating range by adjusting the speed ratio between the runners.

Additional to the steady-state tests, dynamic experiments were performed. To benchmark the dynamic modelling approach, a change of operating point has been experimentally tested and numerically simulated in turbine mode. For this, the measured torques of both drivetrains have been used as an input to the integrated model. The results showed a strong correlation in the transient behaviour between numerical and experimental results. This could be observed for the individual dynamic model components, notably the conduit and two drivetrains. The simulated transients of the rotational speeds of the drivetrains, as well as the flow and pressure variations within the conduit, closely matched the experimental data. These results highlight the accuracy of the integrated numerical modelling approach in representing not only the steady-state RPT performance but also the dynamics within the hydraulic and mechanical subsystems and their coupling. The integrated numerical approach has proven to be a versatile and resource efficient tool.

Subsequently, the model was used to simulate a shutdown sequence in turbine mode, which has been identified to be of high risk for potential transient pressure effects due to its rapid closure of the valve. At the proposed shutdown time and even twice accelerated the resulting pressure fluctuations do not pose a risk to the system. At faster rates, the increased pressure and subsequent potential column separation may cause damage to the conduit and adjacent components.

NUMERICAL EVALUATION OF A POTENTIAL LOW-HEAD PUMPED STORAGE PLANT

In chapter 5, the integrated model is applied to a potential full-scale plant, addressing the final research question by investigating the potential performance outcomes and operational capabilities of low-head pumped hydro storage in supporting grid stability, particularly for energy balancing and frequency regulation services.

A case study is performed evaluating the potential and technical viability of a grid-scale plant with an initial power capacity of 1 GW and net storage capacity of 4 GWh to be deployed in the Dutch North Sea. Furthermore, a sensitivity analysis has investigated the effect of scaling the motor-generators while all other components, notably the RPTs, remain unchanged.

The simulation results demonstrate the potential of the proposed low-head pumped storage technology to achieve high performance at grid scale, effectively supporting both energy balancing and frequency regulation services. The system, applied to the prospective site, has achieved roundtrip efficiencies of 73%. This roundtrip efficiency includes all hydraulic and mechanical losses in the system and was obtained over a full charge and discharge cycle. It was shown that using individual units of PMSMs at the nominal

rating of 10 MW, severely constrain the wider operating range of the RPTs. By scaling up the electric machines alone, the full head range except for one metre of the selected storage site can be utilised. This results in the reduction of the size of the reservoir required to reach the desired energy capacity of 4 GWh to approximately one third. Aside from this reduction in footprint, the average power during operation is also almost doubled.

The dynamic simulations that have been carried out show that fast power ramp rates across its operating range can be achieved. Allocating 20 % of its nominal power for FCR, the new power setpoints are reached between 3.5 and 5 seconds for a full FCR response, depending on the initial state of charge. This fulfils FCR requirements with some margin, enabling it to participate in the provision of frequency regulation services.

6.2. PERSPECTIVES AND RECOMMENDATIONS FOR FUTURE WORK

While the experimental investigation was able to cover tests over a wide operating range, additional tests beyond the known operating range can be performed if the limitations of the presented setup are overcome. If a higher static pressure at the low pressure side of the RPT is achieved, the risk of cavitation would be reduced. This would allow for additional operating conditions as well as reduce uncertainty of the pressure measurements adjacent to the RPT. Adapting the power take-off configuration to incorporate straight shafts instead of bevel gears, the maximum torque could be increased and the uncertainty of the friction torque characterisation avoided. However, such a setup would create additional hydraulic losses in the system and may introduce non-axial flow components. While additional small-scale tests can deliver valuable results on performance and validate numerical methods, to increase the technical readiness of the technology, a large-scale demonstration of the RPT and integrated system would be the appropriate next step. Such a demonstration could, for example, use a single 10 MW set of pump-turbine and axial flux machine.

Due to challenges when it comes to the scaling of tested pump-turbines, large-scale tests would increase the confidence in the performance of the technology and allow for the full-scale integration of RPT, electric machines, control algorithms and energy management strategies. Such a large-scale demonstration would require significant resources though and additional numerical evaluations may be needed.

The presented experimental campaign has shown that a mid-fidelity integrated numerical modelling approach can predict the performance and dynamic behaviour accurately and serve as an efficient and versatile approach to investigate and evaluate low-head pumped storage plants. With this modelling approach, the presented work has demonstrated that low-head pumped storage technology has the technical potential to significantly contribute to grid stability. However, detailed economic and environmental assessments were not within the scope of the conducted case study and are an important next step in assessing the technology for large-scale implementation. The results of the case study can serve as a basis for further economic and environmental investigations. Combined with a detailed assessment of the capital and operating expenditure as well as estimates on the future energy arbitrage margins and the prices of ancillary services, detailed economic analyses including scaling optimisations can be performed.

Further work utilising the developed numerical modelling approach should include the development of energy management strategies, machine-side control algorithms and grid-impact simulations. Due to the flexible control, several energy management strategies, i.e. best efficiency vs. highest power input/output, can be compared for improved LCOS. Furthermore, the integrated model can aid the optimisation of the machine- and grid-side control. This may include the development of the numerical approach into a model predictive control. Of significant relevance would be further studies conducting detailed simulations to quantify the impact of large-scale deployment of low-head PHS on grid stability, especially in regions with a high penetration of renewables. For these applications, the model in its current form should suffice and can be adapted or extended to include varying control strategies or a grid connection.

However, further advancements in the model could unlock additional use cases and widen its predictive capabilities. One avenue could be an upgrade of the hydrodynamic model component to a multidimensional approach. This would allow to approximate localised pressure variations and with that a more precise assessment of cavitation risks under varying operating conditions. Such an upgrade, while coming at the cost of computational expense, would be beneficial in assessing system reliability and preventing potential damage to components in full-scale deployments. Additionally, the steady-state characterisation of the reversible pump-turbine could be replaced with a fully dynamic characterisation to account for unsteady flow effects. This could enable the model to better capture transient effects during rapid operational changes, such as start-ups, shutdowns or the provision of ancillary services. For the applications of the presented study, the steady-state characterisation proved accurate, but for other applications such as investigation of the risk of cavitation during transient state operation this may be beneficial. Beyond these approaches, the model could also be extended to include structural and load modelling. This would enable the evaluation of mechanical stresses and fatigue on critical components under both steady-state and dynamic conditions further aiding the development of the technology.

If the proposed economic, environmental, control and grid-impact investigations are promising and a large-scale technology demonstration further confirms the assumed performance, low-head pumped hydro storage can be deployed as a large-scale storage solution and help facilitate the ongoing energy transition.

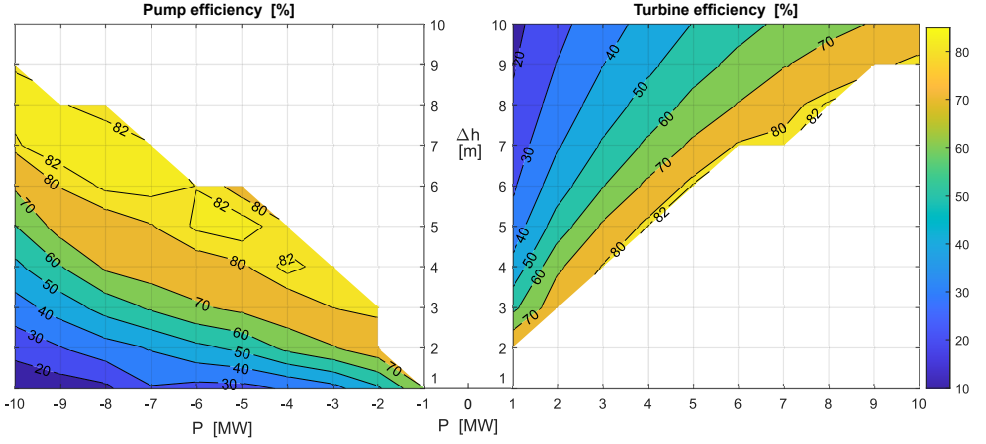
A

APPENDIX

A.1. CONTROL MAPS USED IN THE NUMERICAL MODEL

Four control topologies were evaluated for the maximum RPT efficiency across its operating range in both turbine and pump modes. These topologies are based on the three available control degrees of freedom: the rotational speeds of the two runners and the valve opening angle. Figure A.1 shows the efficiency maps for both operating modes based on the selected control topology (topology 4). It also illustrates the associated valve coefficients (minor loss coefficients corresponding to the valve opening angle) and the ratio of the rotational speeds between the two runners.

A



(a) Topology 4 efficiency map.

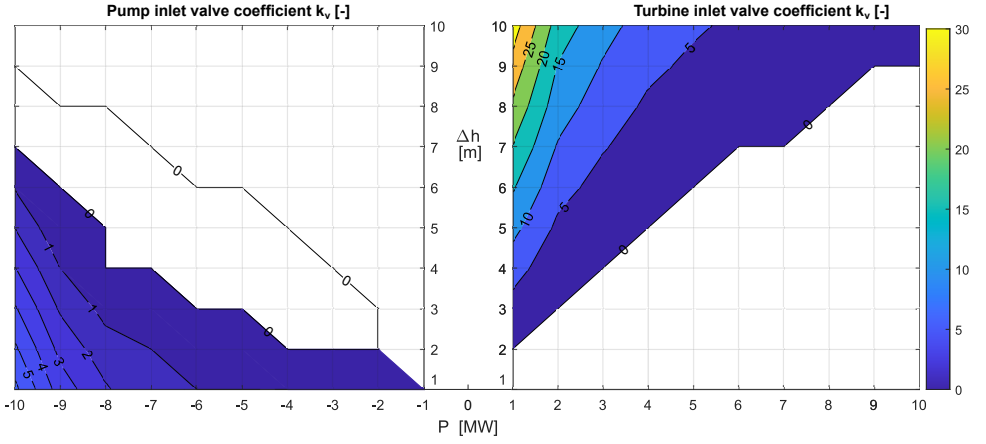
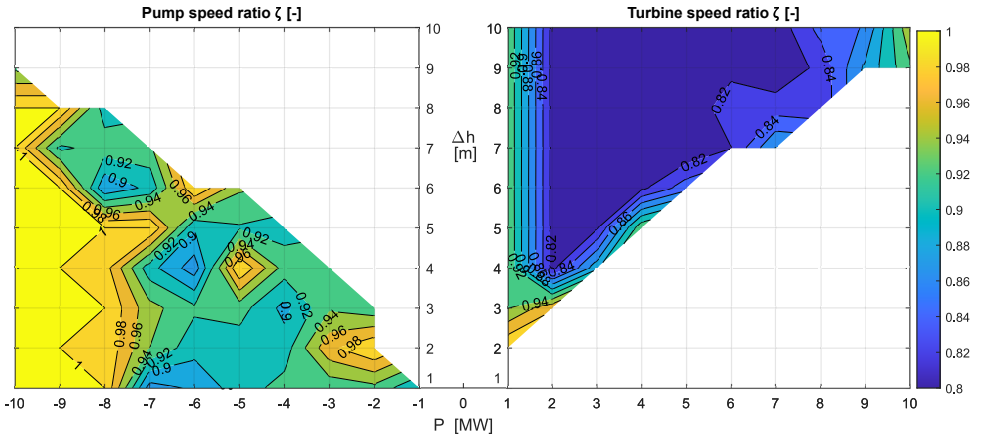
(b) Topology 4 inlet valve coefficient k_v map.(c) Topology 4 speed ratio ζ map.

Figure A.1.: (a) Efficiency, (b) speed ratio and (c) inlet valve coefficient versus power and fallhead for control topology 4. [194] ©2024 IEEE

B

APPENDIX

B.1. STEADY-STATE EXPERIMENTAL RESULTS FOR THE RPT EFFICIENCY AND POWER

During the steady-state experiments a total of 121 operating points of the RPT were tested in turbine and pump modes. The varying operating points were achieved by increasing the rotational speeds of the runners for five different speed ratios between the runners. Additional operating conditions were measured by adjusting the opening angle of the flow valve as well as adjusting the height of the spillway. Figure B.1 shows the results for the efficiency of the RPT as well as the mechanical power. It should be noted though, that these graphs, for the purpose of visual clarity, only include the results of the incremental changes in rotational speeds for the varying speed ratios.

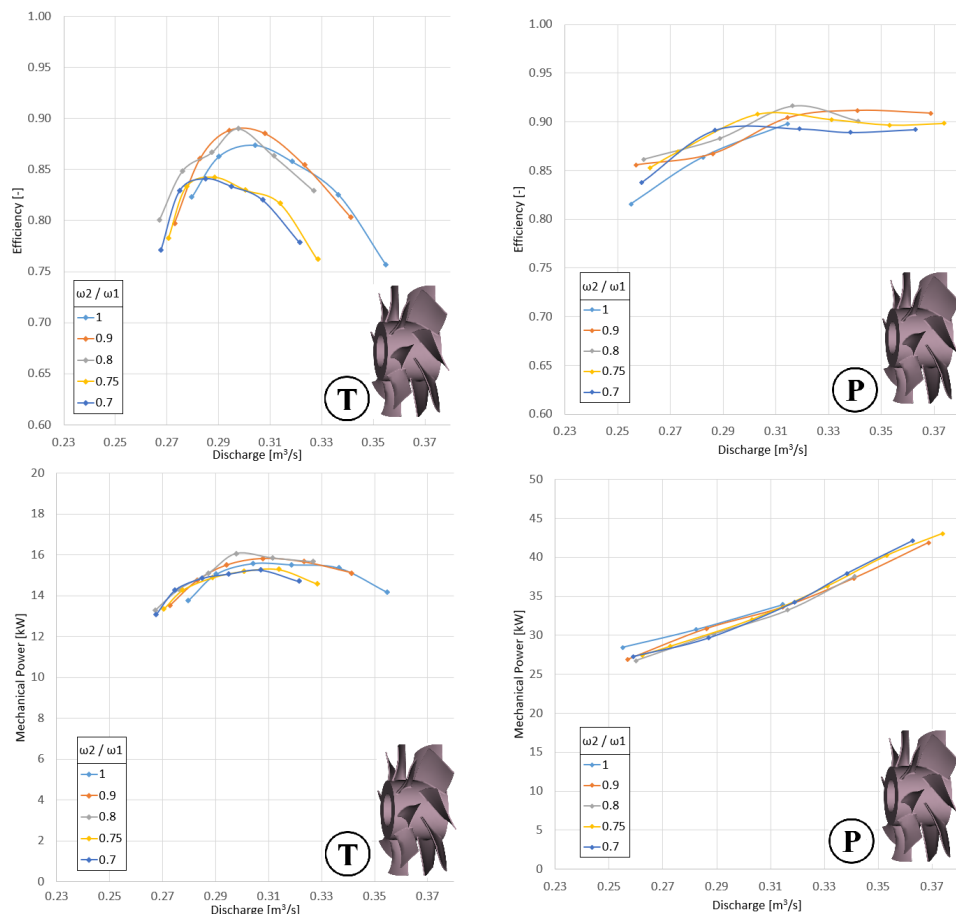


Figure B.1.: Steady-state experimental results for the RPT efficiencies and mechanical powers in turbine and pump modes. Turbine and pump operation are depicted with a T and P respectively.

BIBLIOGRAPHY

- [1] International Energy Agency. *Renewables 2023*. Tech. rep. 2024. URL: https://iea.blob.core.windows.net/assets/96d66a8b-d502-476b-ba94-54ffda84cf72/Renewables_2023.pdf.
- [2] International Energy Agency. *Renewables Information - Overview (2020 Edition)*. Tech. rep. 2020. URL: <https://www.iea.org/reports/renewables-information-2020>.
- [3] A. Q. Al-Shetwi, M. Hannan, K. P. Jern, M. Mansur, and T. Mahlia. "Grid-connected renewable energy sources: Review of the recent integration requirements and control methods". In: *Journal of Cleaner Production* 253 (2020), p. 119831. ISSN: 0959-6526. DOI: <https://doi.org/10.1016/j.jclepro.2019.119831>. URL: <https://www.sciencedirect.com/science/article/pii/S0959652619347018>.
- [4] F. Colas, Q. Taoufik, X. Guillaud, and F. Gruson. *D3.5 - Local Control for Grid-Forming Converters Experimental Validation*. Tech. rep. 2020. DOI: [10.13140/RG.2.2.13327.94881](https://doi.org/10.13140/RG.2.2.13327.94881).
- [5] D. O. Johnson and K. A. Hassan. "Issues of Power Quality in Electrical Systems". In: *International Journal of Energy and Power Engineering* 5 (2016), pp. 148–154. DOI: [10.11648/j.ijepe.20160504.12](https://doi.org/10.11648/j.ijepe.20160504.12).
- [6] A. Castillo and D. F. Gayme. "Grid-scale energy storage applications in renewable energy integration: A survey". In: *Energy Conversion and Management* 87 (2014), pp. 885–894. ISSN: 0196-8904. DOI: <https://doi.org/10.1016/j.enconman.2014.07.063>. URL: <https://www.sciencedirect.com/science/article/pii/S0196890414007018>.
- [7] M. Sterner and I. Stadler. *Handbook of Energy Storage*. 2019. ISBN: 9783662555040. DOI: [10.1007/978-3-662-55504-0](https://doi.org/10.1007/978-3-662-55504-0).
- [8] V. Jülch. "Comparison of electricity storage options using levelized cost of storage (LCOS) method". In: *Applied Energy* 183 (2016), pp. 1594–1606. ISSN: 03062619. DOI: [10.1016/j.apenergy.2016.08.165](https://doi.org/10.1016/j.apenergy.2016.08.165).
- [9] C. J. Barnhart and S. M. Benson. "On the importance of reducing the energetic and material demands of electrical energy storage". In: *Energy and Environmental Science* 6.4 (2013), pp. 1083–1092. ISSN: 17545706. DOI: [10.1039/c3ee24040a](https://doi.org/10.1039/c3ee24040a).
- [10] US Department of Energy. *Pumped Storage Hydropower*. Accessed on 07.08.2024. URL: <https://www.energy.gov/eere/water/pumped-storage-hydropower>.
- [11] W. Richter, K. Vereide, F. G. Píkl, and E. Pummer. "Economic and Sustainable Energy Transition Enabled by Pumped-Storage Hydropower Plants". In: *Hydro Conference 2020*. 2020, pp. 1–10.
- [12] International Hydropower Association (IHA). *Hydropower Status Report 2020*. Tech. rep. International Hydropower Association, 2020. URL: <https://www.hydropower.org/publications/2020-hydropower-status-report>.
- [13] M. Rogner and S. Law. *Pumped Storage Tracking Tool*. 2021. URL: <https://www.hydropower.org/hydropower-pumped-storage-tool>.
- [14] REN21. *Renewables 2021 Global Status Report*. Tech. rep. Accessed: 2024-12-09. Paris, France: REN21 Secretariat, 2021. URL: <https://www.ren21.net/reports/global-status-report/>.

- [15] S. Koohi-Fayegh and M. A. Rosen. "A review of energy storage types, applications and recent developments". In: *Journal of Energy Storage* 27 (2020), p. 101047. ISSN: 2352152X. DOI: [10.1016/j.est.2019.101047](https://doi.org/10.1016/j.est.2019.101047). URL: <https://doi.org/10.1016/j.est.2019.101047>.
- [16] Wissenschaftliche Dienste des Deutschen Bundestages. *Vor- und Nachteile verschiedener Energiespeichersysteme*. 2014. URL: <https://www.bundestag.de/resource/blob/412904/ca2dd030254284687a1763059f1f4c0c/wd-8-032-14-pdf-data.pdf>.
- [17] Statkraft Markets GmbH. *Speicherlösungen für den Energiemarkt der Zukunft*. URL: <https://www.statkraftdirektvermarktung.de/pioniergeist/Stromspeicher/>.
- [18] J. Ren and X. Ren. "Sustainability ranking of energy storage technologies under uncertainties". In: *Journal of Cleaner Production* 170 (2018), pp. 1387–1398. ISSN: 09596526. DOI: [10.1016/j.jclepro.2017.09.229](https://doi.org/10.1016/j.jclepro.2017.09.229). URL: <https://doi.org/10.1016/j.jclepro.2017.09.229>.
- [19] M. Stocks, R. Stocks, B. Lu, C. Cheng, and A. Blakers. "Global Atlas of Closed-Loop Pumped Hydro Energy Storage". In: *Joule* 5.1 (2021), pp. 270–284. ISSN: 25424351. DOI: [10.1016/j.joule.2020.11.015](https://doi.org/10.1016/j.joule.2020.11.015). URL: <https://doi.org/10.1016/j.joule.2020.11.015>.
- [20] A. Blakers, M. Stocks, B. Lu, and C. Cheng. "A review of pumped hydro energy storage". In: *Progress in Energy* 3.2 (2021), p. 022003. DOI: [10.1088/2516-1083/abeb5b](https://doi.org/10.1088/2516-1083/abeb5b).
- [21] S. Rehman, L. M. Al-Hadhrani, and M. M. Alam. "Pumped hydro energy storage system: A technological review". In: *Renewable and Sustainable Energy Reviews* 44 (2015), pp. 586–598. ISSN: 1364-0321. DOI: <https://doi.org/10.1016/j.rser.2014.12.040>. URL: <https://www.sciencedirect.com/science/article/pii/S1364032115000106>.
- [22] E. Barbour, I. A. Wilson, J. Radcliffe, Y. Ding, and Y. Li. "A review of pumped hydro energy storage development in significant international electricity markets". In: *Renewable and Sustainable Energy Reviews* 61 (2016), pp. 421–432. ISSN: 18790690. DOI: [10.1016/j.rser.2016.04.019](https://doi.org/10.1016/j.rser.2016.04.019).
- [23] A. Joseph, T. R. Chelliah, S. S. Lee, and K.-b. Lee. "Reliability of Variable Speed Pumped-Storage Plant". In: *Electronics* 7.10 (2018). ISSN: 2079-9292. DOI: [10.3390/electronics7100265](https://doi.org/10.3390/electronics7100265). URL: <https://www.mdpi.com/2079-9292/7/10/265>.
- [24] J. Feltes, Y. Kazachkov, B. Gong, B. Trouille, P. Donalek, V. Koritarov, L. Guzowski, J. Gevorgian, S. Pti, and M. Americas. *Modeling Ternary Pumped Storage Units*. Tech. rep. US Department of Energy, 2013. DOI: [10.2172/1098020](https://doi.org/10.2172/1098020).
- [25] R. K. Fisher, J. Koutník, L. Meier, V. Loose, K. Engels, and T. Beyer. "A Comparison of Advanced Pumped Storage Equipment Drivers in the US and Europe". In: *Hydrovision*. 2012.
- [26] C. Nicolet and A. Béguin. "Variable Speed and Ternary Units to Mitigate Wind and Solar Intermittent Production". In: *Proc. of the 2014 HydroVision International*. 2014.
- [27] G. Ardizzon, G. Cavazzini, and G. Pavesi. "A new generation of small hydro and pumped-hydro power plants: Advances and future challenges". In: *Renewable and Sustainable Energy Reviews* 31 (2014), pp. 746–761. ISSN: 13640321. DOI: [10.1016/j.rser.2013.12.043](https://doi.org/10.1016/j.rser.2013.12.043). URL: <http://dx.doi.org/10.1016/j.rser.2013.12.043>.
- [28] I. Kougias, G. Aggidis, F. Avellan, S. Deniz, U. Lundin, A. Moro, S. Muntean, D. Novara, J. I. Pérez-Díaz, E. Quaranta, P. Schild, and N. Theodossiou. "Analysis of emerging technologies in the hydropower sector". In: *Renewable and Sustainable Energy Reviews* 113 (2019), p. 109257. ISSN: 1364-0321. DOI: [10.1016/j.rser.2019.109257](https://doi.org/10.1016/j.rser.2019.109257). URL: <https://doi.org/10.1016/j.rser.2019.109257>.
- [29] M. S. Javed, D. Zhong, T. Ma, A. Song, and S. Ahmed. "Hybrid pumped hydro and battery storage for renewable energy based power supply system". In: *Applied Energy* 257 (2020), p. 114026. ISSN: 03062619. DOI: [10.1016/j.apenergy.2019.114026](https://doi.org/10.1016/j.apenergy.2019.114026). URL: <https://doi.org/10.1016/j.apenergy.2019.114026>.

- [30] K. Bódis, F. Monforti, and S. Szabó. "Could Europe have more mini hydro sites? A suitability analysis based on continentally harmonized geographical and hydrological data". In: *Renewable and Sustainable Energy Reviews* 37 (2014), pp. 794–808. ISSN: 13640321. DOI: [10.1016/j.rser.2014.05.071](https://doi.org/10.1016/j.rser.2014.05.071).
- [31] J. P. Deane, B. P. Ó Gallachóir, and E. J. McKeogh. "Techno-economic review of existing and new pumped hydro energy storage plant". In: *Renewable and Sustainable Energy Reviews* 14.4 (2010), pp. 1293–1302. ISSN: 13640321. DOI: [10.1016/j.rser.2009.11.015](https://doi.org/10.1016/j.rser.2009.11.015).
- [32] R. Juhlin and M. Assadi. "Harnessing ocean depths for energy: A theoretical framework for evaluating the feasibility of Subsea Pumped Hydro Storage". In: *Journal of Energy Storage* 83 (2024), p. 110510. ISSN: 2352-152X. DOI: <https://doi.org/10.1016/j.est.2024.110510>. URL: <https://www.sciencedirect.com/science/article/pii/S2352152X24000951>.
- [33] A. H. Slocum, G. E. Fennell, G. Dundar, B. G. Hodder, J. D. C. Meredith, and M. A. Sager. "Ocean Renewable Energy Storage (ORES) System: Analysis of an Undersea Energy Storage Concept". In: *Proceedings of the IEEE* 101.4 (2013), pp. 906–924. DOI: [10.1109/JPROC.2013.2242411](https://doi.org/10.1109/JPROC.2013.2242411).
- [34] M. Puchta, J. Bard, C. Dick, D. Hau, B. Krautkremer, F. Thalemann, and H. Hahn. "Development and testing of a novel offshore pumped storage concept for storing energy at sea - Stensea". In: *Journal of Energy Storage* 14 (2017), pp. 271–275. ISSN: 2352152X. DOI: [10.1016/j.est.2017.06.004](https://doi.org/10.1016/j.est.2017.06.004). URL: <https://doi.org/10.1016/j.est.2017.06.004>.
- [35] A. Pradhan, M. Marencé, and M. J. Franca. "The adoption of Seawater Pump Storage Hydropower Systems increases the share of renewable energy production in Small Island Developing States". In: *Renewable Energy* 177 (2021), pp. 448–460. ISSN: 18790682. DOI: [10.1016/j.renene.2021.05.151](https://doi.org/10.1016/j.renene.2021.05.151).
- [36] A. Berrada, K. Loudiyi, and I. Zorkani. "System design and economic performance of gravity energy storage". In: *Journal of Cleaner Production* 156 (2017), pp. 317–326. ISSN: 09596526. DOI: [10.1016/j.jclepro.2017.04.043](https://doi.org/10.1016/j.jclepro.2017.04.043). URL: <https://www.sciencedirect.com/science/article/pii/S0959652617307515>.
- [37] J. Novgorodcev Andre R., F. Mols, and A. Jarquin Laguna. "Subsea Buoyancy and Gravity Energy Storage System for Deep-Water Applications: A Preliminary Assessment". In: *Ocean Renewable Energy*. Vol. Volume 8. International Conference on Offshore Mechanics and Arctic Engineering. June 2022, V008T09A012. DOI: [10.1115/OMAE2022-80422](https://doi.org/10.1115/OMAE2022-80422). eprint: <https://asmedigitalcollection.asme.org/OMAE/proceedings-pdf/OMAE2022/85932/V008T09A012/6929503/v008t09a012-omae2022-80422.pdf>.
- [38] N. McIlwaine, A. M. Foley, D. J. Morrow, D. Al Kez, C. Zhang, X. Lu, and R. J. Best. "A state-of-the-art techno-economic review of distributed and embedded energy storage for energy systems". In: *Energy* 229 (2021), p. 120461. ISSN: 0360-5442. DOI: <https://doi.org/10.1016/j.energy.2021.120461>. URL: <https://www.sciencedirect.com/science/article/pii/S0360544221007106>.
- [39] I. Loots, M. Van Dijk, B. Barta, S. J. Van Vuuren, and J. N. Bhagwan. "A review of low head hydropower technologies and applications in a South African context". In: *Renewable and Sustainable Energy Reviews* 50.2015 (2015), pp. 1254–1268. ISSN: 1364-0321. DOI: <https://doi.org/10.1016/j.rser.2015.05.064>. URL: <https://www.sciencedirect.com/science/article/pii/S1364032115005353>.
- [40] A. M. Foley, P. G. Leahy, K. Li, E. J. McKeogh, and A. P. Morrison. "A long-term analysis of pumped hydro storage to firm wind power". In: *Applied Energy* 137.2015 (2015), pp. 638–648. ISSN: 03062619. DOI: [10.1016/j.apenergy.2014.07.020](https://doi.org/10.1016/j.apenergy.2014.07.020).
- [41] K. Mongird, V. Fotedar, V. Viswanathan, V. Koritarov, P. Balducci, B. Hadjerioua, and J. Alam. *Energy Storage Technology and Cost Characterization Report*. U.S. Department of Energy, 2019.

- [42] B. Zakeri and S. Syri. "Electrical energy storage systems: A comparative life cycle cost analysis". In: *Renewable and Sustainable Energy Reviews* 42 (2015), pp. 569–596. ISSN: 18790690. DOI: [10.1016/j.rser.2014.10.011](https://doi.org/10.1016/j.rser.2014.10.011). URL: <http://dx.doi.org/10.1016/j.rser.2014.10.011>.
- [43] J. Liu, C. Hu, A. Kimber, and Z. Wang. "Uses, Cost-Benefit Analysis, and Markets of Energy Storage Systems for Electric Grid Applications". In: *Journal of Energy Storage* 32 (2020), p. 101731. ISSN: 2352-152X. DOI: <https://doi.org/10.1016/j.est.2020.101731>. URL: <https://www.sciencedirect.com/science/article/pii/S2352152X20315681>.
- [44] G. F. Frate, L. Ferrari, and U. Desideri. "Energy storage for grid-scale applications: Technology review and economic feasibility analysis". In: *Renewable Energy* 163 (2021), pp. 1754–1772. ISSN: 0960-1481. DOI: <https://doi.org/10.1016/j.renene.2020.10.070>. URL: <https://www.sciencedirect.com/science/article/pii/S0960148120316360>.
- [45] I. Kougias and S. Szabó. "Pumped hydroelectric storage utilization assessment: Forerunner of renewable energy integration or Trojan horse?" In: *Energy* 140 (2017), pp. 318–329. ISSN: 03605442. DOI: [10.1016/j.energy.2017.08.106](https://doi.org/10.1016/j.energy.2017.08.106).
- [46] T. Ida, T. Kubota, J. Kurokawa, and H. Tanaka. "Recent Development of Studies on Scale Effect". In: *Hydraulic Machinery and Cavitation*. Ed. by E. Cabrera, V. Espert, and F. Martínez. Dordrecht: Springer Netherlands, 1996, pp. 313–322. ISBN: 978-94-010-9385-9.
- [47] T. Ida. "Analysis of scale effects on performance characteristics of hydraulic turbines". In: *Journal of Hydraulic Research* 28.1 (1990), pp. 93–104. DOI: [10.1080/00221689009499149](https://doi.org/10.1080/00221689009499149). eprint: <https://doi.org/10.1080/00221689009499149>. URL: <https://doi.org/10.1080/00221689009499149>.
- [48] S. Waters and G. A. Aggidis. "Over 2000 years in review: Revival of the Archimedes Screw from Pump to Turbine". In: *Renewable and Sustainable Energy Reviews* 51 (2015), pp. 497–505. ISSN: 1364-0321. DOI: <https://doi.org/10.1016/j.rser.2015.06.028>. URL: <https://www.sciencedirect.com/science/article/pii/S136403211505985>.
- [49] M. Maisuria, L. Ratadiya, and A. Patel. "Computational investigation and optimization of the bulb turbine for ultra-low head application". In: *Renewable Energy* 230 (2024), p. 120876. ISSN: 0960-1481. DOI: <https://doi.org/10.1016/j.renene.2024.120876>. URL: <https://www.sciencedirect.com/science/article/pii/S0960148124009443>.
- [50] E. McLean and D. Kearney. "An Evaluation of Seawater Pumped Hydro Storage for Regulating the Export of Renewable Energy to the National Grid". In: *Energy Procedia* 46 (2014). 8th International Renewable Energy Storage Conference and Exhibition (IRES 2013), pp. 152–160. ISSN: 1876-6102. DOI: <https://doi.org/10.1016/j.egypro.2014.01.168>. URL: <https://www.sciencedirect.com/science/article/pii/S1876610214001842>.
- [51] M. Qudaih, B. Engel, D. P. K. Truijen, J. D. M. De Kooning, K. Stockman, J. P. Hoffstaedt, A. Jarquin-Laguna, R. Ansoarena Ruiz, N. Goseberg, L. de Vilder, J. D. Bricker, M. Joseph, M. Zangeneh, and K. Terheiden. "The contribution of low-head pumped hydro storage to grid stability in future power systems". In: *IET Renewable Power Generation* (2022), pp. 1–15. ISSN: 1752-1424. DOI: [10.1049/RPG2.12668](https://doi.org/10.1049/RPG2.12668).
- [52] J. Fahlbeck, H. Nilsson, S. Salehi, M. Zangeneh, and M. Joseph. "Numerical analysis of an initial design of a counter-rotating pump-turbine". In: *IOP Conference Series: Earth and Environmental Science* 774.1 (2021), p. 12066. ISSN: 1755-1315. DOI: [10.1088/1755-1315/774/1/012066](https://doi.org/10.1088/1755-1315/774/1/012066).

- [53] E. Prasasti, M. Joseph, X. Miao, M. Zangeneh, and K. Terheiden. "Design of shaft- and rim-driven contra-rotating reversible pump-turbine to optimize novel low-head pumped hydro energy storages". In: *Energy* 306 (2024), p. 132237. ISSN: 0360-5442. DOI: <https://doi.org/10.1016/j.energy.2024.132237>. URL: <https://www.sciencedirect.com/science/article/pii/S0360544224020115>.
- [54] J. Fahlbeck, H. Nilsson, and S. Salehi. "Surrogate based optimisation of a pump mode startup sequence for a contra-rotating pump-turbine using a genetic algorithm and computational fluid dynamics". In: *Journal of Energy Storage* 62 (2023), p. 106902. ISSN: 2352-152X. DOI: <https://doi.org/10.1016/j.est.2023.106902>. URL: <https://www.sciencedirect.com/science/article/pii/S2352152X23002992>.
- [55] J. Fahlbeck, H. Nilsson, and S. Salehi. "Flow Characteristics of Preliminary Shutdown and Startup Sequences for a Model Counter-Rotating Pump-Turbine". In: *Energies* 14.12 (2021), p. 3593. DOI: [10.3390/en14123593](https://doi.org/10.3390/en14123593).
- [56] E. Prasasti, M. Aouad, M. Joseph, M. Zangeneh, and K. Terheiden. "Optimization of pumped hydro energy storage design and operation for offshore low-head application and grid stabilization". In: *Renewable and Sustainable Energy Reviews* 191 (2024), p. 114122. ISSN: 1364-0321. DOI: <https://doi.org/10.1016/j.rser.2023.114122>. URL: <https://www.sciencedirect.com/science/article/pii/S1364032123009802>.
- [57] H. Wang, F. Wang, C. Wang, B. Wang, C. Li, and D. Li. "A prospective assessment of scale effects of energy conversion in ultra-low-head pumped hydro energy storage units". In: *Energy Conversion and Management* 315 (2024), p. 118798. ISSN: 0196-8904. DOI: <https://doi.org/10.1016/j.enconman.2024.118798>. URL: <https://www.sciencedirect.com/science/article/pii/S0196890424007398>.
- [58] J. Shen, J. Pei, W. Wang, and S. Yuan. "Instability characteristics regarding the saddle-shaped region in a reversible mixed-flow pump applied to the low-head pumped storage". In: *Journal of Energy Storage* 63 (2023), p. 107035. ISSN: 2352-152X. DOI: <https://doi.org/10.1016/j.est.2023.107035>. URL: <https://www.sciencedirect.com/science/article/pii/S2352152X23004322>.
- [59] H. Wang, F. Wang, B. Wang, J. Wu, H. Lu, and C. Wang. "Partial flow separation in guide-vane region of large-capacity/low-head pumped hydro energy storage system with horizontal shaft". In: *Journal of Energy Storage* 71 (2023), p. 108173. ISSN: 2352-152X. DOI: <https://doi.org/10.1016/j.est.2023.108173>. URL: <https://www.sciencedirect.com/science/article/pii/S2352152X23015700>.
- [60] R. Ansorena Ruiz, L. de Vilder, E. Prasasti, M. Aouad, A. De Luca, B. Geisseler, K. Terheiden, S. Scanu, A. Miccoli, V. Roeber, M. Marencé, R. Moll, J. Bricker, and N. Goseberg. "Low-head pumped hydro storage: A review on civil structure designs, legal and environmental aspects to make its realization feasible in seawater". In: *Renewable and Sustainable Energy Reviews* 160 (2022), p. 112281. ISSN: 1364-0321. DOI: <https://doi.org/10.1016/j.rser.2022.112281>. URL: <https://www.sciencedirect.com/science/article/pii/S1364032122002003>.
- [61] J. Hunt, E. Byers, K. Riahi, and S. Langan. "Comparison between seasonal pumped-storage and conventional reservoir dams from the water, energy and land nexus perspective". In: *Energy Conversion and Management* 166 (2018), pp. 385–401. ISSN: 0196-8904. DOI: [10.1016/j.enconman.2018.04.044](https://doi.org/10.1016/j.enconman.2018.04.044). URL: <https://www.sciencedirect.com/science/article/pii/S0196890418303790>.
- [62] D. K. Okot. "Review of small hydropower technology". In: *Renewable and Sustainable Energy Reviews* 26 (2013), pp. 515–520. ISSN: 1364-0321. DOI: <https://doi.org/10.1016/j.rser.2013.05.006>. URL: <https://www.sciencedirect.com/science/article/pii/S1364032113003092>.
- [63] J. D. Hunt, B. Zakeri, R. Lopes, P. S. F. Barbosa, A. Nascimento, N. J. d. Castro, R. Brandão, P. S. Schneider, and Y. Wada. "Existing and new arrangements of pumped-hydro storage plants". In: *Renewable and Sustainable Energy Reviews* 129 (Sept. 2020), p. 109914. ISSN: 1364-0321. DOI: [10.1016/j.rser.2020.109914](https://doi.org/10.1016/j.rser.2020.109914).

- [64] K. R. Vasudevan, V. K. Ramachandaramurthy, G. Venugopal, J. B. Ekanayake, and S. K. Tiong. "Variable speed pumped hydro storage: A review of converters, controls and energy management strategies". In: *Renewable and Sustainable Energy Reviews* 135 (2021), p. 110156. ISSN: 13640321. DOI: [10.1016/j.rser.2020.110156](https://doi.org/10.1016/j.rser.2020.110156). URL: <https://www.sciencedirect.com/science/article/pii/S1364032120304470>.
- [65] J. M. Chapallaz, P. Eichenberger, and G. Fischer. *Manual on Pumps Used as Turbines*. Vol. 11. Deutsches Zentrum für Entwicklungstechnologien GATE, 1992, p. 229. ISBN: 3-528-02069-5.
- [66] S. L. Dixon and C. A. Hall. *Fluid Mechanics and Thermodynamics of Turbomachinery*. Seventh. Butterworth-Heinemann, 2014. ISBN: 978-0-12-415954-9. DOI: <https://doi.org/10.1016/C2011-0-05059-7>.
- [67] A. J. Stepanoff. *Centrifugal and axial flow pumps : theory, design and application*. Wiley, 1948.
- [68] M. Ak, E. Kentel, and S. Kucukali. "A fuzzy logic tool to evaluate low-head hydropower technologies at the outlet of wastewater treatment plants". In: *Renewable and Sustainable Energy Reviews* 68 (2017), pp. 727–737. ISSN: 13640321. DOI: [10.1016/j.rser.2016.10.010](https://doi.org/10.1016/j.rser.2016.10.010).
- [69] T. W. Hogan, G. F. Cada, and S. V. Amaral. "The Status of Environmentally Enhanced Hydropower Turbines". In: *Fisheries* 39.4 (2014), pp. 164–172. DOI: <https://doi.org/10.1080/03632415.2014.897195>. URL: <https://afspubs.onlinelibrary.wiley.com/doi/abs/10.1080/03632415.2014.897195>.
- [70] I. J. Karassik, J. P. Messina, P. Cooper, and C. C. Heald. "Pump handbook, Fourth Edition". In: New York: McGraw-Hill Education, 2008. ISBN: 9780071460446.
- [71] A. Carravetta, S. Derakhshan Houreh, and H. M. Ramos. "Introduction". In: *Pumps as Turbines: Fundamentals and Applications*. Springer Tracts in Mechanical Engineering. Cham: Springer International Publishing, 2018, pp. 3–26. ISBN: 978-3-319-67507-7. DOI: [10.1007/978-3-319-67507-7_1](https://doi.org/10.1007/978-3-319-67507-7_1). URL: https://doi.org/10.1007/978-3-319-67507-7_1.
- [72] W. Bogenrieder. "2.6. Pumped storage power plants". In: *Renewable Energy*. Ed. by K. Heinloth. Vol. 3C. Springer-Verlag Berlin Heidelberg, 2006, pp. 165–196. ISBN: 978-3-540-42962-3. DOI: [10.1007/10858992_7](https://doi.org/10.1007/10858992_7). URL: http://materials.springer.com/lb/docs/sm_lbs_978-3-540-45662-9_7.
- [73] P. Breeze. "Chapter 8 - Pumped Storage Hydropower". In: *Hydropower*. Ed. by P. Breeze. Academic Press, 2018, pp. 73–78. ISBN: 978-0-12-812906-7. DOI: [10.1016/B978-0-12-812906-7.00008-9](https://doi.org/10.1016/B978-0-12-812906-7.00008-9).
- [74] A. Morabito, G. de Oliveira e Silva, and P. Hendrick. "Deriaz pump-turbine for pumped hydro energy storage and micro applications". In: *Journal of Energy Storage* 24 (Aug. 2019), p. 100788. ISSN: 2352-152X. DOI: [10.1016/j.est.2019.100788](https://doi.org/10.1016/j.est.2019.100788).
- [75] F. M. White. *Fluid Mechanics, Eighth Edition*. New York, NY, USA: McGraw-Hill Education, 2016. ISBN: 9780073398273.
- [76] W. Braitsch and H. Haas. "2.7 Turbines for hydroelectric power". In: *Renewable Energy*. Ed. by K. Heinloth. Vol. 3C. Springer Berlin Heidelberg, 2006, pp. 197–222. ISBN: 978-3-540-42962-3. DOI: [10.1007/10858992_8](https://doi.org/10.1007/10858992_8).
- [77] D. Novara and A. McNabola. "A model for the extrapolation of the characteristic curves of Pumps as Turbines from a datum Best Efficiency Point". en. In: *Energy Conversion and Management* 174 (Oct. 2018), pp. 1–7. ISSN: 0196-8904. DOI: [10.1016/j.enconman.2018.07.091](https://doi.org/10.1016/j.enconman.2018.07.091). (Visited on 10/27/2021).
- [78] M. Binama, W.-T. Su, X.-B. Li, F.-C. Li, X.-Z. Wei, and S. An. "Investigation on pump as turbine (PAT) technical aspects for micro hydropower schemes: A state-of-the-art review". In: *Renewable and Sustainable Energy Reviews* 79 (Nov. 2017), pp. 148–179. ISSN: 1364-0321. DOI: [10.1016/j.rser.2017.04.071](https://doi.org/10.1016/j.rser.2017.04.071).
- [79] J. Delgado, L. Andolfatto, D. I. C. Covas, and F. Avellan. "Hill chart modelling using the Hermite polynomial chaos expansion for the performance prediction of pumps running as turbines". en. In: *Energy Conversion and Management* 187 (May 2019), pp. 578–592. ISSN: 0196-8904. DOI: [10.1016/j.enconman.2019.02.051](https://doi.org/10.1016/j.enconman.2019.02.051). (Visited on 10/27/2021).

- [80] A. Furukawa, T. Shigemitsu, and S. Watanabe. "Performance test and flow measurement of contra-rotating axial flow pump". In: *Journal of Thermal Science* 16.1 (2007), pp. 7–13. ISSN: 1993-033X. DOI: [10.1007/s11630-007-0007-4](https://doi.org/10.1007/s11630-007-0007-4). URL: <https://doi.org/10.1007/s11630-007-0007-4>.
- [81] J.-W. Kim, J.-W. Suh, Y.-S. Choi, K.-Y. Lee, T. Kanemoto, and J.-H. Kim. "Optimized Blade Design of Counter-Rotating-Type Pump-Turbine Unit Operating in Pump and Turbine Modes". In: *International Journal of Rotating Machinery* (Apr. 2018). DOI: <https://doi.org/10.1155/2018/6069780>.
- [82] J.-H. Kim, R. Kasahara, T. Kanemoto, T. Miyaji, Y.-S. Choi, J.-H. Kim, K.-Y. Lee, and A. M. Galal. "Multiobjective Optimization of a Counterrotating Type Pump-Turbine Unit Operated at Turbine Mode". In: *Advances in Mechanical Engineering* 6 (2014), p. 467235. ISSN: 1687-8140. DOI: [10.1155/2014/467235](https://doi.org/10.1155/2014/467235).
- [83] A. YoosefDoost and W. D. Lubitz. "Archimedes Screw Turbines: A Sustainable Development Solution for Green and Renewable Energy Generation—A Review of Potential and Design Procedures". In: *Sustainability* 12.18 (2020), p. 7352. DOI: [10.3390/su12187352](https://doi.org/10.3390/su12187352). URL: <https://www.mdpi.com/2071-1050/12/18/7352>.
- [84] D. Zhou and Z. (Deng. "Ultra-low-head hydroelectric technology: A review". In: *Renewable and Sustainable Energy Reviews* 78.May (2017), pp. 23–30. ISSN: 18790690. DOI: [10.1016/j.rser.2017.04.086](https://doi.org/10.1016/j.rser.2017.04.086).
- [85] M. A. Sari, M. Badruzzaman, C. Cherchi, M. Swindle, N. Ajami, and J. G. Jacangelo. "Recent innovations and trends in in-conduit hydropower technologies and their applications in water distribution systems". In: *Journal of Environmental Management* 228 (2018), pp. 416–428. ISSN: 0301-4797. DOI: <https://doi.org/10.1016/j.jenvman.2018.08.078>. URL: <https://www.sciencedirect.com/science/article/pii/S0301479718309496>.
- [86] P. Krampe and P. R. Ørke. "Four-Quadrant Operation of Rotary Lobe Pumps and Regenerative Throttling". In: *Pump Users International Forum 2012, International Rotating Equipment Conference 2012*. 2012.
- [87] J. Kurokawa, J. Matsui, and Y.-D. Choi. "Flow Analysis in Positive Displacement Micro-Hydro Turbine and Development of Low Pulsation Turbine". In: *International Journal of Fluid Machinery and Systems* 1.1 (2008), pp. 76–85. DOI: <https://doi.org/10.5293/ijfms.2008.1.1.076>. URL: <http://koreascience.or.kr/article/JAKO200820065114333.page>.
- [88] D. Phommachanh, J. Kurokawa, Y.-D. Choi, and N. Nakajima. "Development of a Positive Displacement Micro-Hydro Turbine". In: *Jsm International Journal Series B-fluids and Thermal Engineering* 49 (2006), pp. 482–489.
- [89] A. Sonawat, Y.-S. Choi, K. M. Kim, and J.-H. Kim. "Parametric study on the effect of inlet and outlet pipe shape on the flow fluctuation characteristics associated with a positive displacement hydraulic turbine". In: *Renewable Energy* 163 (2021), pp. 1046–1062. ISSN: 0960-1481. DOI: <https://doi.org/10.1016/j.renene.2020.09.025>. URL: <https://www.sciencedirect.com/science/article/pii/S0960148120314336>.
- [90] A. Sonawat, S.-J. Kim, H.-M. Yang, Y.-S. Choi, K.-M. Kim, Y.-K. Lee, and J.-H. Kim. "Positive displacement turbine - A novel solution to the pressure differential control valve failure problem and energy utilization". In: *Energy* 190 (2020), p. 116400. ISSN: 0360-5442. DOI: <https://doi.org/10.1016/j.energy.2019.116400>. URL: <https://www.sciencedirect.com/science/article/pii/S036054421932095X>.
- [91] A. Bocquel and J. Janning. "Analysis of a 300 MW variable speed drive for pump-storage plant applications". In: *2005 European Conference on Power Electronics and Applications*. 2005, 10 pp.–P.10. DOI: [10.1109/EPE.2005.219434](https://doi.org/10.1109/EPE.2005.219434).
- [92] M. S. Javed, T. Ma, J. Jurasz, and M. Y. Amin. "Solar and wind power generation systems with pumped hydro storage: Review and future perspectives". In: *Renewable Energy* 148 (2020), pp. 176–192. ISSN: 0960-1481. DOI: [10.1016/j.renene.2019.11.157](https://doi.org/10.1016/j.renene.2019.11.157).

- [93] M. Alizadeh Bidgoli, W. Yang, and A. Ahmadian. "DFIM versus synchronous machine for variable speed pumped storage hydropower plants: A comparative evaluation of technical performance". In: *Renewable Energy* 159 (2020), pp. 72–86. ISSN: 0960-1481. DOI: <https://doi.org/10.1016/j.renene.2020.05.163>. URL: <https://www.sciencedirect.com/science/article/pii/S0960148120308685>.
- [94] L. Belhadji, S. Bacha, I. Munteanu, A. Rumeau, and D. Roze. "Adaptive MPPT Applied to Variable-Speed Microhydropower Plant". In: *IEEE Transactions on Energy Conversion* 28.1 (2013), pp. 34–43. DOI: [10.1109/TEC.2012.2220776](https://doi.org/10.1109/TEC.2012.2220776).
- [95] B. Guo, S. Bacha, M. Alamir, A. Mohamed, and C. Boudinet. "LADRC applied to variable speed micro-hydro plants: Experimental validation". In: *Control Engineering Practice* 85 (2019), pp. 290–298. ISSN: 0967-0661. DOI: <https://doi.org/10.1016/j.conengprac.2019.02.008>. URL: <https://www.sciencedirect.com/science/article/pii/S0967066119300218>.
- [96] J. L. Márquez, M. G. Molina, and J. M. Pacas. "Dynamic modeling, simulation and control design of an advanced micro-hydro power plant for distributed generation applications". In: *International Journal of Hydrogen Energy* 35.11 (2010), pp. 5772–5777. ISSN: 0360-3199. DOI: <https://doi.org/10.1016/j.ijhydene.2010.02.100>. URL: <https://www.sciencedirect.com/science/article/pii/S0360319910004003>.
- [97] I. Ducar and C. Marinescu. "Increasing the efficiency of motor-pump systems using a vector controlled drive for PMSM application". In: *2014 International Symposium on Fundamentals of Electrical Engineering (ISFEE)*. 2014, pp. 1–5. DOI: [10.1109/ISFEE.2014.7050545](https://doi.org/10.1109/ISFEE.2014.7050545).
- [98] H. Iman-Eini, D. Frey, S. Bacha, C. Boudinet, and J.-L. Schanen. "Evaluation of loss effect on optimum operation of variable speed micro-hydropower energy conversion systems". In: *Renewable Energy* 131 (2019), pp. 1022–1034. ISSN: 0960-1481. DOI: <https://doi.org/10.1016/j.renene.2018.07.122>. URL: <https://www.sciencedirect.com/science/article/pii/S0960148118309194>.
- [99] W. Abd El Maguid Ahmed, M. M. Adel, M. Taha, and A. A. Saleh. "PSO technique applied to sensorless field-oriented control PMSM drive with discretized RL-fractional integral". In: *Alexandria Engineering Journal* 60.4 (2021), pp. 4029–4040. ISSN: 1110-0168. DOI: <https://doi.org/10.1016/j.aej.2021.02.049>. URL: <https://www.sciencedirect.com/science/article/pii/S1110016821001393>.
- [100] J. Bonifacio, N. Amann, and R. Kennel. "Silent low speed self-sensing strategy for permanent magnet synchronous machines based on subtractive filtering". In: *2017 Brazilian Power Electronics Conference (COBEP)*. 2017, pp. 1–6. DOI: [10.1109/COBEP.2017.8257377](https://doi.org/10.1109/COBEP.2017.8257377).
- [101] D. Borkowski. "Maximum Efficiency Point Tracking (MEPT) for Variable Speed Small Hydropower Plant With Neural Network Based Estimation of Turbine Discharge". In: *IEEE Transactions on Energy Conversion* 32.3 (2017), pp. 1090–1098. DOI: [10.1109/TEC.2017.2690447](https://doi.org/10.1109/TEC.2017.2690447).
- [102] A. G. Sanchez, M. G. Molina, and A. M. R. Lede. "Dynamic model of wind energy conversion systems with PMSG-based variable-speed wind turbines for power system studies". In: *International Journal of Hydrogen Energy* 37.13 (2012), pp. 10064–10069. ISSN: 0360-3199. DOI: <https://doi.org/10.1016/j.ijhydene.2011.12.077>. URL: <https://www.sciencedirect.com/science/article/pii/S0360319911027704>.
- [103] S. M. Tripathi, A. N. Tiwari, and D. Singh. "Grid-integrated permanent magnet synchronous generator based wind energy conversion systems: A technology review". In: *Renewable and Sustainable Energy Reviews* 51 (2015), pp. 1288–1305. ISSN: 1364-0321. DOI: <https://doi.org/10.1016/j.rser.2015.06.060>. URL: <https://www.sciencedirect.com/science/article/pii/S1364032115006322>.

- [104] G. Dubrovskiy, S. Peter, E.-M. Lappeen, A. Mikerov, V. Dzhanhotov, and J. Pyrhonen. "General comparison of direct and geared drives for control applications". In: *2014 16th European Conference on Power Electronics and Applications*. 2014, pp. 1–6. DOI: [10.1109/EPE.2014.6910754](https://doi.org/10.1109/EPE.2014.6910754).
- [105] K. Touimi, M. Benbouzid, and P. Tavner. "Tidal stream turbines: With or without a Gearbox?" In: *Ocean Engineering* 170 (2018), pp. 74–88. ISSN: 0029-8018. DOI: <https://doi.org/10.1016/j.oceaneng.2018.10.013>. URL: <https://www.sciencedirect.com/science/article/pii/S0029801818313155>.
- [106] A. Cavagnino, M. Lazzari, F. Profumo, and A. Tenconi. "A comparison between the axial flux and the radial flux structures for PM synchronous motors". In: *IEEE Transactions on Industry Applications* 38.6 (2002), pp. 1517–1524. DOI: [10.1109/TIA.2002.805572](https://doi.org/10.1109/TIA.2002.805572).
- [107] J. Gieras, R.-J. Wang, and M. Kamper. *Axial Flux Permanent Magnet Brushless Machines*. Springer, 2008, pp. 55–56. ISBN: 978-1-4020-6993-2. DOI: [10.1007/978-1-4020-8227-6](https://doi.org/10.1007/978-1-4020-8227-6).
- [108] H. Vansompel, P. Sergeant, and L. Dupré. "Optimized Design Considering the Mass Influence of an Axial Flux Permanent Magnet Synchronous Generator With Concentrated Pole Windings". In: *IEEE Transactions on Magnetics* 46.12 (2010), pp. 4101–4107. DOI: [10.1109/TMAG.2010.2070075](https://doi.org/10.1109/TMAG.2010.2070075).
- [109] K. Sitapati and R. Krishnan. "Performance comparisons of radial and axial field, permanent-magnet, brushless machines". In: *IEEE Transactions on Industry Applications* 37.5 (2001), pp. 1219–1226. DOI: [10.1109/28.952495](https://doi.org/10.1109/28.952495).
- [110] A. A. Pop, F. Jurca, C. Oprea, M. Chirca, S. Breban, and M. M. Radulescu. "Axial-flux vs. radial-flux permanent-magnet synchronous generators for micro-wind turbine application". In: *2013 15th European Conference on Power Electronics and Applications (EPE)*. 2013, pp. 1–10. DOI: [10.1109/EPE.2013.6634639](https://doi.org/10.1109/EPE.2013.6634639).
- [111] S. Kahourzade, A. Mahmoudi, H. W. Ping, and M. N. Uddin. "A Comprehensive Review of Axial-Flux Permanent-Magnet Machines". In: *Canadian Journal of Electrical and Computer Engineering* 37.1 (2014), pp. 19–33. DOI: [10.1109/CJECE.2014.2309322](https://doi.org/10.1109/CJECE.2014.2309322).
- [112] K. Wirtayasa, P. Irasari, M. Kasim, P. Widiyanto, and M. Hikmawan. "Design of an axial-flux permanent-magnet generator (AFPMG) 1 kW, 220 volt, 300 rpm, 1 phase for pico hydro power plants". In: *2017 International Conference on Sustainable Energy Engineering and Application (ICSEEA)*. 2017, pp. 172–179. DOI: [10.1109/ICSEEA.2017.8267704](https://doi.org/10.1109/ICSEEA.2017.8267704).
- [113] S. Djebbari, J. F. Charpentier, F. Scullier, and M. Benbouzid. "Design and Performance Analysis of Double Stator Axial Flux PM Generator for Rim Driven Marine Current Turbines". In: *IEEE Journal of Oceanic Engineering* 41.1 (2016), pp. 50–66. DOI: [10.1109/JOE.2015.2407691](https://doi.org/10.1109/JOE.2015.2407691).
- [114] S. Mengesha, S. Rajput, S. Lineykin, and M. Averbukh. "The Effects of Cogging Torque Reduction in Axial Flux Machines". In: *Micromachines* 12 (2021), p. 323. DOI: [10.3390/mi12030323](https://doi.org/10.3390/mi12030323).
- [115] S. S. Laxminarayan, M. Singh, A. H. Saifee, and A. Mittal. "Design, modeling and simulation of variable speed Axial Flux Permanent Magnet Wind Generator". In: *Sustainable Energy Technologies and Assessments* 19 (2017), pp. 114–124. ISSN: 2213-1388. DOI: <https://doi.org/10.1016/j.seta.2017.01.004>. URL: <https://www.sciencedirect.com/science/article/pii/S2213138817300310>.
- [116] J. Jin, J. F. Charpentier, and T. Tang. "Preliminary design of a TORUS type axial flux generator for direct-driven tidal current turbine". In: *2014 First International Conference on Green Energy ICGE 2014*. 2014, pp. 20–25. DOI: [10.1109/ICGE.2014.6835391](https://doi.org/10.1109/ICGE.2014.6835391).
- [117] N. Anitha and R. Bharanikumar. "Design and Analysis of Axial Flux Permanent Magnet Machine for Wind Power Applications". In: *2019 International Conference on Power Electronics Applications and Technology in Present Energy Scenario (PETPES)*. 2019, pp. 1–4. DOI: [10.1109/PETPES47060.2019.9003866](https://doi.org/10.1109/PETPES47060.2019.9003866).

- [118] T. S. El-Hasan. "Development of axial flux permanent magnet generator for direct driven micro wind turbine". In: *2016 IEEE International Conference on Renewable Energy Research and Applications (ICRERA)*. 2016, pp. 169–172. DOI: [10.1109/ICRERA.2016.7884531](https://doi.org/10.1109/ICRERA.2016.7884531).
- [119] C. Lok, V. Balakrishnan, and R. T. Subramaniam. "Implementation of hybrid pattern search-genetic algorithm into optimizing axial-flux permanent magnet coreless generator (AFPMG)". In: *Electrical Engineering* 99 (2017). DOI: [10.1007/s00202-016-0443-9](https://doi.org/10.1007/s00202-016-0443-9).
- [120] D. Kowal, P. Sergeant, L. Dupre, and A. den Bossche. "Comparison of Nonoriented and Grain-Oriented Material in an Axial Flux Permanent-Magnet Machine". In: *IEEE Transactions on Magnetics* 46.2 (2010), pp. 279–285. DOI: [10.1109/TMAG.2009.2032145](https://doi.org/10.1109/TMAG.2009.2032145).
- [121] J. He, C. Somogyi, A. Strandt, and N. A. O. Demerdash. "Diagnosis of stator winding short-circuit faults in an interior permanent magnet synchronous machine". In: *2014 IEEE Energy Conversion Congress and Exposition (ECCE)*. 2014, pp. 3125–3130. DOI: [10.1109/ECCE.2014.6953825](https://doi.org/10.1109/ECCE.2014.6953825).
- [122] L. Verkroost, H. Vansompel, F. De Belie, and P. Sergeant. "Distributed control strategies for modular permanent magnet synchronous machines taking into account mutual inductances". In: *2020 IEEE/ASME International Conference on Advanced Intelligent Mechatronics (AIM), Proceedings*. IEEE, 2020, pp. 66–71. ISBN: 9781728167947. URL: <http://dx.doi.org/10.1109/aim43001.2020.9158834>.
- [123] A.H.R. Mohamed, H. Vansompel, and P. Sergeant. "An integrated modular motor drive with shared cooling for axial flux motor drives". In: *IEEE Transactions on Industrial Electronics* (2020), pp. 1–10. ISSN: 0278-0046. URL: <http://dx.doi.org/10.1109/tie.2020.3028818>.
- [124] Y. Chen, S. Liang, W. Li, H. Liang, and C. Wang. "Faults and Diagnosis Methods of Permanent Magnet Synchronous Motors: A Review". In: *Applied sciences* 9.2116 (2019). DOI: [10.3390/app9102116](https://doi.org/10.3390/app9102116).
- [125] K. Kudelina, B. Asad, T. Vaimann, A. Rassölkin, A. Kallaste, and H. V. Khang. "Methods of Condition Monitoring and Fault Detection for Electrical Machines". In: *Energies* 14.22 (2021). ISSN: 1996-1073. URL: <https://www.mdpi.com/1996-1073/14/22/7459>.
- [126] A. Stetco, F. Dinmohammadi, X. Zhao, V. Robu, D. Flynn, M. Barnes, J. Keane, and G. Nenadic. "Machine learning methods for wind turbine condition monitoring: A review". In: *Renewable Energy* 133 (2019), pp. 620–635. ISSN: 0960-1481. DOI: <https://doi.org/10.1016/j.renene.2018.10.047>. URL: <https://www.sciencedirect.com/science/article/pii/S096014811831231X>.
- [127] Y. Lei, B. Yang, X. Jiang, F. Jia, N. Li, and A. K. Nandi. "Applications of machine learning to machine fault diagnosis: A review and roadmap". In: *Mechanical Systems and Signal Processing* 138 (2020), p. 106587. ISSN: 0888-3270. DOI: <https://doi.org/10.1016/j.ymssp.2019.106587>. URL: <https://www.sciencedirect.com/science/article/pii/S0888327019308088>.
- [128] H. Lee, H. Jeong, G. Koo, J. Ban, and S. W. Kim. "Attention Recurrent Neural Network-Based Severity Estimation Method for Interturn Short-Circuit Fault in Permanent Magnet Synchronous Machines". In: *IEEE Transactions on Industrial Electronics* 68.4 (2021), pp. 3445–3453. DOI: [10.1109/TIE.2020.2978690](https://doi.org/10.1109/TIE.2020.2978690).
- [129] B. M. Ebrahimi and J. Faiz. "Feature Extraction for Short-Circuit Fault Detection in Permanent-Magnet Synchronous Motors Using Stator-Current Monitoring". In: *IEEE Transactions on Power Electronics* 25.10 (2010), pp. 2673–2682. DOI: [10.1109/TPEL.2010.2050496](https://doi.org/10.1109/TPEL.2010.2050496).
- [130] I.-H. Kao, W.-J. Wang, Y.-H. Lai, and J.-W. Perng. "Analysis of Permanent Magnet Synchronous Motor Fault Diagnosis Based on Learning". In: *IEEE Transactions on Instrumentation and Measurement* 68.2 (2019), pp. 310–324. DOI: [10.1109/TIM.2018.2847800](https://doi.org/10.1109/TIM.2018.2847800).

- [131] E. J. Piedad, Y.-T. Chen, H.-C. Chang, and C.-C. Kuo. "Frequency Occurrence Plot-Based Convolutional Neural Network for Motor Fault Diagnosis". In: *Electronics* 9.10 (2020). ISSN: 2079-9292. DOI: [10.3390/electronics9101711](https://doi.org/10.3390/electronics9101711).
- [132] Z. Liu, W. Chen, C. Zhang, C. Yang, and H. Chu. "Data Super-Network Fault Prediction Model and Maintenance Strategy for Mechanical Product Based on Digital Twin". In: *IEEE Access* 7 (2019), pp. 177284–177296. DOI: [10.1109/ACCESS.2019.2957202](https://doi.org/10.1109/ACCESS.2019.2957202).
- [133] A. Rassõlkin, T. Orosz, G. L. Demidova, V. Kuts, V. Rjabtšikov, T. Vaimann, and A. Kallaste. "Implementation of Digital Twins for electrical energy conversion systems in selected case studies". In: *PROCEEDINGS OF THE ESTONIAN ACADEMY OF SCIENCES* 70.1 (2021), pp. 19–39. DOI: [10.3176/PROC.2021.1.03](https://doi.org/10.3176/PROC.2021.1.03).
- [134] G. Falekas and A. Karlis. "Digital Twin in Electrical Machine Control and Predictive Maintenance: State-of-the-Art and Future Prospects". In: *Energies* 14.18 (2021). ISSN: 1996-1073. DOI: [10.3390/en14185933](https://doi.org/10.3390/en14185933). URL: <https://www.mdpi.com/1996-1073/14/18/5933>.
- [135] M. M. Chowdhury, M. E. Haque, S. Saha, M. A. Mahmud, A. Gargoom, and A. M. T. Oo. "An Enhanced Control Scheme for an IPM Synchronous Generator Based Wind Turbine With MTPA Trajectory and Maximum Power Extraction". In: *IEEE Transactions on Energy Conversion* 33.2 (2018), pp. 556–566. DOI: [10.1109/TEC.2017.2769126](https://doi.org/10.1109/TEC.2017.2769126).
- [136] B. Demirkov. "Improved wind turbine control using maximum torque per ampere control strategy taking into account the magnetic saturation". In: *Electrotechnica & Electronica (E+E)* 54.2 (2019), pp. 26–34. ISSN: 0861-4717. URL: <https://epluse.ceec.bg/wp-content/uploads/2019/03/20190102-05.pdf>.
- [137] W. A. A. Salem, G. F. Osman, and S. H. Arfa. "Adaptive Neuro-Fuzzy Inference System Based Field Oriented Control of PMSM Speed Estimation". In: *2018 Twentieth International Middle East Power Systems Conference (MEPCON)*. 2018, pp. 626–631. DOI: [10.1109/MEPCON.2018.8635179](https://doi.org/10.1109/MEPCON.2018.8635179).
- [138] K. Scicluna, C. S. Staines, and R. Raute. "Sensorless position control of a PMSM for steer-by-wire applications". In: *2016 International Conference on Control, Decision and Information Technologies (CoDIT)*. 2016, pp. 46–51. DOI: [10.1109/CoDIT.2016.7593533](https://doi.org/10.1109/CoDIT.2016.7593533).
- [139] N. P. Gupta and P. Gupta. "Performance analysis of direct torque control of PMSM drive using SVPWM - inverter". In: *2012 IEEE 5th India International Conference on Power Electronics (IICPE)*. 2012, pp. 1–6. DOI: [10.1109/IICPE.2012.6450421](https://doi.org/10.1109/IICPE.2012.6450421).
- [140] Y. El Mourabit, A. Derouich, A. El Ghzizal, N. El Ouanjli, and O. Zamzoum. "DTC-SVM Control for Permanent Magnet Synchronous Generator based Variable Speed Wind Turbine". In: *International Journal of Power Electronics and Drive Systems* 8.4 (2017), pp. 1732–1743. ISSN: 20888694. URL: <https://www.proquest.com/scholarly-journals/dtc-svm-control-permanent-magnet-synchronous/docview/1982896402/se-2?accountid=11077>.
- [141] G. Foo and M. F. Rahman. "Sensorless Direct Torque and Flux-Controlled IPM Synchronous Motor Drive at Very Low Speed Without Signal Injection". In: *IEEE Transactions on Industrial Electronics* 57.1 (2010), pp. 395–403. DOI: [10.1109/TIE.2009.2030815](https://doi.org/10.1109/TIE.2009.2030815).
- [142] G. F. H. Beng. "Sensorless direct torque and flux control of interior permanent magnet synchronous motors at very low speeds including standstill". PhD thesis. The University of New South Wales, 2010.
- [143] H. Mesloub, R. Boumaaraf, M. T. Benchouia, A. Goléa, N. Goléa, and K. Srairi. "Comparative study of conventional DTC and DTC-SVM based control of PMSM motor — Simulation and experimental results". In: *Mathematics and Computers in Simulation* 167 (2020), pp. 296–307. ISSN: 0378-4754. DOI: <https://doi.org/10.1016/j.matcom.2018.06.003>.
- [144] T. Staubli and A. Abgottspon. "Discharge measurement in low head hydro power plants". In: *2017 International Conference on ENERGY and ENVIRONMENT (CIEM)*. 2017, pp. 226–230. DOI: [10.1109/CIEM.2017.8120820](https://doi.org/10.1109/CIEM.2017.8120820).

- [145] V. Krishnakumar R., K. R. Vigna, V. Gomathi, J. B. Ekanayake, and S. K. Tiong. "Modelling and simulation of variable speed pico hydel energy storage system for microgrid applications". In: *Journal of Energy Storage* 24 (2019), p. 100808. ISSN: 2352-152X. DOI: <https://doi.org/10.1016/j.est.2019.100808>. URL: <https://www.sciencedirect.com/science/article/pii/S2352152X19300556>.
- [146] S.-H. Mozafarpour-Khoshrodi and G. Shahgholian. "Improvement of perturb and observe method for maximum power point tracking in wind energy conversion system using fuzzy controller". In: *Energy Equipment and Systems* 4.2 (2016), pp. 111–122. ISSN: 2383-1111. DOI: [10.22059/ees.2016.23031](https://doi.org/10.22059/ees.2016.23031).
- [147] R. Putri, M. Pujiantara, A. Priyadi, T. Ise, and M. Purnomo. "Maximum power extraction improvement using sensorless controller based on adaptive perturb and observe algorithm for PMSG wind turbine application". In: *IET Electric Power Applications* 12.4 (2018), pp. 455–462. DOI: [10.1049/iet-epa.2017.0603](https://doi.org/10.1049/iet-epa.2017.0603).
- [148] A. Shahi and C. Bhattacharjee. "A study analysis of fuzzy based P&O MPPT scheme in PMSG based wind turbine". In: *2018 Technologies for Smart-City Energy Security and Power (ICSESP)*. 2018, pp. 1–4. DOI: [10.1109/ICSESP.2018.8376738](https://doi.org/10.1109/ICSESP.2018.8376738).
- [149] A. Borghetti, G. Naldi, M. Paolone, and M. Alberti. "Maximum Efficiency Point Tracking for Adjustable-Speed Small Hydro Power Plant". In: (2008), pp. 1–7.
- [150] R.-M. Chao, S.-H. Ko, H.-K. Lin, and I.-K. Wang. "Evaluation of a Distributed Photovoltaic System in Grid-Connected and Standalone Applications by Different MPPT Algorithms". In: *Energies* 11.6 (2018). ISSN: 1996-1073. DOI: [10.3390/en11061484](https://doi.org/10.3390/en11061484). URL: <https://www.mdpi.com/1996-1073/11/6/1484>.
- [151] K. T. Atta, A. Johansson, M. J. Cervantes, and T. Gustafsson. "Phasor extremum seeking and its application in Kaplan turbine control". In: *2014 IEEE Conference on Control Applications (CCA)*. 2014, pp. 298–303. DOI: [10.1109/CCA.2014.6981362](https://doi.org/10.1109/CCA.2014.6981362).
- [152] J. Zhang, V. Leontidis, A. Dazin, A. Tounzi, P. Delarue, G. Caignaert, F. Piriou, and A. Libaux. "Canal lock variable speed hydropower turbine design and control". In: *IET Renewable Power Generation* 12.14 (2018), pp. 1698–1707. ISSN: 0360-3199. DOI: <https://doi.org/10.1049/iet-rpg.2018.5312>.
- [153] D. Borkowski. "Analytical Model of Small Hydropower Plant Working at Variable Speed". In: *IEEE Transactions on Energy Conversion* 33.4 (2018), pp. 1886–1894. DOI: [10.1109/TEC.2018.2849573](https://doi.org/10.1109/TEC.2018.2849573).
- [154] J. I. Pérez-Díaz and J. Fraile-Ardanuy. "Neural networks for optimal operation of a run-of-river adjustable speed hydro power plant with axial-flow propeller turbine". In: *16th Mediterranean Conference on Control and Automation Congress Centre*. 2008, pp. 309–314. URL: <https://ieeexplore.ieee.org/stamp/stamp.jsp?arnumber=4602228>.
- [155] G. Heckelsmueller. "Application of variable speed operation on Francis Turbines". In: *Ingeniería e Investigación* 35 (2015), pp. 12–16. DOI: [10.15446/ing.investig.v35n1.44995](https://doi.org/10.15446/ing.investig.v35n1.44995).
- [156] J. Fraile-Ardanuy, J. R. Wilhelmi, J. Fraile-Mora, J. Pérez-Díaz, and I. Sarasúa. "Speed control of run-of-river variable speed hydro plants". In: (2006).
- [157] Y. Pannatier, B. Kawkabani, C. Nicolet, J.-J. Simond, A. Schwery, and P. Allenbach. "Investigation of Control Strategies for Variable-Speed Pump-Turbine Units by Using a Simplified Model of the Converters". In: *IEEE Transactions on Industrial Electronics* 57.9 (2010), pp. 3039–3049. DOI: [10.1109/TIE.2009.2037101](https://doi.org/10.1109/TIE.2009.2037101).
- [158] J. D. M. De Kooning, T. L. Vandoorn, J. Van de Vyver, B. Meersman, and L. Vandevelde. "Displacement of the maximum power point caused by losses in wind turbine systems". In: *Renewable Energy* 85 (2016), pp. 273–280. ISSN: 0960-1481. DOI: <https://doi.org/10.1016/j.renene.2015.06.052>. URL: <https://www.sciencedirect.com/science/article/pii/S0960148115300768>.

- [159] C. Wei, Z. Zhang, W. Qiao, and L. Qu. "Reinforcement-Learning-Based Intelligent Maximum Power Point Tracking Control for Wind Energy Conversion Systems". In: *IEEE Transactions on Industrial Electronics* 62.10 (2015), pp. 6360–6370. DOI: [10.1109/TIE.2015.2420792](https://doi.org/10.1109/TIE.2015.2420792).
- [160] N. Tomin, V. Kurbatsky, and H. Gulyev. "Intelligent Control of a Wind Turbine based on Reinforcement Learning". In: *2019 16th Conference on Electrical Machines, Drives and Power Systems (ELMA)*. 2019, pp. 1–6. DOI: [10.1109/ELMA.2019.8771645](https://doi.org/10.1109/ELMA.2019.8771645).
- [161] H. Fang, L. Chen, N. Dlakavu, and Z. Shen. "Basic Modeling and Simulation Tool for Analysis of Hydraulic Transients in Hydroelectric Power Plants". In: *IEEE Transactions on Energy Conversion* 23.3 (2008), pp. 834–841. DOI: [10.1109/TEC.2008.921560](https://doi.org/10.1109/TEC.2008.921560).
- [162] D. Borkowski and M. Majdak. "Small Hydropower Plants with Variable Speed Operation—An Optimal Operation Curve Determination". In: *Energies* 13.23 (2020). ISSN: 1996-1073. DOI: [10.3390/en13236230](https://doi.org/10.3390/en13236230). URL: <https://www.mdpi.com/1996-1073/13/23/6230>.
- [163] C. Li, Y. Mao, J. Yang, Z. Wang, and Y. Xu. "A nonlinear generalized predictive control for pumped storage unit". In: *Renewable Energy* 114 (2017), pp. 945–959. ISSN: 0960-1481. DOI: <https://doi.org/10.1016/j.renene.2017.07.055>. URL: <https://www.sciencedirect.com/science/article/pii/S0960148117306699>.
- [164] L. Liang, Y. Hou, and D. J. Hill. "GPU-Based Enumeration Model Predictive Control of Pumped Storage to Enhance Operational Flexibility". In: *IEEE Transactions on Smart Grid* 10.5 (2019), pp. 5223–5233. DOI: [10.1109/TSG.2018.2879226](https://doi.org/10.1109/TSG.2018.2879226).
- [165] J.-F. Mennemann, L. Marko, J. Schmidt, W. Kemmetmüller, and A. Kugi. "Nonlinear Model Predictive Control of a Variable-Speed Pumped-Storage Power Plant". In: *IEEE Transactions on Control Systems Technology* 29.2 (2021), pp. 645–660. DOI: [10.1109/TCST.2019.2956910](https://doi.org/10.1109/TCST.2019.2956910).
- [166] K. Abughalieh and S. Alawneh. "A Survey of Parallel Implementations for Model Predictive Control". In: *IEEE Access* (Mar. 2019), pp. 1–1. DOI: [10.1109/ACCESS.2019.2904240](https://doi.org/10.1109/ACCESS.2019.2904240).
- [167] M. C. Jover. "Optimal joint day-ahead energy and secondary regulation reserve scheduling of pumped-storage power plants operating with variable speed or in hydraulic short-circuit mode in the Iberian electricity market". PhD thesis. Technical University of Madrid, 2017. URL: http://oa.upm.es/47652/1/Manuel_Chazarra_Jover.pdf.
- [168] Next Kraftwerke GmbH. "What are ancillary services?" In: (). URL: <https://www.next-kraftwerke.com/knowledge/ancillary-services>.
- [169] M. Qudaih, B. Engel, D. Truijen, J. Kooning, K. Stockman, J. Hoffstaedt, A. Jarquin Laguna, R. Ansorena Ruiz, N. Goseberg, J. Bricker, J. Fahlbeck, H. Nilsson, L. Bossi, M. Joseph, and M. Zangeneh. "The Contribution of Low-Head Pumped Hydro Storage to a Successful Energy Transition". In: *Virtual 19th Wind Integration Workshop*. 2020.
- [170] Siemens AG. *Parallel compensation Comprehensive solutions for safe and reliable grid operation*. Tech. rep. 2016. URL: <https://assets.siemens-energy.com/siemens/assets/api/uuid:14331eadd9b9b70a911fe4e238c96a5a67041eeb/263-160391-ws-parallel-compensation-us-o2e-1611.pdf>.
- [171] ENTSO-E. "Synchronous condenser". In: *ENTSO-E Technopedia* (2021). URL: <https://www.entsoe.eu/Technopedia/techsheets/synchronous-condenser>.
- [172] P. Unruh, M. Nuschke, P. Strauß, and F. Welck. "Overview on Grid-Forming Inverter Control Methods". In: *Energies* 13.10 (2020). ISSN: 1996-1073. DOI: [10.3390/en13102589](https://doi.org/10.3390/en13102589). URL: <https://www.mdpi.com/1996-1073/13/10/2589>.

- [173] S. Laudahn, J. Seidel, B. Engel, T. Bülo, and D. Premm. "Substitution of synchronous generator based instantaneous frequency control utilizing inverter-coupled DER". In: *2016 IEEE 7th International Symposium on Power Electronics for Distributed Generation Systems (PEDG)*. 2016, pp. 1–8. DOI: [10.1109/PEDG.2016.7527020](https://doi.org/10.1109/PEDG.2016.7527020).
- [174] EU. *DIRECTIVE (EU) 2019/944 OF THE EUROPEAN PARLIAMENT AND OF THE COUNCIL of 5 June 2019 on common rules for the internal market for electricity and amending Directive 2012/27/EU*. Tech. rep. 2019. URL: <https://eur-lex.europa.eu/legal-content/EN/TXT/PDF/?uri=CELEX:32019L0944&from=EN>.
- [175] T. Kerdphol, M. Watanabe, Y. Mitani, and V. Phunpeng. "Applying Virtual Inertia Control Topology to SMES System for Frequency Stability Improvement of Low-Inertia Microgrids Driven by High Renewables". In: *Energies* 12.20 (2019). ISSN: 1996-1073. DOI: [10.3390/en12203902](https://doi.org/10.3390/en12203902). URL: <https://www.mdpi.com/1996-1073/12/20/3902>.
- [176] T. Kerdphol, F. S. Rahman, and Y. Mitani. "Virtual Inertia Control Application to Enhance Frequency Stability of Interconnected Power Systems with High Renewable Energy Penetration". In: *Energies* 11.4 (2018). ISSN: 1996-1073. DOI: [10.3390/en11040981](https://doi.org/10.3390/en11040981). URL: <https://www.mdpi.com/1996-1073/11/4/981>.
- [177] J. Hu, J. Yang, W. Zeng, and J. Yang. "Transient Pressure Analysis of a Prototype Pump Turbine: Field Tests and Simulation". In: *Journal of Fluids Engineering* 140.7 (Mar. 2018), p. 071102. ISSN: 0098-2202. DOI: [10.1115/1.4039258](https://doi.org/10.1115/1.4039258). eprint: https://asmedigitalcollection.asme.org/fluidsengineering/article-pdf/140/7/071102/6058810/fe_140_07_071102.pdf. URL: <https://doi.org/10.1115/1.4039258>.
- [178] G. Tiwari, J. Kumar, V. Prasad, and V. K. Patel. "Utility of CFD in the design and performance analysis of hydraulic turbines — A review". In: *Energy Reports* 6 (2020), pp. 2410–2429. ISSN: 2352-4847. DOI: <https://doi.org/10.1016/j.egy.2020.09.004>. URL: <https://www.sciencedirect.com/science/article/pii/S2352484720312920>.
- [179] E. Casartelli, A. Del Rio, L. Mangani, and A. Schmid. "Capturing the S-Shape of Pump-Turbines by Computational Fluid Dynamics Simulations Using an Anisotropic Turbulence Model". In: *Journal of Fluids Engineering* 144.2 (Aug. 2021), p. 021203. ISSN: 0098-2202. DOI: [10.1115/1.4051809](https://doi.org/10.1115/1.4051809). eprint: https://asmedigitalcollection.asme.org/fluidsengineering/article-pdf/144/2/021203/6739636/fe_144_02_021203.pdf. URL: <https://doi.org/10.1115/1.4051809>.
- [180] H. A. Mrope, Y. A. Chande Jande, and T. T. Kivevele. "A Review on Computational Fluid Dynamics Applications in the Design and Optimization of Crossflow Hydro Turbines". In: *Journal of Renewable Energy* (2021), pp. 1–13. ISSN: 2314-4386. DOI: [10.1155/2021/5570848](https://doi.org/10.1155/2021/5570848).
- [181] W. E. Schiesser. *The numerical method of lines: integration of partial differential equations*. Elsevier, 2012.
- [182] M. Mohanpurkar, A. Ouroua, R. Hovsopian, Y. Luo, M. Singh, E. Muljadi, V. Gevorgian, and P. Donalek. "Real-time co-simulation of adjustable-speed pumped storage hydro for transient stability analysis". In: *Electric Power Systems Research* 154 (2018), pp. 276–286. ISSN: 03787796. DOI: [10.1016/j.epsr.2017.08.010](https://doi.org/10.1016/j.epsr.2017.08.010). URL: <https://doi.org/10.1016/j.epsr.2017.08.010>.
- [183] E. Wylie and V. Streeter. "Fluid Transients in Systems". In: *Journal of Fluid Mechanics* 264 (1994), p. 375.
- [184] J. S. Stecki and D. C. Davis. "Fluid transmission lines-distributed parameter models Part 1: a review of the state of the art." In: *Proc. Inst. Mech. Engrs. Part A* 200.A4, 1986 (1986), pp. 215–228. ISSN: 02637138.
- [185] M. S. Ghidaoui, M. Zhao, D. A. McInnis, and D. H. Axworthy. "A Review of Water Hammer Theory and Practice". In: *Applied Mechanics Reviews* 58.1 (Jan. 2005), pp. 49–76. ISSN: 0003-6900. DOI: [10.1115/1.1828050](https://doi.org/10.1115/1.1828050). URL: <https://asmedigitalcollection-asme-org.tudelft.idm.oclc.org/appliedmechanicsreviews/article/58/1/49/458451/A-Review-of-Water-Hammer-Theory-and-Practice>.

- [186] J. D. Sharma and A. Kumar. "Development and Implementation of Non- Linear Hydro Turbine Model with Elastic Effect of Water Column and Surge Tank". In: *International Journal of Electrical and Electronics Research* 2.4 (2014), pp. 234–243.
- [187] M. S. Ghidaoui. "On the fundamental equations of water hammer". In: *Urban Water Journal* 1.2 (June 2004), pp. 71–83. ISSN: 1573-062X. DOI: [10.1080/15730620412331290001](https://doi.org/10.1080/15730620412331290001).
- [188] G. Janevska, S. Panovski, and C. Stefanovska. "Comparative Analysis of Mathematical Models of Penstock Dynamics at Hydropower Plants". In: *International Journal of Scientific and Engineering Research* Volume 9 (Oct. 2018), pp. 652–657.
- [189] M. H. Chaudhry. *Applied hydraulic transients*. Springer, 2014. ISBN: 0442215177. DOI: [10.13182/nt81-a32632](https://doi.org/10.13182/nt81-a32632).
- [190] G. Brown. "The History of the Darcy-Weisbach Equation for Pipe Flow Resistance". In: *Environmental and Water Resources History* 38 (2002), pp. 34–43. DOI: [10.1061/40650\(2003\)4](https://doi.org/10.1061/40650(2003)4).
- [191] J. J. Benito, F. Ureña, and L. Gavete. "Influence of several factors in the generalized finite difference method". In: *Applied Mathematical Modelling* 25.12 (Dec. 2001), pp. 1039–1053. ISSN: 0307-904X. DOI: [10.1016/S0307-904X\(01\)00029-4](https://doi.org/10.1016/S0307-904X(01)00029-4).
- [192] Z. Lubis, T. Manik, M. Rinkanto, and T. Sitorus. "Design of a heat exchanger of three concentric tube layer on contrary flow". In: *IOP Conference Series: Materials Science and Engineering* 505 (July 2019), p. 012091. DOI: [10.1088/1757-899X/505/1/012091](https://doi.org/10.1088/1757-899X/505/1/012091).
- [193] W. E. Leithead and B. Connor. "Control of variable speed wind turbines: Dynamic models". In: *International Journal of Control* 73.13 (2000), pp. 1173–1188. ISSN: 1366-5820. DOI: [10.1080/002071700417830](https://doi.org/10.1080/002071700417830). URL: <https://www.tandfonline.com/action/journalInformation?journalCode=tcon20>.
- [194] D. P. K. Truijen, J. P. Hoffstaedt, J. Fahlbeck, A. Jarquin Laguna, H. Nilsson, K. Stockman, and J. D. M. de Kooning. "Impact of Dual Variable Speed and Inlet Valve Control on the Efficiency and Operating Range of Low-Head Contra-Rotating Pump-Turbines". In: *IEEE Access* 12 (2024), pp. 86854–86868. DOI: [10.1109/ACCESS.2024.3416679](https://doi.org/10.1109/ACCESS.2024.3416679).
- [195] J. Hoffstaedt, R. Ansorena Ruiz, D. Schürenkamp, A. Jarquin Laguna, and N. Goseberg. "Experimental setup and methods for a novel low-head pumped storage system". English. In: *7th Offshore Energy & Storage Symposium (OSES 2023)*. IET Digital Library, 2023, pp. 341–348. ISBN: 978-1-83953-922-0.
- [196] S. Riedelbauch and C. Stens. "Pump to turbine transient for a pump-turbine in a model test circuit and a real size power plant". In: *IOP Conference Series: Earth and Environmental Science* 240.7 (Mar. 2019), p. 072039. DOI: [10.1088/1755-1315/240/7/072039](https://doi.org/10.1088/1755-1315/240/7/072039). URL: <https://dx.doi.org/10.1088/1755-1315/240/7/072039>.
- [197] B. Zhu, X. Wang, L. Tan, D. Zhou, Y. Zhao, and S. Cao. "Optimization design of a reversible pump–turbine runner with high efficiency and stability". In: *Renewable Energy* 81 (2015), pp. 366–376. ISSN: 0960-1481. DOI: <https://doi.org/10.1016/j.renene.2015.03.050>. URL: <https://www.sciencedirect.com/science/article/pii/S0960148115002323>.
- [198] R. Tao and Z. Wang. "Comparative numerical studies for the flow energy dissipation features in a pump-turbine in pump mode and turbine mode". In: *Journal of Energy Storage* 41 (2021), p. 102835. ISSN: 2352-152X. DOI: <https://doi.org/10.1016/j.est.2021.102835>. URL: <https://www.sciencedirect.com/science/article/pii/S2352152X21005600>.
- [199] The Government of the Netherlands. *Climate Agreement*. Ministry of Economic Affairs and Climate Policy, 2019. URL: <https://www.government.nl/topics/renewable-energy/documents/reports/2019/06/28/climate-agreement>.

- [200] The Government of the Netherlands. *Offshore wind energy*. Accessed: 10.03.2023. URL: <https://www.government.nl/topics/renewable-energy/offshore-wind-energy>.
- [201] K. VanGraafeiland. *Global Tidal Range*. Accessed: 07.06.2023. URL: <https://www.arcgis.com/home/item.html?id=d5354dea41b14f0689860bf4b2cf5e8a#>.
- [202] H. Hahn, D. Hau, C. Dick, and M. Puchta. "Techno-economic assessment of a subsea energy storage technology for power balancing services". In: *Energy* 133 (2017), pp. 121–127. ISSN: 0360-5442. DOI: <https://doi.org/10.1016/j.energy.2017.05.116>. URL: <https://www.sciencedirect.com/science/article/pii/S0360544217308733>.
- [203] A. Berrada, A. Emrani, and A. Ameer. "Life-cycle assessment of gravity energy storage systems for large-scale application". In: *Journal of Energy Storage* 40 (2021), p. 102825. ISSN: 2352-152X. DOI: <https://doi.org/10.1016/j.est.2021.102825>. URL: <https://www.sciencedirect.com/science/article/pii/S2352152X2100551X>.
- [204] J. Menéndez, J. M. Fernández-Oro, M. Galdo, and J. Loredó. "Efficiency analysis of underground pumped storage hydropower plants". In: *Journal of Energy Storage* 28 (2020), p. 101234. ISSN: 2352-152X. DOI: <https://doi.org/10.1016/j.est.2020.101234>. URL: <https://www.sciencedirect.com/science/article/pii/S2352152X20300323>.
- [205] Y. Chen, Y. Kang, Y. Zhao, L. Wang, J. Liu, Y. Li, Z. Liang, X. He, X. Li, N. Tavajohi, and B. Li. "A review of lithium-ion battery safety concerns: The issues, strategies, and testing standards". In: *Journal of Energy Chemistry* 59 (2021), pp. 83–99. ISSN: 2095-4956. DOI: <https://doi.org/10.1016/j.jechem.2020.10.017>. URL: <https://www.sciencedirect.com/science/article/pii/S2095495620307075>.
- [206] C. Costa, J. Barbosa, R. Gonçalves, H. Castro, F. D. Campo, and S. Lanceros-Méndez. "Recycling and environmental issues of lithium-ion batteries: Advances, challenges and opportunities". In: *Energy Storage Materials* 37 (2021), pp. 433–465. ISSN: 2405-8297. DOI: <https://doi.org/10.1016/j.ensm.2021.02.032>. URL: <https://www.sciencedirect.com/science/article/pii/S2405829721000829>.
- [207] Tennet SOP-SYS. *FCR Manual for BSP's*. Tech. rep. Tennet, 2022. URL: <https://tennet-drupal.s3.eu-central-1.amazonaws.com/default/2023-04/Handboek%20FCR%20voor%20BSPs%20-%20EN%20version.pdf>.
- [208] 50hertz, Amprion, Tennet, Transnet bw. *Prequalification Process for Balancing Service Providers (FCR, aFRR, mFRR) in Germany ("PQ conditions")*. Tech. rep. Regelleistung.net, 2022. URL: [https://www.regelleistung.net/Portals/1/downloads/regelenergieanbieter_werden/pr%C3%A4qualifikationsbedingungen/PQ%20Bedingungen%20-%2003.06.2022%20\(englisch\).pdf?ver=4rD5rRjAmi_tqY0oI3Q2Mw%3d%3d](https://www.regelleistung.net/Portals/1/downloads/regelenergieanbieter_werden/pr%C3%A4qualifikationsbedingungen/PQ%20Bedingungen%20-%2003.06.2022%20(englisch).pdf?ver=4rD5rRjAmi_tqY0oI3Q2Mw%3d%3d).
- [209] U. Akram, M. Nadarajah, R. Shah, and F. Milano. "A review on rapid responsive energy storage technologies for frequency regulation in modern power systems". In: *Renewable and Sustainable Energy Reviews* 120 (2020), p. 109626. ISSN: 1364-0321. DOI: <https://doi.org/10.1016/j.rser.2019.109626>. URL: <https://www.sciencedirect.com/science/article/pii/S1364032119308330>.
- [210] X. Ma, D. Wu, D. Wang, B. Huang, K. Desomber, T. Fu, and M. Weimar. "Optimizing pumped storage hydropower for multiple grid services". In: *Journal of Energy Storage* 51 (2022), p. 104440. ISSN: 2352-152X. DOI: <https://doi.org/10.1016/j.est.2022.104440>. URL: <https://www.sciencedirect.com/science/article/pii/S2352152X22004637>.

ACKNOWLEDGEMENTS

Those who have embarked on a PhD journey before me have compared it to solving a jigsaw puzzle without the picture on the box—or, for the more dramatic, to building a plane while flying it. Surely, these comparisons are exaggerated. Yet, after years of navigating this academic endeavour, I must admit they might be onto something. The process is a curious blend of confusion, self-doubt, and the persistent feeling that the greatest challenge is always just ahead—much like hurtling through the air, uncertain if you’ve installed the wings correctly.

And yet, I have been incredibly lucky not to have undertaken this journey alone. I have been surrounded by wonderful people who, knowingly or unknowingly, helped keep this aircraft level. After all, flying a plane can be exhilarating, and the views are often spectacular. To all those who have offered guidance, support, and encouragement, I want to express my deepest gratitude

First and foremost, I want to thank Antonio, my daily supervisor and copromotor. Over the years, he has been an exceptional mentor – offering unwavering support, sharp insights, and a generosity of time and effort that has profoundly shaped my journey. Beyond the academic work, I cherish the memories from conferences and moments shared outside the office. I am deeply grateful to my original promotor, Cees, who tragically passed away before he could see the completion of this PhD. I am equally grateful to my new promotor, Rudy, who kindly stepped in to guide me toward the finish line. Thank you both for playing such significant roles in this journey.

I was fortunate to be part of a larger research project that brought together colleagues from across the world. My heartfelt thanks go to my ALPHEUS colleagues for the brilliant collaboration and the many enjoyable moments we shared. A special thank you to Ruben, Daan, Jonathan, Mohammed and Luiz, whose contributions and teamwork have directly shaped this dissertation. Your efforts, particularly in the review paper, played a crucial role in laying the foundation for this work.

The life I built in the Netherlands while working on this PhD would not have been the same without the incredible colleagues and friends who surrounded me. I wouldn’t have wanted to do it without you all. Thank you, Stella, Filippo, Frida, Marco, Fede, my lovely roomies, and so many more, for the wonderful times we shared.

To Leon and Tobi – thank you for shaping my life in all the best ways. To Alex, Vinni, and Kay—thank you for being the most incredible friends through all the years we have known each other. There are countless others I want to acknowledge, but three more deserve a special mention. Elad, Noam, and Ryan — you are three of the best people I have ever met. Your friendship, wisdom, and the example you set of how to live with purpose and integrity have been an inspiration. I have learned so much from you, thank you.

I would also like to thank my family. First, my wonderful new family, Ali, Lesley, and

Robin—you have been an incredible source of support and joy, and I couldn't be happier to have you in my life. To my sister Anne —thank you for everything you have taught me and for laying the foundation that helped me embark on this long journey. To my dad—thank you for answering the endless questions I had as a child, setting me on the path of curiosity.

Finally, I want to thank the two people to whom I have dedicated this thesis – my mother, Ulrike, and my wife, Charlie. I cannot imagine what my life would look like without you. Your unwavering love, patience, and encouragement have meant everything. I am endlessly grateful for all the support you have given me, and I dedicate this achievement to you both.

CURRICULUM VITAE

Justus HOFFSTÄDT

23-02-1994 Born in Düsseldorf, Germany.

EDUCATION

2014–2017 Bachelor of Engineering - Engineering and Business
Administration - Major: Electrical Engineering
Cooperative State University Baden Württemberg

2018–2019 Master of Science - Sustainable Energy Systems
University of Edinburgh

2020-2024 Doctor of Philosophy
Faculty of Mechanical Engineering, Delft University
of Technology

Thesis: Low-Head Pumped Hydro Storage with Contra-
Rotating Pump-Turbines - A Study on its Perfor-
mance and Potential Contribution to Grid Stability

Promoters: Prof. Dr. ir. C. van Rhee (†)
Dr. ir. R.I.J. Helmons

Copromotor: Dr. ir. A. Jarquin Laguna

AWARDS

2018 M.Sc. Dissertation - Best Project Providing Tangible Benefits
to Industry

PROFESSIONAL EXPERIENCE

2014–2017	Dual Student, Siemens AG Stuttgart, Germany
2016	In-House Intern, Siemens AG Helsinki, Finland
2017–2018	Intern, German Development Cooperation (GIZ) Nairobi, Kenya
2018–2020	Engineering Consultant, Comet-ME Hebron, Palestine
2020–2024	PhD Researcher, Delft University of Technology Delft, Netherlands

LIST OF PUBLICATIONS

JOURNAL PUBLICATIONS

5. **J. P. Hoffstaedt**, A. Jarquin-Laguna, R. Ansorena Ruiz, D. Schuerenkamp, N. Goseberg, D. Truijen, J. De Kooning, K. Stockmann, J. Fahlbeck, and H. Nilsson. “Analysis of a Contra-Rotating Pump-Turbine for Low-Head Applications: An Experimental Study and Numerical Comparison”. In: *Energy Conversion and Management* n/a.n/a (2025). [Submitted]
4. **J.P. Hoffstaedt**, D. Truijen, A. Jarquin-Laguna, J. De Kooning, K. Stockmann, J. Fahlbeck, and H. Nilsson. “Low-Head Pumped Hydro Storage: An Evaluation of Energy Balancing and Frequency Support”. In: *IET Renewable Power Generation* n/a.n/a (2024). DOI: <https://doi.org/10.1049/rpg2.13125>
3. D. P. K. Truijen, **J.P. Hoffstaedt**, J. Fahlbeck, A. Jarquin Laguna, H. Nilsson, K. Stockman, and J. D. M. de Kooning. “Impact of Dual Variable Speed and Inlet Valve Control on the Efficiency and Operating Range of Low-Head Contra-Rotating Pump-Turbines”. In: *IEEE Access* 12 (2024), pp. 86854–86868. DOI: [10.1109/ACCESS.2024.3416679](https://doi.org/10.1109/ACCESS.2024.3416679)
2. **J.P. Hoffstaedt**, D. P. K. Truijen, J. Fahlbeck, L. H. A. Gans, M. Qudaih, A. J. Laguna, J. D. M. De Kooning, K. Stockman, H. Nilsson, P.-T. Storli, B. Engel, M. Marence, and J. D. Bricker. “Low-head pumped hydro storage: A review of applicable technologies for design, grid integration, control and modelling”. In: *Renewable and Sustainable Energy Reviews* 158 (2022), p. 112119. ISSN: 1364-0321. DOI: <https://doi.org/10.1016/j.rser.2022.112119>
1. M. Qudaih, B. Engel, D. P. K. Truijen, J. D. M. De Kooning, K. Stockman, **J.P. Hoffstaedt**, A. Jarquin-Laguna, R. Ansorena Ruiz, N. Goseberg, L. de Vilder, J. D. Bricker, M. Joseph, M. Zangeneh, and K. Terheiden. “The contribution of low-head pumped hydro storage to grid stability in future power systems”. In: *IET Renewable Power Generation* (2022), pp. 1–15. ISSN: 1752-1424. DOI: [10.1049/RPG2.12668](https://doi.org/10.1049/RPG2.12668)

CONFERENCE PUBLICATIONS

4. D. P. K. Truijen, **J.P. Hoffstaedt**, J. Fahlbeck, A. Jarquin-Laguna, H. Nilsson, K. Stockman, and J. D. M. De Kooning. “Hardware-in-the-loop emulator test-setup for a dual-rotor contra-rotating pump-turbine”. In: *13th International Conference on Power Electronics, Machines and Drives (PEMD 2024)*. Vol. 2024. 2024, pp. 81–88. DOI: [10.1049/icp.2024.2140](https://doi.org/10.1049/icp.2024.2140)
3. **J.P. Hoffstaedt**, R. Ansorena Ruiz, D. Schürenkamp, A. Jarquin Laguna, and N. Goseberg. “Experimental setup and methods for a novel low-head pumped storage system”. English. In: *7th Offshore Energy & Storage Symposium (OSES 2023)*. IET Digital Library, 2023, pp. 341–348. ISBN: 978-1-83953-922-0
2. **J.P. Hoffstaedt**, A. Jarquín-Laguna, J. Fahlbeck, and H. Nilsson. “System model development and numerical simulation of low-head pumped hydro storage”. In: *Trends in Renewable Energies Offshore*. 2022, pp. 757–763. DOI: [10.1201/9781003360773-85](https://doi.org/10.1201/9781003360773-85)
1. M. Qudaih, B. Engel, D. Truijen, J. De Kooning, K. Stockman, **J.P. Hoffstaedt**, A. Jarquin-Laguna, R. Ansorena Ruiz, N. Goseberg, J. Bricker, J. Fahlbeck, H. Nilsson, L. Bossi, M. Joseph, and M. Zangeneh. “The contribution of low-head pumped hydro storage to a successful energy transition”. In: *Proceedings of the Virtual 19th Wind Integration Workshop*. Online, 2020, p. 8

